

https://dspace.org/

# Prospectivity mapping using stream sediment geochemistry along the Orange River Catchment for base metal, Prieska, Northern Cape, South Africa

**Mashale, Hilda Nthabiseng**

**2020**

https://hdl.handle.net/10539/31599

Mashale, Hilda Nthabiseng (2020) Prospectivity mapping using stream sediment geochemistry along the Orange River Catchment for base metal, Prieska, Northern Cape, South Africa, University of the Witwatersrand, Johannesburg, <http://hdl.handle.net/10539/31599>

Downloaded from a DSpace repository. https://dspace.org/




# Prospectivity Mapping using Stream Sediment Geochemistry Along the Orange River Catchment for Base Metal, Prieska, Northern Cape, South Africa.

**By**

**Hilda Nthabiseng Mashale**

**A research report submitted to the Faculty of Science, University of the Witwatersrand, Johannesburg, in partial fulfilment of the requirement for the degree of Masters of Science.**

**2020**

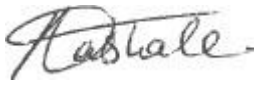
**Declaration**

I **Hilda Nthabiseng Mashale** (Student number: **0607122X**) am a student registered for MSc Economic Geology (Research and Course work) in the year 2017-2018. I hereby declare the following:

- That this research report has been composed solely by me and that it has not been submitted, in whole or in part, in any previous application for a degree. Except where states otherwise by reference or acknowledgment, the work presented is entirely my own.

- I am aware that plagiarism (the use of someone else's work without their permission and/or without acknowledging the original source) is wrong.

- I understand that the University of the Witwatersrand may take disciplinary action against me if there is a belief that this is not my own unaided work or that I have failed to acknowledge the source of the ideas or words in my writing



20/02/2020

…… …….

Hilda Nthabiseng Mashale Date

**Abstract**

The Areachap Terrane which is part of the Namaqua Sector of the Namaqua-Natal Belt in the Northern Cape Province host volcanic-hosted Zn-Cu deposits at volcanic centres. Major deposits that were mined till early 1990's include Copperton (at Prieska) and Areachap deposits. Currently, Orion mining/exploration Company is further exploring some of the best target areas including Copperton, Areachap and Kantienpan base metal occurrences.

The primary objective was to map base metal mineralisation, determine the heavy metal contents of sediments, locate the source of anomalies and delineate targets for follow-up studies. A total of 9314 stream sediments samples were collected and analysed using XRF at the Council for Geoscience laboratory. Spatial joint analysis tool was used to calculate the element associated with their respective lithostratigraphy. Fuzzy OR Overlay operation was applied to combine maps of relevant indicator elements associated with the geology.

The results for elements associated with the known base metals occurring in Prieska area as well as relevant multi-element groups were plotted on distribution maps using ArcGIS. The mineralisation target M1, M2, and M3 are delineated as potential VMS mineralisation zone and considered for further follow-up study. The M13 and M14 anomalies are delineated for Co_Ni (±Cu) mineralisation. M13 and M14 anomalies are sourced from ultramafic debris transported from the Ghaap Group, however this potential target will require follow-up studies for verification. The correlation of the Cu-Pb-Zn anomaly with alkali elements (Nb, Zr, Th, and U) and REEs (in Table 3.3) suggests there is a possibility that the M26 –M29 anomaly are alkali-granitic genetic origin. The As, Ba, Ce, Cr, Cu, Hf, Nd, Ni, Rb, Sr, S, V, Zr and Zn contents showed a heterogeneous spatial distribution, reflected by high coefficient of variation and large standard deviation; these elements concentrations are extremely elevated in stream sediments. There is a very high Cu-Zn correlation coefficient calculated for samples near the Copperton deposit. Normal Q-Q plots for S, Zn, Pb, and Ba have similar trends with outliers of the high coefficient of variations which might be sourced from the mine wastes. The high Cu, Zn and Pb are derived from the ore minerals related VMS deposits. The Fe elevated concentration are derived from both primary minerals which are not directly related to the VMS or Co_Ni (±Cu) mineralisation.

**Acknowledgements**

I acknowledge Council for Geoscience for financial contribution to this study. I extend my gratitude to S. Schalk, R. Lusunzi, M Bensid, and J.H Elsenbroek for their knowledge and help with effective utilization of the computer ArcGIS software which was used to process the data and produce all the Maps. My late daughter Lethabo Mashale (2015-2018), your strength kept me hopeful and rest assured that the Almighty is forever with us and nothing is impossible.

# Table of Content

Declaration ..... 2

Abstract ..... 3

Acknowledgements ..... 0

List of Figures ..... 2

List of Table ..... 3

Appendix ..... 3

**CHAPTER 1 ..... 4**

**Introduction ..... 4**

1.1 Background ..... 4

1.2 Research statement ..... 5

1.3 Justification ..... 6

1.4 Objectives of the Study ..... 6

1.5 Hypothesis ..... 6

**CHAPTER 2 ..... 7**

**Geological Setting ..... 7**

2.1 Regional Geology ..... 7

2.2 Local Geological Settings. ..... 11

2.2.1 The Areachap Terrane ..... 11

2.2.2 The Kaaien Terrane ..... 13

2.2.3 The geology of 2922 Prieska sheet on ArcGIS ..... 15

2.2.3.1 Kalahari Group ..... 17

2.2.3.2 Dwyka Group ..... 17

2.2.3.3 Waterkop Suite ..... 17

2.2.3.4 Jacomynspan Formation ..... 17

2.2.3.5 Spioenkop Formation ..... 17

2.2.3.6 Groblershoop Formation ..... 17

2.2.3.7 The Olifantshoek Supergroup ..... 18

2.2.3.8 Ghaap Group ..... 19

2.2.3.9 Marydale Group ..... 20
2.3 Exploration History ..... 22
2.3.1 The Economic geological work done in the study area. ..... 22
2.3.1.1 The main Prieska Ore body ..... 22
**CHAPTER 3 ..... 24**
**Methodology ..... 24**
3.1 Desktop Study ..... 25
3.2 Fieldwork ..... 25
3.3 Laboratory Work ..... 25
***3.3.1 Drying and Milling*** ..... 25
***3.3.2 Sample Analysis*** ..... 25
3.3.3 Quality Control and Quality Assurance ..... 26
3.4 Data Processing and Evaluation ..... 28
3.4.1 Statistical Data Analysis ..... 28
**CHAPTER 4 ..... 34**
**Data presentation and interpretation ..... 34**
4.1 Univariate Stream Sediment Geochemistry ..... 34
4.1.1 Barium (Ba) ..... 34
4.1.2 Cobalt (Co) ..... 36
4.1.3 Copper (Cu) ..... 38
4.1.4 Molydenum (Mo) ..... 39
4.1.5 Lead (Pb) ..... 41
4.1.6 Uranium ..... 43
4.1.7 Vanadium (V) ..... 44
4.1.8 Zinc (Zn) ..... 46
4.1.9 Sulphur(S) ..... 47
4.1.10 Nickel (Ni) ..... 49
4.1.11 $Fe_2O_3$ (%) ..... 50
4.2 Normal Quantile-Quantile plots ..... 52
4.3 Stream Sediment Exploration Target generation: Geology and Economic geology synthesis Map of Prieska area. ..... 53
4.3.1 Spioenkop Formation ..... 54
4.3.2 Ongeluk lava Formation ..... 55
4.3.3 Brulsand ..... 57
4.4 Stream Sediment Exploration Target generation: Economic geology synthesis Map of Prieska area ..... 58

4.4.1 Cu_Zn index for VMS deposit ..... 58
4.4.2 Ni_Co_Cr for the ultramafic Ni_Cr (±Cu) deposit ..... 59
4.4.3 Zr_Nb_U_Th_Hf_Ta for the heavy mineral deposits ..... 60
**CHAPTER 5 ..... 62**
**Conclusions and Recommendations ..... 62**
**5.1 Recommendations** ..... 63
References ..... 64
Appendices ..... 68

**List of Figures**

Figure 1.1: The Map of different terranes in the Namaqua Sector. (Duchesne et al., 2007) ..... 5
Figure 2.1: a) The NNMP stretching from Namibia to the Tugela Valley and b) The Tectono-stratigraphic position of the Namaqua sector of the NNMP. : GT= Groothoek Thrust; OT = Onseepkans Thrust; PSZ = Pofadder Shear-zone; HRT = Hartbees River Thrust; BRSZ = Buffels River Shear-zone; NSZ = Neusberg Shear-zone; BoSZ = Boven Rugzeer Shear-zone; BSZ = Brakbos Shear-zone; DT= Dabeep Thrust. ..... 8
Figure 2.2: The composite stratigraphic column across the Kaapvaal, from Thabazimbi through Vryburg to Prieska (Almond, 2018). ..... 10
Figure 2.3: The Map illustrating the Areachap Group volcanic centres Lithostratigraphy (after Cornell et al., 2006 and references therein). ..... 12
Figure 2.4: The Map illustrating the Lithostratigraphy of the Kaaien Terrane and Kheis Province (van Schijndel et al., 2019). ..... 14
Figure 2.5: Geological Setting of the 2922 Prieska Map sheet (CGS ArcGIS database, 2020). ..... 16
Figure 2.6: The stratigraphy of the Olifantshoek Supergroup. (Cornell et al., 2016). ..... 18
Figure 2.7: The Lithostratigraphy of the upper Transvaal Supergroup as preserved in the Griqualand West basin (Gumsley, A. 2017). ..... 19
Figure 2.8: The 2922 Prieska map illustrating the lithostratigraphy from the Maritzdam Granite to the Copperton Formation. (Modified after Anhaeusser, 2019). ..... 21
Figure 2.9: A simplified architecture of the Copperton deposit as related to a model of a biomodal felsic type of VMS deposit. (Bailie and Gutzmer, 2011 and reference therein; Theart et al., 1989). ..... 23
Figure 3.1 Flow chart indicating methods and procedures applied during the study. ..... 24
Figure 4.1.1 a) Histogram frequency distribution showing the skewness and Kurtosis of Ba (ppm) dataset, b) The Regional geochemical distribution map illustrating the location of Ba (ppm) anomalies. ..... 35
Figure 4.1.2 a) Histogram frequency distribution showing the skewness and Kurtosis of Co (ppm) dataset, b) The Regional geochemical distribution map illustrating the location of Co (ppm) anomalies. ..... 37
Figure 4.1.3 a) Histogram frequency distribution showing the skewness and Kurtosis of Cu (ppm) dataset, b) The Regional geochemical distribution map illustrating the location of Cu (ppm) anomalies. ..... 38
Figure 4.1.4 a) Histogram frequency distribution showing the skewness and Kurtosis of Mo (ppm) dataset, b) The Regional geochemical distribution map illustrating the location of Mo (ppm) anomalies. ..... 40
Figure 4.1.5 a) Histogram frequency distribution showing the skewness and Kurtosis of Pb (ppm) dataset, b) The Regional geochemical distribution map illustrating the location of Pb (ppm) anomalies. ..... 42
Figure 4.1.6 a) Histogram frequency distribution showing the skewness and Kurtosis of U (ppm) dataset, b) The Regional geochemical distribution map illustrating the location of U (ppm) anomalies. ..... 43
Figure 4.1.7 a) Histogram frequency distribution showing the skewness and Kurtosis of V (ppm) dataset, b) The Regional geochemical distribution map illustrating the location of V (ppm) anomalies. ..... 45
Figure 4.1.8 a) Histogram frequency distribution showing the skewness and Kurtosis of Zn (ppm) dataset, b) The Regional geochemical distribution map illustrating the location of Zn (ppm) anomalies. ..... 46
Figure 4.1.9 a) Histogram frequency distribution showing the skewness and Kurtosis of S (ppm) dataset, b) The Regional geochemical distribution map illustrating the location of S (ppm) anomalies. ..... 48
Figure 4.1.10 a) Histogram frequency distribution showing the skewness and Kurtosis of Ni (ppm) dataset, b)

The Regional geochemical distribution map illustrating the location of Ni (ppm) anomalies. ..... 49
Figure 4.1.11 a) Histogram frequency distribution showing the skewness and Kurtosis of Fe2O3 (ppm) dataset, b) The Regional geochemical distribution map illustrating the location of Fe2O3 (ppm) anomalies ..... 51
Figure 4.2: Normal Q-Q plots for data after none transformation, in order to preserve symmetry for the expected values (y-axis) negative values (observed values) on the x-axis are included. ..... 52
Figure 4.3.1: Fuzzy OR overlay multi-element map index of Cu, Ga, Zn, and Rb ..... 54
Figure 4.3.2: the Fuzzy OR overlay multi-element map index of Co and Ni ..... 56
Figure 4.3.3: the Fuzzy OR overlay of Mo, Nb, Sc, Ta, and U ..... 57
Figure 4.4.1: the Fuzzy OR overlay map for Cu_Zn index. ..... 58
Figure 4.4.2: the Fuzzy OR overlay map for Ni, Co and Cr index. ..... 59
Figure 4.4.3: the Fuzzy OR overlay of Zr_Nb_U_Th_Hf_Ta ..... 61

**List of Table**

Table 1: Summary of tectonic subdivisions and their geological features of The Namaqua Metamorphic Province (Eglington, 2006). ..... 9
Table 3.1. The lower limit of detection (LLD) of each element and the reference material obtained results. .... 27
Table 3.2.The Average abundance of relevant element in the continental crust ..... 30
Table 3.3. The Correlation matrix showing the correlation between elements from negative correlation to very strong positive correlation. ..... 32
Table 4.3: Elements relative or in association to the lithostratigraphic unit ..... 53

**Appendix**

*Appendix 1: XRF and its principles.* ..... 68
*Appendix 2: The mean statistics of the each element relative or in association to the lithostratigraphic unit* .... 69
*Appendix 3: The descriptive statistics on geochemistry data of the Prieska area, and box plot.* ..... 72
*Appendix 4. The box plot of high coefficient of variation.* ..... 74

# CHAPTER 1

# Introduction

## 1.1 Background

The Republic of South Africa (RSA) is known to be among one of the world's most active mining countries. RSA hosts several deposits such as gold in the Witwatersrand basin, diamonds in Kimberly, platinum group elements (PGE) in the Bushveld Complex and manganese in the Griqualand West Basin, all of which contribute to the economy of the country (Bokana, 2015). The Namaqua Sector of Namaqua- Natal Metamorphic Province (NNMP) is the remarkable mineralised sector in the country hosting the Copperton deposit, which according to Cornell et al., (1986), and Bailie and Gutzmer (2011) is one of the world's giant Volcanogenic Massive Sulphide (VMS) deposits.

The Namaqua-Natal Metamorphic Province is a tectono-stratigraphic province that stretches 1 400 km across South Africa. It is made up of Namaqua Sector which outcrops in the Northern Cape Province and Natal Sector which outcrops in Kwa-Zulu Natal. The NNMP is characterised by igneous and metamorphic rocks formed or metamorphosed during the Namaqua Orogeny at 1200 Ma - 1000 Ma (Cornell *et al.,* 2006). It is 400 km wide and has borders with the Kaapvaal Craton to the north and Pan-African (Gariep and Saldana) belts in the west and south (Cornell *et al.,* 2006; Fransson, 2008).

The Namaqua Sector of the Namaqua-Natal Province is divided into a number of distinct, discontinuity-bounded domains: Richtersveld Subprovince, Bushmanland Subprovince, Gordonia Subprovince, and Kaaien Terrane (Figure 1.1). The locality of the study area is in the western degree of the 2922 Prieska sheet, Northern Cape Province, South Africa. The study area of this research covers the Areachap terrane, Kaaien terrane and Griqualand West basin on the Kaapvaal Craton.

Geochemical data combined with mineralogical and other additional data sets such as geological maps, mineral distributions, geophysical data, amongst others, provide a foundation for classifying and evaluating the mineral resource endowment and natural hazards. A mineral resource produces diagnostic textural, geological, geophysical, and geochemical signatures when exposed at or near the surface of the Earth. Geochemical exploration is based on outlining such dispersion halos and in the present study that will be done by chemical analyses of stream-drainage sediments.

There is a difference between regional and detailed surveys in terms of objective, size of area being surveyed, sampling density, and type of material sampled. Ginzburg (1960) recognised three scales of geochemical mapping and surveys depending on purpose and objective, namely, reconnaissance, prospecting and detailed. A regional survey can be conveniently discussed based on the number of stream sediment samples taken per square kilometres (Bradshow *et al.,* 1972).

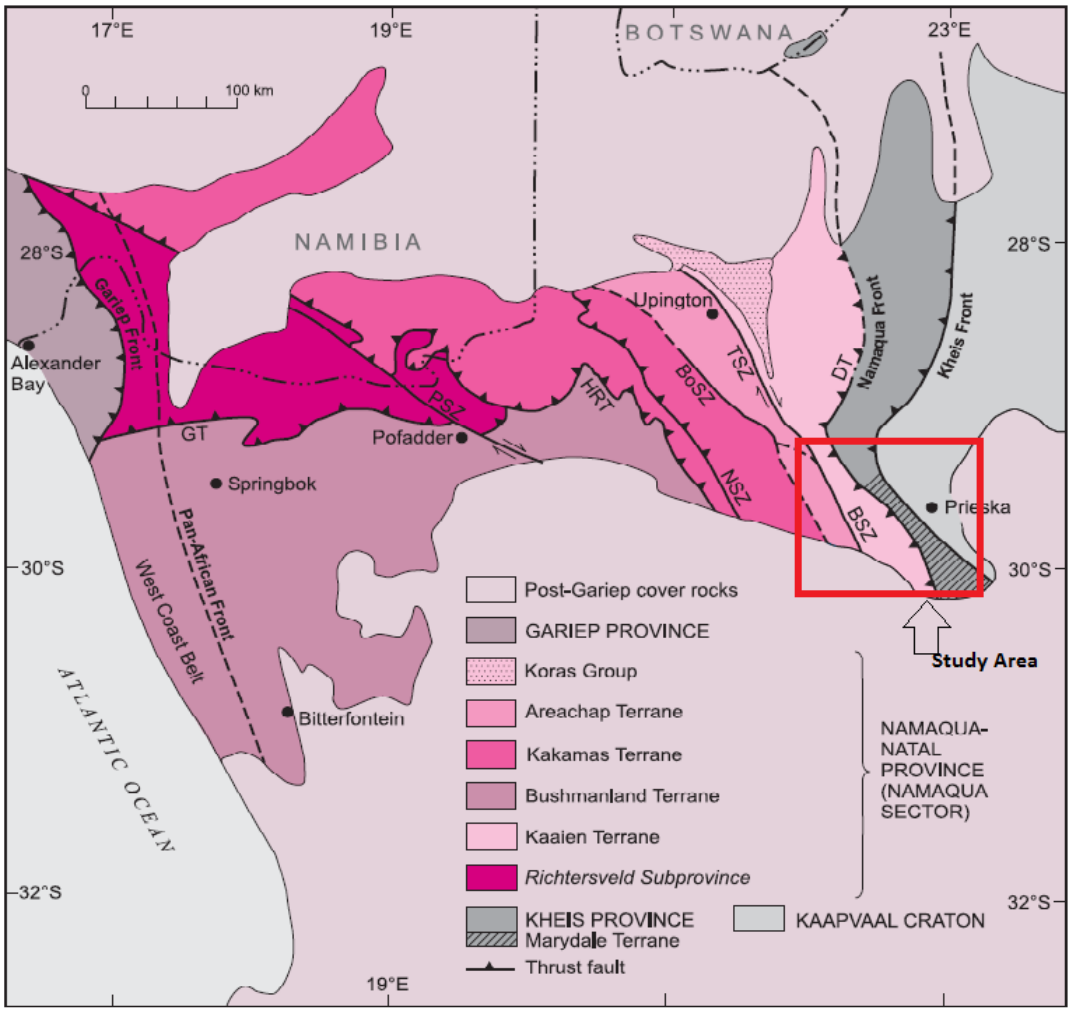



**Figure 1.1: The Map of different terranes in the Namaqua Sector. (Duchesne et al., 2007)**

Regional geochemical mapping has been part of the core mapping function of the Council for Geoscience (CGS) since the 1970s. The regional geochemical mapping programme followed a systematic approach focussed on providing high quality- and high density datasets that will contribute to resolving issues relevant to a modern South African geological society, namely, exploration, geological mapping, groundwater, environmental studies, and geological modelling. The principal objective of this geochemical orientation survey is to define the patterns of primary and secondary dispersion occurring in the study area particularly those of economically interesting elements. During the 1986 the stream sediment sample collection was conducted in the Prieska area and the analysis of the samples took place during 2004 and 2005 at the Council for Geoscience Laboratory. The geochemical dataset is used in this report to map the VMS mineralisation potential.

### 1.2 Research statement

The regional geochemical survey was conducted to study the chemical element distribution patterns in order to better understand the geochemistry of stream sediments in relation to the underlying geology of the 2922 Prieska Map sheet. The survey was standardised by taking one stream sediment sample per square kilometre. Numerous deposits had been discovered by stream sediments programmes

worldwide, one of the examples is the discovery of Wolitu Pb-Zn deposit through stream sediments geochemical prospecting by Yang *et al.* (2017).

### 1.3 Justification

The geochemical patterns obtained from this study are used to link element deficiencies and abundances with the underlying geology, structures, known mineral occurrences and mines. This will assist in tracing the source of anomalies encountered in stream sediments and delineate targets for follow-up studies within the Orange River catchment area.

### 1.4 Objectives of the Study

The main objective of this study is to determine the back ground values of each chemical element in the stream sediment on its associated lithology in order to map the VMS mineralisation potential in the Prieska area. This will enable the recognition of anomalies within the catchment area and has the potential to trace their sources.

The following specific objectives need to be met:

- To determine the background values of each chemical element geochemistry in the stream sediments in the study area;
- To determine heavy metals content of the sediments;
- To map the element anomalies to locate the source and delineate targets for verification and follow-up studies.

### 1.5 Hypothesis

- That the geochemical anomalies of the sediments in the Orange River can be determined;
- Targets for follow up studies can be delineated;
- That the sources of resulted anomalies within the Orange River catchment can be traced.

# CHAPTER 2

# Geological Setting

## 2.1 Regional Geology

The study area is the western degree of 2922 Prieska Map sheet. The study area consists of four terranes, which are the Areachap Terrane, the Kaaien Terrane, Kheis Province, and the Kaapvaal Craton (Cornell *et al.,* 2006). The area generally forms part of the Namaqua Metamorphic Province and the Griqualand-West Basin. The Namaqua Metamorphic Province is a tectonically distinct region that developed adjacent to the Kaapvaal Craton, approximately between 2.0 and 1.0 Ga. The Namaqua Metamorphic Province is truncated by the Neoproterozoic Gariep belt. The Kheis Belt intervenes along the west and northwest margins of the Kaapvaal Craton (Dewey *et al.,* 2006).

The Namaqua Metamorphic Province consists of mid- to lower-crustal igneous and high-grade metamorphic rocks in a belt that extends for more than 1 500 km across southern Africa and attains a maximum width in excess of 500 km (McCourt *et al.,* 2006). The Namaqua Metamorphic Province is exposed to the west- and east coast of southern Africa and in the central parts of South Africa. It is covered by Karoo basin sedimentary rocks in the central South Africa (Cornell *et al.,* 2006). The Namaqua Metamorphic Province consists of three main components: 1) The reworked ~ 2000 ma Kheisian rocks; 2) The juvenile supracrustal and plutonic rocks that formed during 1600 to 1200 Ma rifting, ocean spreading and subduction phases of the Namaqua Wilson cycle; and 3) voluminous syn- and post-tectonic granitoids (Cornell *et al.,* 2006) .

The Namaqua Metamorphic Province consists of a number of shear zone-bound provinces and terranes (summarised in Table 1) that were juxtaposed and assembled during the Namaqua Orogeny from 1100-1020 Ma (Cornell *et al.,* 2006; Diener *et al.,* 2012). The Richtersveld and Bushmanland Subprovince are comprised of a micro-continent that collided with the margin of the Kaapvaal Craton during the 1.2 to 1.0 Ga Namaqua Orogeny (Figure 2.1). The Gordonia Subprovince separates the Kaapvaal Craton to the Bushmanland Subprovince (Cornell *et al.,* 2006). The Gordonia Subprovince contains a central domain of volcano-sedimentary amphibolite to granulite grade rocks (Cornell *et al.,* 2006). The Kheis Subprovince to the immediate east of the Gordonia Subprovince; consists of thick quartzitic and arenitic meta-sedimentary rocks (Cornell *et al.,* 2006).

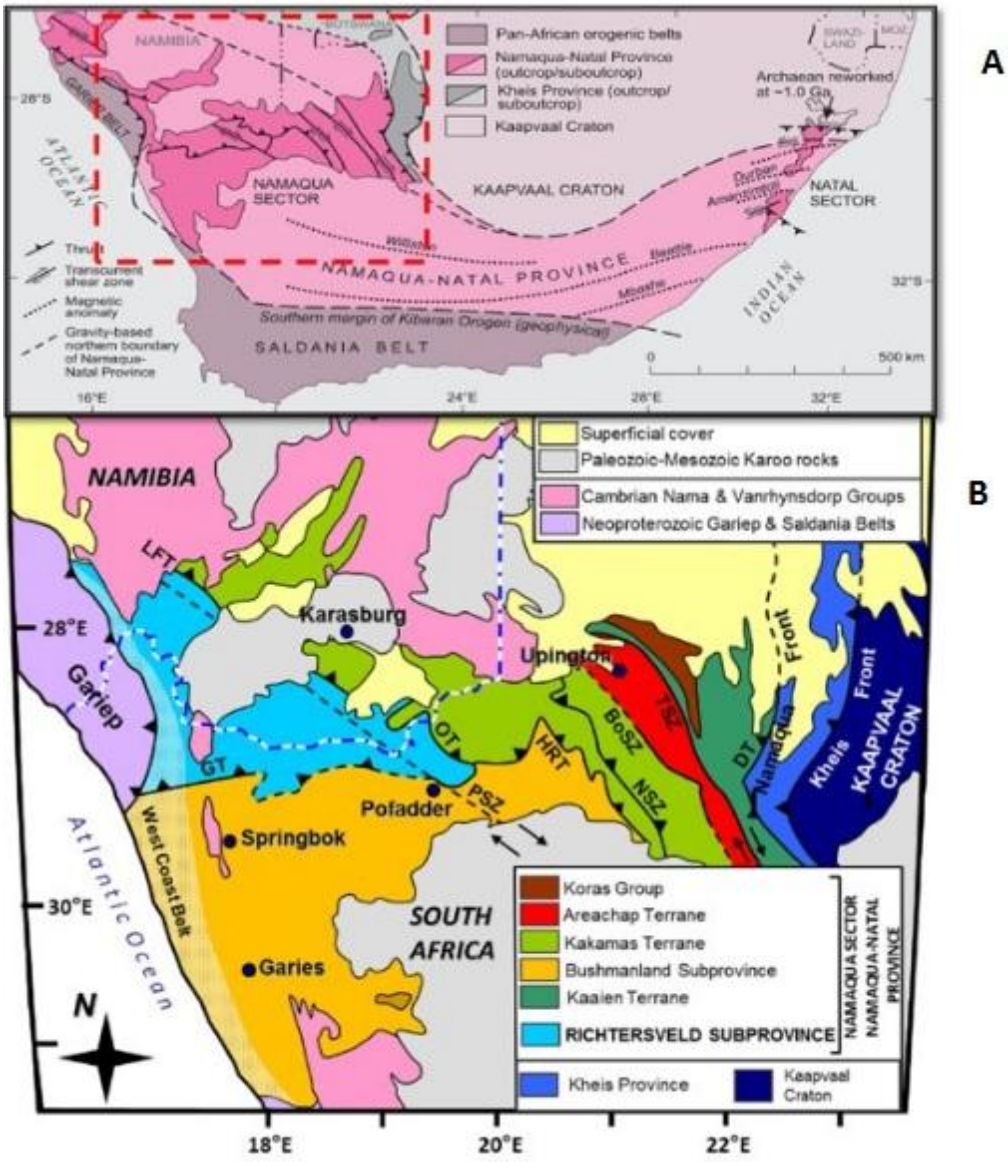



**Figure 2.1: a) The NNMP stretching from Namibia to the Tugela Valley and b) The Tectono-stratigraphic position of the Namaqua sector of the NNMP. : GT= Groothoek Thrust; OT = Onseepkans Thrust; PSZ = Pofadder Shear-zone; HRT = Hartbees River Thrust; BRSZ = Buffels River Shear-zone; NSZ = Neusberg Shear-zone; BoSZ = Boven Rugzeer Shear-zone; BSZ = Brakbos Shear-zone; DT= Dabeep Thrust.**

Table 1: Summary of tectonic subdivisions and their geological features of The Namaqua Metamorphic Province (Eglington, 2006).

| Sub-province | Terrane | Major geological features |
|---|---|---|
| Richtersveld | Not subdivided | Calc-alkaline lavas, and granitoids, thrust southwards over the Aggeneys terrane along the Groothoek thrust boundary with the Kakamas terrane. Richtersveld is bound by the Onseepkans Thrust (Moen and Toogood, 2007), synonymous with the Hartebees River Thrust. |
| Bushmanland | Aggeneys | Para- and ortho-gneisses, metavolcanics and granites. Significant stratiform mineralization. Several phases of deformation, including early S-verging recumbent folds and thrust and late NW dextral shear zones. |
| | Okiep | Para- and ortho-gneisses, voluminous granites and charnockites. Significant Cu mineralisation associated with steep structures. Several phases of deformation, including early-S-verging recumbent folds and thrusts and late NW dextral shear zones. Boundary with the Gariep terrane occurs at the Buffels River shear zone. Poorly defined boundary with the Aggeneys terrane. Para- and ortho-gneisses, voluminous granites and charnockites. |
| | Gariep | Several phases of deformation. Southern boundary not known. |
| Gordonia | Kakamas | High-grade supracrustal gneisses, charnockites and granites. Early SW-verging thrust and late NW, dextral shear zones. Boundary with the Areachap terrane is defined by the BSZT. Transitional zone between high-grade gneisses of the Kakamas terrane and low-grade metasediments and metavolcanics of the Kheis sub-province. NE-verging folding and thrusting, late NW dextral shearing. Boundary with the Kheis sub-province is defined by the Brakbosch and Trooilapspan shear zone and faults |
| | Areachap | |
| Kheis | Not Subdivided | Thin-skinned fold and thrust belt. Quartzite, phyllite and meta-basalt. Eastern limit of the Kheis Subprovince is the Dabep Fault. |

The Kaapvaal Craton hosts the Archaean to Palaeoproterozoic sedimentary successions that were deposited between 3 105 Ma and 1 700 Ma (Bumby *et al.,* 2012). The younger sedimentary sequences either outcrops on the margin of the Kaapvaal Craton or are underlain by orogenic belts off the edge of the craton (Moore *et al.,* 2001; Bumby *et al.,* 2012). The Kaapvaal Craton underlies most of the northern part of South Africa,

Swaziland and the eastern portion Botswana (Figure 2.1a). It is considered to be one of the most stable and long-lived examples of continental crust (Moore *et al.,* 2001; Summer and Beukes, 2006).

The Kaapvaal Craton hosts major Precambrian-aged basins which were deposited between the 3105 Ma (Dominion Group) and the 1700 Ma (Waterberg Group). These basins include Archaean Witwatersrand- , the Ventersdorp-, the Transvaal Sequence-, Griqualand-west- and the Waterberg Basins. The study area of the research covers the southern portion the Griqualand-West Basin near the Prieska area (Figure 2.1 ), the Kaaien terrane and the Areachap terrane, Northern Cape Province, South Africa (Moore *et al.,* 2001; Summer and Beukes, 2006). The Griqualand-West sediments were deposited in three major tectono-sedimentary environments, a shallow water platform, a platform edge and a deeper basin to the west and southwest of the continent (Bumby *et al.,* 2012). These environments correspond stratigraphically to the Schmidtsdrif Formation, the limestone and chert of the Ghaap Plateau Formation and Asbesberge Formation Jaspilite respectively (see Figure 2.2) (Moore *et al.,* 2001; Greyling *et al.,* 2001, Summer and Beukes, 2006). The Griqualand West basin is subdivided into the Ghaap Plateau and Prieska sub-basins. The Ghaap Group is additionally subdivided into the Schmidtsdrif, Campbell Rand, Asbestos Hills and Koegas Subgroups (in stratigraphic order) (Truswell, 1990; Turner, 1992; Greylings *et al.,* 2001; Moore *et al.,* 2001).

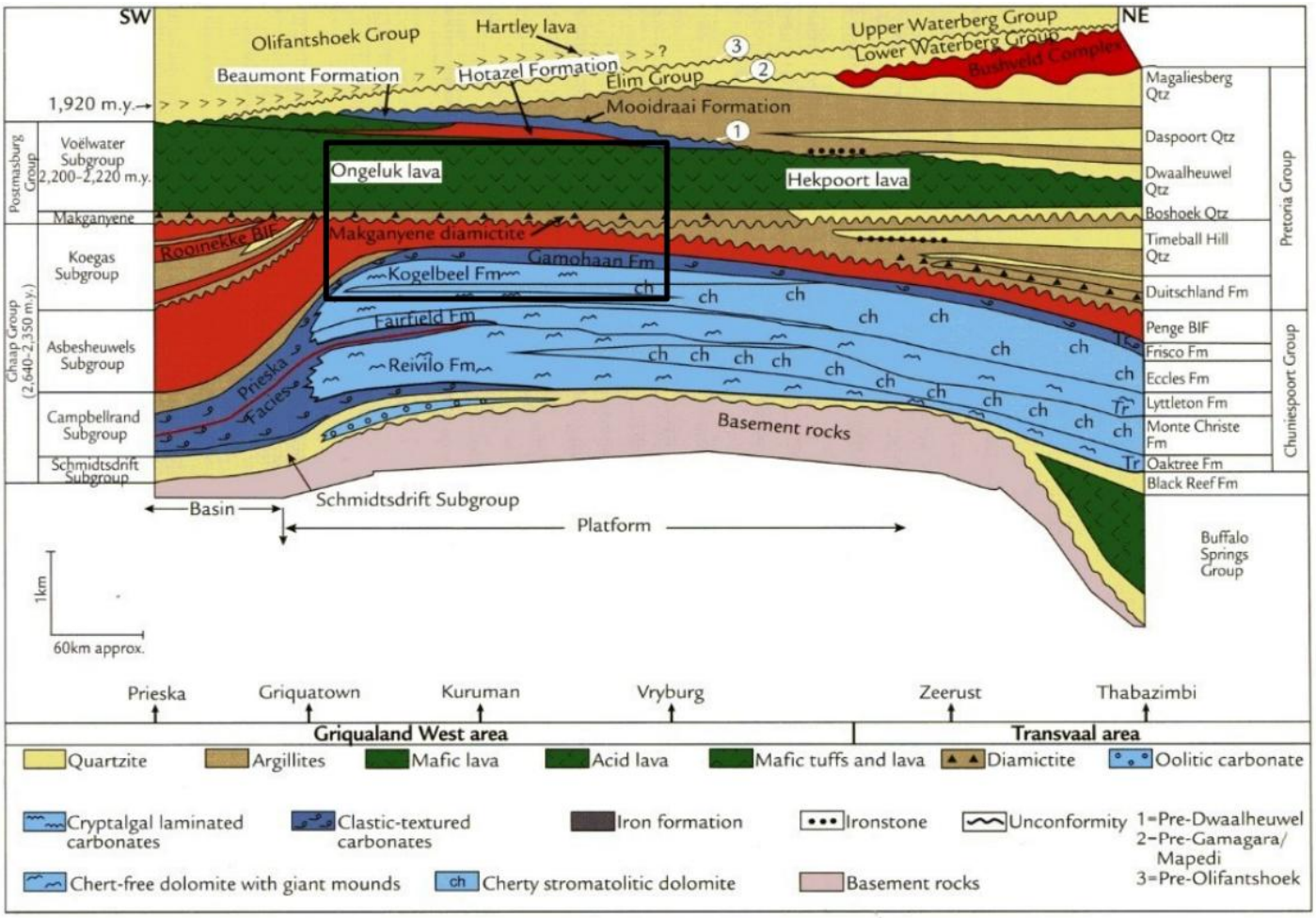



**Figure 2.2: The composite stratigraphic column across the Kaapvaal, from Thabazimbi through Vryburg to Prieska (Almond, 2018).**

## 2.2 Local Geological Settings.

### *2.2.1 The Areachap Terrane*

The Areachap Terrane comprises of Areachap Group and the Keimoes Suite, overlies the Kaaien Terrane along the Brakbosch-Trooilapsan Shear Zone (BTSZ) and is sandwiched between the Kaaien and the Kakamas Terrane (Figure 2.1). The Areachap terrane consists of only juvenile material, of an age of ~1 300 Ma (Cornell *et al.,* 2006). Some of the alkaline and mafic bodies in the terrane were metamorphosed to amphibolite-grade (Cornell *et al.,* 2006). It comprises metabasics and intermediate supracustal gneisses in a NNW-trending belt, granitoids intrusions of the Keimoes Suite, volcanic rocks and volcanogenic ore deposits (Cornell *et al.,* 2006). Some massive sulphide ores containing pyrites and pyrrhotite have been mined (Eglington, 2006; Cornell *et al.,* 2006; Fransson, 2008). It is characterised by the Besshi-type massive sulphides and metavolcanic components (Cornell *et al.,* 2006; Fransson, 2008). Other geological features are summarised in Table 1.2. The Prieska Cu-Zn mine at Copperton and old Areachap mine are situated within the Areachap Terrain (Eglington, 2006; Cornell *et al.,* 2006; Fransson, 2008).

The Areachap Group is an island arc; its succession contains numerous Zn-Cu deposits of varying size and economic significance along its exposed strike length of ~280 km (Bailey *et al.,* 2007). Based on Geringer et al. (1994), the Areachap Terrane consists of four volcanic centres (refer to figure 2.3), namely the Copperton, Boksputs-, Vanwykspan, Kleinbegin, and Upington centres, each distinguished according to the volcanism and type of sediment occurring within them. The general type of sediment units are a variety of gneisses occurring with calc-silicate and banded iron formations. The suggested succession is presented in the figure 2.3 below.

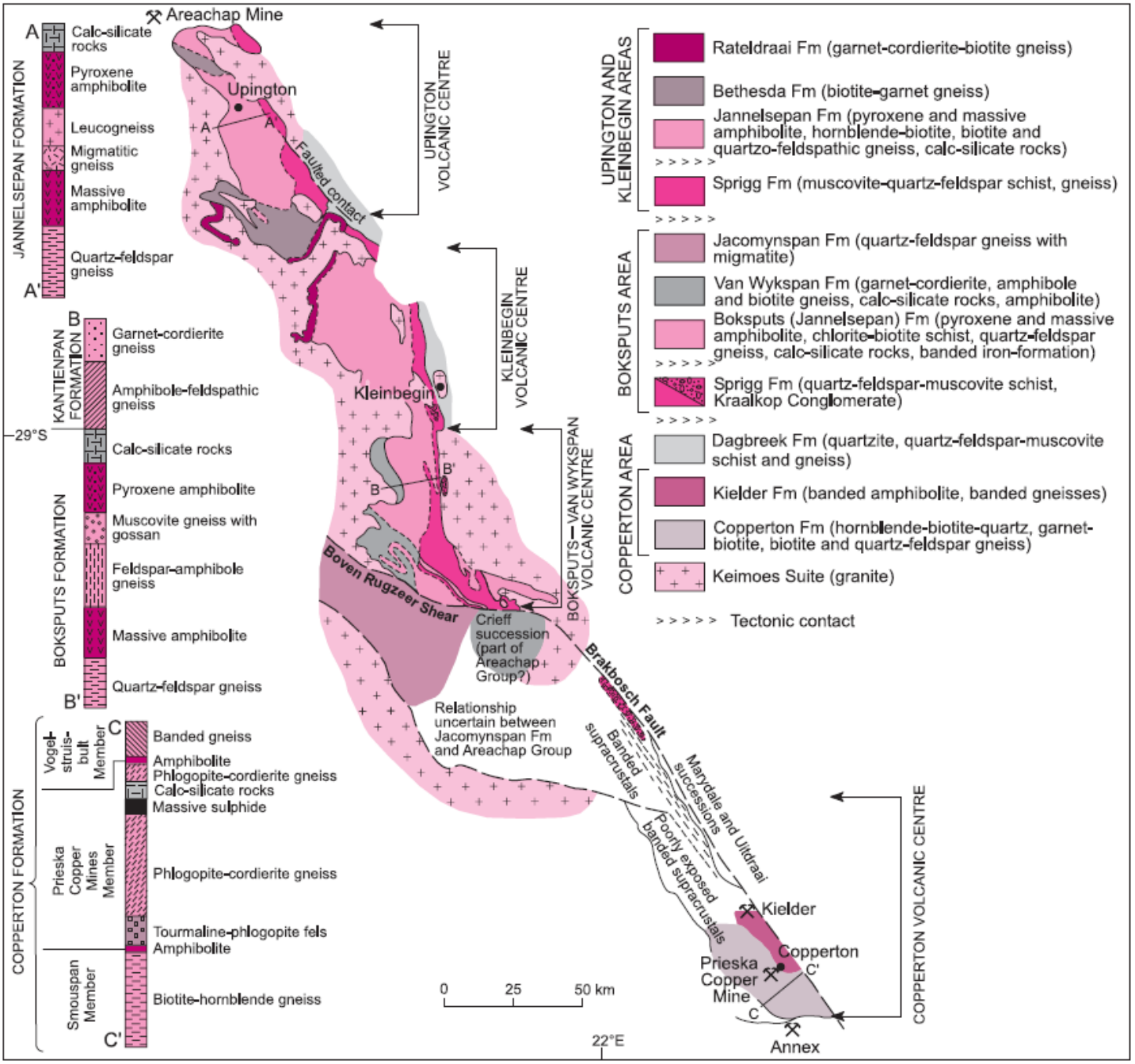



**Figure 2.3: The Map illustrating the Areachap Group volcanic centres Lithostratigraphy (after Cornell et al., 2006 and references therein).**

The Copperton Formation comprises three members (Figure 2.3), the Smouspan Gneiss Member, the Prieska Copper Mines Member and the Vogelstruisbuilt Member (Humphreys, 1985; Ghavami-Riabi, 2006, Cornell *et al.,* 2006; Fransson, 2008). The Copperton Formation is partly obscured in many places by the Dwyka Group tillite cover which thickens southwards (Figure 2.5) (Cornell, 2019).The Smouspan Gneiss Member consists mainly of a biotite-hornblende-quartz-plagioclase gneiss; this Member forms the base of the Copperton Formation and it is considered to have originated as a dacitic lava (Humphreys, 1985; Ghavami-Riabi, 2006, Bumby *et al.,* 2012). The Prieska Copper Mines Member consists of peraluminous silicate rocks and hosts the massive sulphide ore of the Prieska Zn-Cu mine (Bumby *et al.,* 2012). The Prieska Copper Mines Member mainly consist of a gedrite fels, the hydrothermally altered dacite protolith of the Smouspan Gneiss Member, and a quartz-perthite-sillimanite gneiss, originating from precipitation of 53 silica, sericite and trace minerals in the basin-floor sediments close to the fumarolic vent (Bumby *et al.,* 2012). The Vogelstruisbult Member consists of tholeiitic banded hornblende gneiss of intermediate composition, laminated amphibole, originating from a basaltic lava or subaqueous tuff (Humphreys, 1985; Ghavami-Riabi, 2006, Bumby *et al.,* 2012).

The Jannelsepan rocks are juxtaposed against the Bethesda Formation, the Jannelsepan rocks comprise of pyroxene, massive amphibolite, hornblende-biotite, biotite and quartz-feldspar gneiss (refer to Figure 2.3) (Ghavami-Riabi, 2006, Oriolo and Becker, 2018). The Bethesda Formation is comprised mostly of metapelitic gneisses and biotite-muscovite schist. Rocks of the Kantienpan Formation are bounded by the Rooiputs shear to the east. Rooiputs shear occur mainly in the western portion on the farm Kantienpan and in the northern portion on the farm Van Wyks Pan (Ghavami-Riabi, 2006 and references therein). The Van Wyks Pan Formation consists dominantly of granitic-biotite gneisses and quartz-feldspar gneisses which are intercalated with thin layers of amphibole gneisses and amphibolites (Ghavami-Riabi, 2006).

### 2.2.2 The Kaaien Terrane

The Kaaien Terrane on the far east of the Namaqua Sector is surrounded by the Kheis Province, Koras Group and the Areachap Terrane (Figure 2.1) (Cornell *et al.,* 2006). It is a thick sequence of deformed quartzite forming a transition from the Kaapvaal Craton and Kheis Province to Areachap high- grade rocks (Cornell *et al.,* 2006). Based on van Schijndel (2013), the Kaaien Terrane is part of the complex suture zone between the Kaapvaal Craton, Kheis Province, Rehoboth Province and the Namaqua-Natal Province, and the Kaaien Terrane. (Cornell *et al.,* 2006; van Schijndel, 2013). The Kaaien Terrane is the area between the Dabep thrust and Brakbosch Fault which extends into the Trooilapspan Shear Zone (Cornell *et al.,* 2006) as shown in Figure 2.1.

The Kaaien Terrane is characterised by highly metamorphosed sedimentary formations in different areas and different types of low-grade metamorphosed sediments, which are mostly covered by the grey gneissic granite (Miller, 2012; Cornell *et al.,* 2006). The granite in the terrane is covered with patches of granulites and schists (de Villiers and Sohnge, 1959; Cornell *et al.,* 2006). Some formations in the terrane show severe folding and major faulting, i.e. in Rosyntjiebos Formation (de Villiers and Sohnge, 1959; Cornell *et al.,* 2006). The lithologies in the area are white quartzite alternating with schists, chlorite schists, muscovite granite, grey gneissic granite of different sizes and shapes, gneisses and the quartzite and the schists correlate with the Stinkfontein Formation (Cornell *et al.,* 2006). The Kaaien Terrane (Figure 2.4) is characterised by quartzite and quartz-mica schist called the Kaaien Series, which is subdivided into several formations and units (Cornell *et al.,* 2006; Miller, 2012; Oriolo and Becker, 2018). The Groblershoop Formation consists of quartz-muscovite schist and schistose quartzite that is up to ~ 2000 m thick. The Bokpoort Member near Groblershoop consists of garbenschiefer schists with a complex mineralogy with poikiloblastic garnet and subhedral hornblende and white mica (Cornell *et al.,* 2006; Miller, 2012; Oriolo and Becker, 2018).

The Kaaien Terrane consists of meta-quartzites and quartz-mica schist in the Brulpan and Vaalkoppies group and meta-volcano-sedimentary sequence of the Wilgenhoutsdrif Group, with mafic to felsic intrusions (Figure2.4). The Koras Group (Figure 2.4) unconformably overlies all the units (Petterson *et al.,* 2009). According to the Sm-Nd dating studies conducted by Petterson *et al.,* (2009) the Kaaien Terrane shows a dominance of Sm-Nd model ages between 1.98 and 1.57 Ga (Oriolo and Becker, 2018).

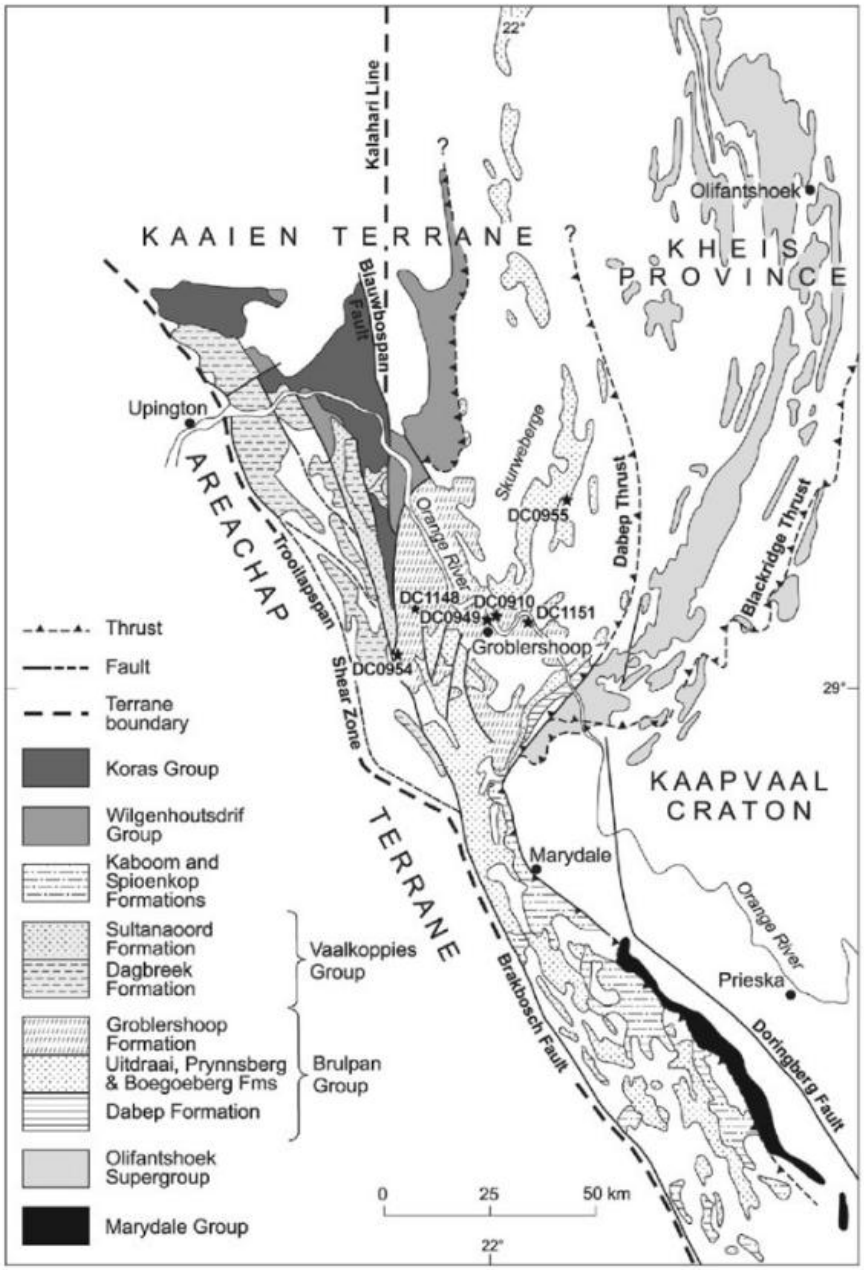



**Figure 2.4: The Map illustrating the Lithostratigraphy of the Kaaien Terrane and Kheis Province (van Schijndel et al., 2019).**

### 2.2.3 The geology of 2922 Prieska sheet on ArcGIS

The geology map retrieved from the CGS database, was compiled on ArcGIS software (Figure 2.5). The area is comprised of the Transvaal Sequence, Olifantshoek Supergroup, Kaaien Terrane, Areachap Group and Karoo Supergroup. The Transvaal Sequence is confined to the north-central part of the Kaapvaal Craton (Eriksson *et al.,* 2009). It overlies the Witwatersrand foreland basin (Supergroup) and is overlain by Bushveld Complex (Eriksson *et al.,* 2009; Eriksson *et al.,* 2001). The three basins – the Transvaal basin, and Griqualand West basin, in South Africa, and the Kanye basin in Botswana basins are preserved on the Kaapvaal Craton (Eriksson *et al.,* 2009).

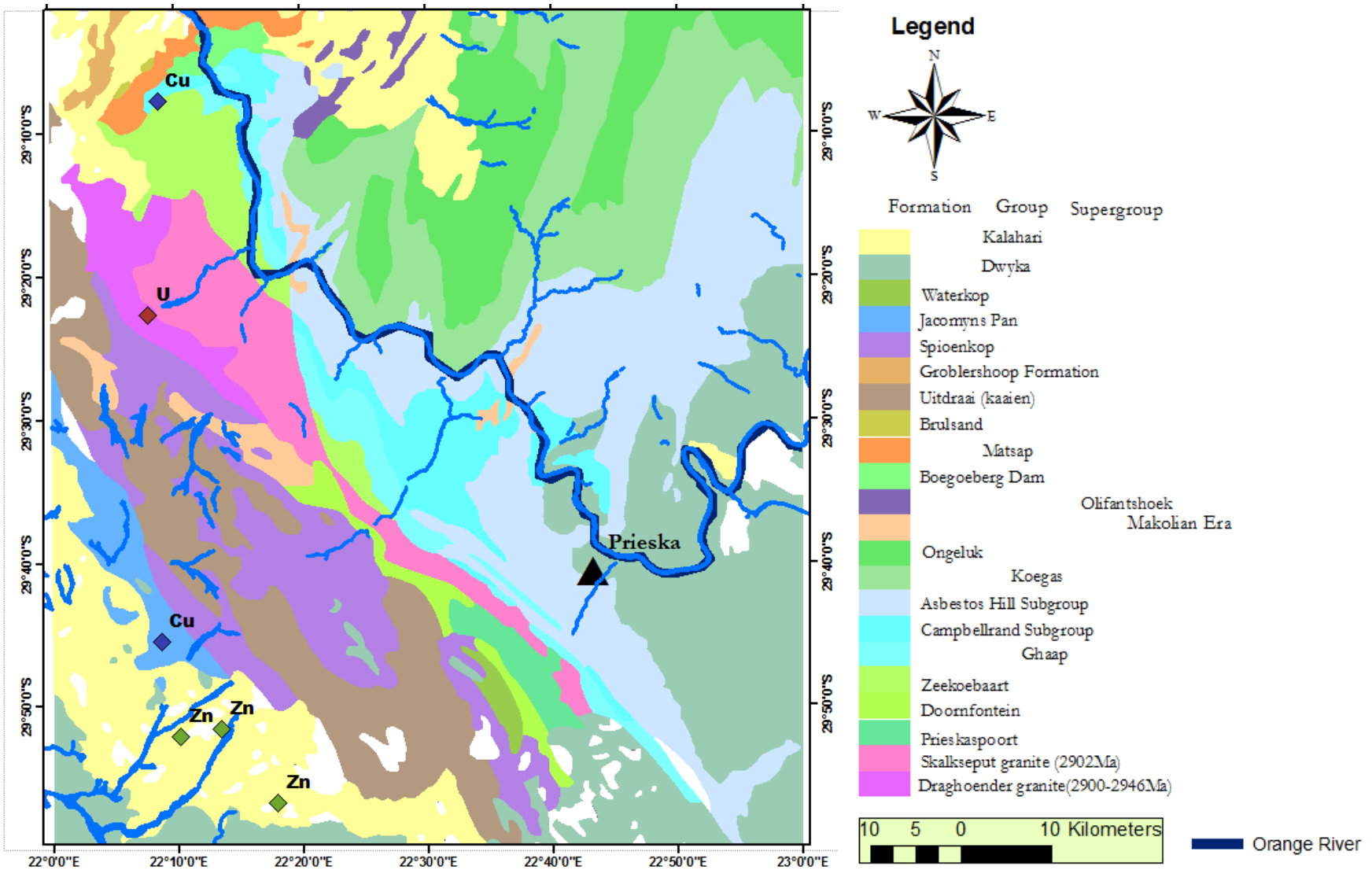



**Figure 2.5: Geological Setting of the 2922 Prieska Map sheet (CGS ArcGIS database, 2020).**

#### *2.2.3.1 Kalahari Group*

The Kalahari Group is dominated by an extensive blanket of unconsolidated sand comprising one of the largest continuous sand bodies on earth covering $2.5 \times 10^6$ km$^2$ of central southern Africa (Matmon *et al.,* 2015). Based on Puchner (2002), the Kalahari Group includes continental sedimentary strata of Quaternary alluvium and aeolian sand, terrace gravels, surface limestone and silcrete, which unconformably overlies calcified sand and gravel (Puchner, 2002). The Kalahari Group is up to 65m in thickness and unconformably overlies a 30m thick red clay layer (Puchner, 2002). Puchner (2002) further discussed that the Kalahari Group sediments are probably an aggrading fluvial fan (proximal and distal) deposit that formed as a result of epeiorogenic uplift along the Griqualand- Transvaal axis to the south of Kuruman during the Late Cretaceous period. The conglomerate layer is considered to be the basal unit of the aggrading Kalahari Group.

#### *2.2.3.2 Dwyka Group*

The Karoo Supergroup stratigraphy is divided into five groups, which are in ascending order, the Dwyka Group, Ecca Group, Beaufort, Stormberg and Drakensberg Group (Johnson et al, 2006). The Dwyka formation is made up of 1 000 m of massive and interbedded diamictites as well as deformed sandstone bodies. Most of the Dwyka rocks are interpreted as true tillites and they form the major component of the Dwyka Group (Johnson et al., 2006). According to Johnson et al.(2006), there are seven lithofacies that have been identified in the Dwyka Group, the facies include massive diamictites, stratified diamictites, massive carbonate-rich diamictites, mudrock facies, sandstone facies, mudrock with drop-stone facies and lastly conglomerate facies (Johnson et al., 2006).

#### *2.2.3.3 Waterkop Suite*

The Waterkop Suite consists of the products of several intrusive pulses, varying from jotunite, pyroxene syenite and quartz syenite to granite (Geringer et al., 1998). Waterkop Syenite is a sodalite-nepheline syenite exposed in a cutting along the Prieska-Copperton road, 18 km from Keikamspoort. The extent of the Waterkop Syenite body is unknown (Verwoerd, 1993). The Waterkop Syenite is dominated by the K-feldspar with up to 10% plagioclase and nepheline, the mafic minerals are predominantly biotite and clinopyroxene (Geringer et al., 1998). The colour variation of syenite is mainly attributed to the differences in the colour of the K-feldspar (Geringer et al., 1998).

#### *2.2.3.4 Jacomynspan Formation*

The Jacomynspan Formation is a metasedimentary sequence of quartzite, leucogneiss, amphibolite and calc-silicate. Based on Boelema (1994), Jacomynspan Formation is comprised of aluminous metapelitic gneiss with interbanded quartzite, leucocratic quarts-feldspar gneiss, amphibolite, calc-silicate and marble. Along the fault margin of the Jacomynspan Formation, there is a mafic-ultramafic sill with potential to host Ni-Cu mineralisation. The sill is locally deformed and subjected to low-grade metamorphism of which the intensity of deformation is said to be less than the host gneiss (Orion Minerals, 2018).

#### *2.2.3.5 Spioenkop Formation*

Spioenkop Formation, a metamorphosed sedimentary unit in the highly deformed zone was previously considered to be part of the 3.0 Ga Marydale Group (Humphreys et al., 1988; Hillard, 1999). Scott(1987) suggested that the Spioenkop Formation is part of the Kaaien Group (Scott, 1987; Hillard, 1999), whilst SACS(1980) interpreted the Spioenkop Formation to be part of the Namaqua Metamorphic Province with a Mokolian metamorphic age (2 070 – 1 180 Ma). The Spioenkop Formation consists of quartzite, quartz-mica schist, quartz-feldspar gneiss and amphibolite (Hillard, 1999).

#### *2.2.3.6 Groblershoop Formation*

The Groblershoop Formation can be defined in general as a schistose unit. The Groblershoop Formation

occurs above the Marydale Formation and below the Kaaien Formation (Figure 2.4) (Botha, 1976; Hillard, 1999). The Groblershoop Formation comprises quartz-mica pelitic schist, micaceous quartzite and orthoquartzite with minor amounts of amphibolite and amphibolitic-schist (Hillard, 1999). The Groblershoop Formation is exposed in a synclinorium, so that duplication of individual units occur several times between the Kaaien Hills and the Langeberg Range (Botha, 1976).

### *2.2.3.7 The Olifantshoek Supergroup*

The Olifantshoek Supergroup (2 050 Ma to 1 750 Ma) overlies rocks of the Transvaal Sequence with angular unconformity. The Olifantshoek Supergroup (Figure 2.6) is subdivided into Volop Group which is further subdivided into Matsap Subgroup and Brulsand Subgroup, and its lower part is composed of the Gamara Formation & Mapedi Formation, Lucknow Formation and Hartley Formation & Boegoeberg Dam Formation (Cornell *et al.,* 2016; Land *et al.,* 2018). Brulsand Subgroup is comprised of grey and white quartzite and subordinate shale (Cornell *et al.,* 2016). Boegoeberg Dam Formation consists of Greenstone, quartz-chlorite-epidote schist, subgreywacke and conglomerate (Cornell *et al.,* 2016).

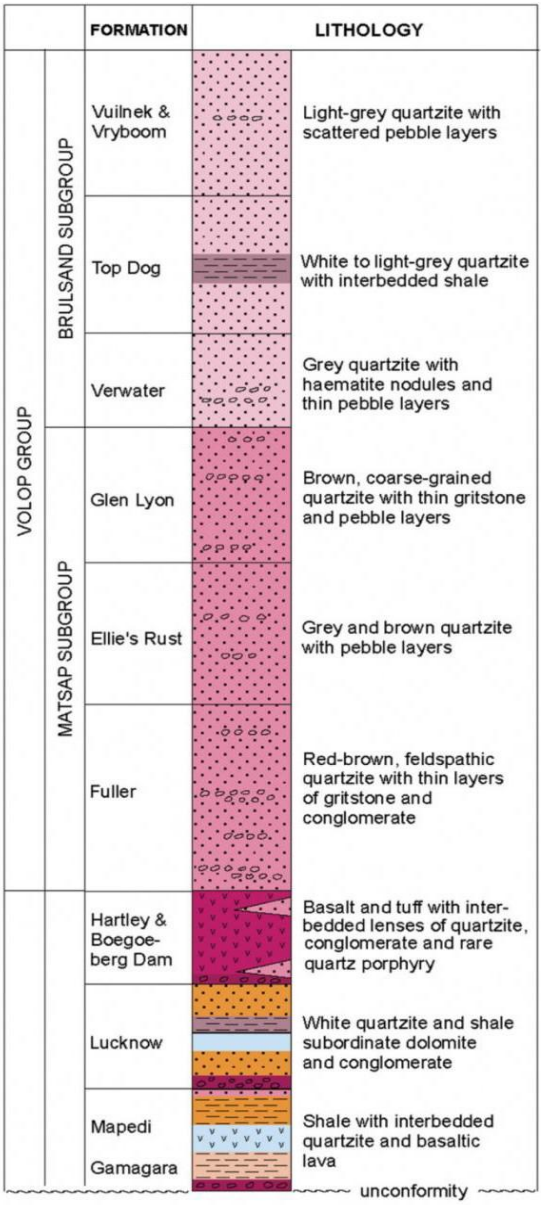



**Figure 2.6: The stratigraphy of the Olifantshoek Supergroup. (Cornell et al., 2016).**

### *2.2.3.8 Ghaap Group*

There are four subgroups of the Ghaap Group recorded from the older to the younger; Schmidtsdrif Subgroup, Campbell Rand, Asbestos Hills and Koegas Subgroup (Hilliard, 1999; Moore *et al.,* 2001; Eriksson *et al.,* 2006). This group consists predominantly of limestone, dolomite, chert, and iron-formation (Truswell, 1990). Ghaap Group is overlain unconformably by the volcano-sedimentary Postmasburg Group (Moore *et al.,* 2001) (Figure 2.7). The deposition of the Campbell Rand Subgroup occurred on a shallow-marine platform; it bounded by the Kuruman Iron Formation at its top and bounded by the Schmidtsdrif Subgroup at its base (Truswell, 1990; Moore *et al.,* 2001).

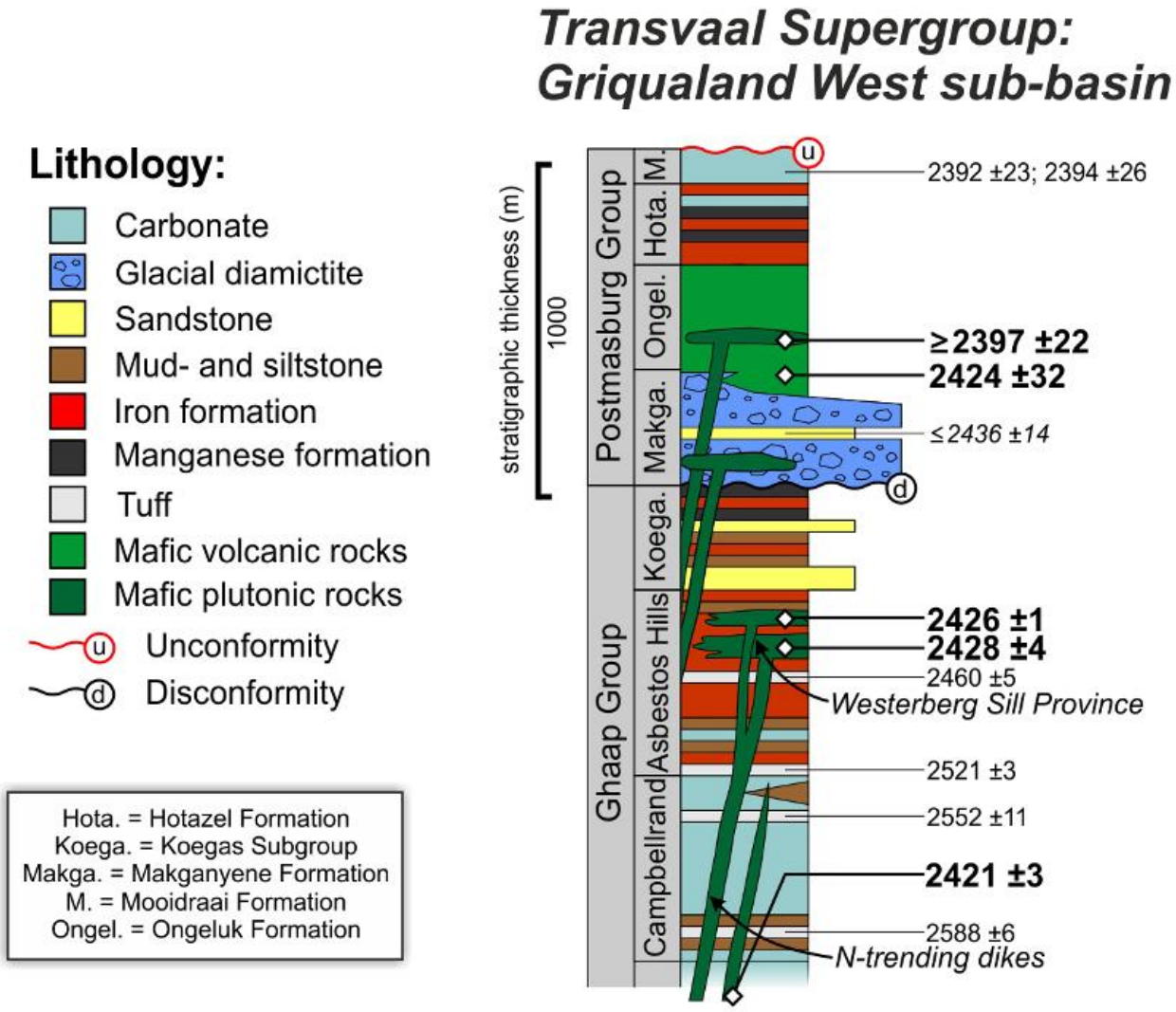



**Figure 2.7: The Lithostratigraphy of the upper Transvaal Supergroup as preserved in the Griqualand West basin (Gumsley, A. 2017).**

Campbell Rand Subgroup are characterised by thin intercalations of black shale, withlight-colouredcherty dolomite in the central section of the Subgroup (Truswell, 1990; Hilliard, 1999; Philip Nel, 2013; Moore *et al.,* 2012). The Campbell Rand Subgroup is an extensive carbonate platform. The Asbestos Hills Subgroup is a transgressive–regressive cycle of chert and banded iron formation following the drowning of the carbonate platform (Eriksson *et al.,* 2006). The younger subgroup of the four is Koegas Subgroup, which are multiple transgressive–regressive cycles along a pro-grading delta or submarine fan system (Hilliard, 1999; Moore *et al.,* 2001; Kendall, 2013).

#### *2.2.3.9 Marydale Group*

The Marydale Group occurs as a narrow belt along the south-western edge of the Kaapvaal Craton (Figure 2.1) (Potgieter and Botha, 1982). The narrow belt is about 120 km in length, and extends from Soetvlei, 35 km south-east of Prieska to Marydale (Potgieter and Botha, 1982). The group is best exposed west of Prieska, between Prieskapoort and Copperton (Potgieter and Botha, 1982). Marydale Group consists of alternation of immature clastic and volcanoclastic rocks and lava. Marydale is dated 3 100Ma (Potgieter and Botha, 1982; Vajner, 1974).

##### *2.2.3.9.1 Skalkseput Granite and Draghoender Granite*

The Skalkseput Granite is the youngest granite recorded in the study area and is composed of biotite-muscovite (Vajner, 1974). Skalkseput Granite was dated at 2 718±8 Ma (Mapukule, 2009; Vajner, 1974). In the west, Skalkseput Granite is bounded by the Draghoender Granite (Figure. 2.8). To the east it is bounded by the Doringberg Fault (Vajner, 1974). The rocks are medium to coarse grained, consisting of light grey granitoid containing cataclastic biotite and muscovite (Vajner, 1974). The Skalkseput Granite is lithologically more uniform than the Draghoender Granite; contains variability in mineral composition, grain-size and structure (Vajner, 1974). The pegmatite vein strike north-easterly in the north-western part of Skalkseputand is unzoned homogeneous type consisting mainly of silica minerals (Vajner, 1974).

Shear zones are less in the Draghoender Granite than in the Skalkseput Granite (Vajner, 1974). There are three types of shears zones; the minor shear zone marked by quartz (± feldspar and muscovite) veins, the minor shear zone type are of smaller extent and less numerous than the other two shear zone types (Vajner, 1974). Silicified shear zones and quartz veins striking mostly north north-easterly, characterized by more pronounced brittle deformation of granite and by frequently occurrence of quartz-veins (Vajner, 1974). Lastly the zone of shearing, silicification and partial recrystallization of granite in the southern part of the Skalkseput Granite has the most intense shearing zone, which is cataclastic and passes into foliated types in which chlorite and chloritized biotite is coated (Vajner, 1974).

The Draghoender Granite is a granitoid volcanic breccia (Vajner, 1974; Hilliard, 1999). According to Hilliard (1999) the Draghoender Granite was dated ~ 2.9 Ga. The Draghoender Granite comprises of biotite-muscovite granite and adamellite and has a strong foliation in places defined by layers of biotite (Vajner, 1974; Hilliard, 1999). There are three distinct groups of granitoid recognised within the Draghoender Granite (Vajner, 1974; Hilliard, 1999). Muscovite-biotite granite of normal type, which are the common type within the Draghoender Granite; they are usually medium-grained and white- grey biotite granite. Biotite-muscovite granite and adamellite of the leucocratic type are more coarse-grained than the normal type and sometimes resembles the Skalkseput Granite. They occur in the Marydale River, in road cuttings along the Upington-Prieska road to some 8 to 15 km north-northeast of Marydale. Intrusive rocks are characterised by megacysts of opalescent quartz (Vajner, 1974).

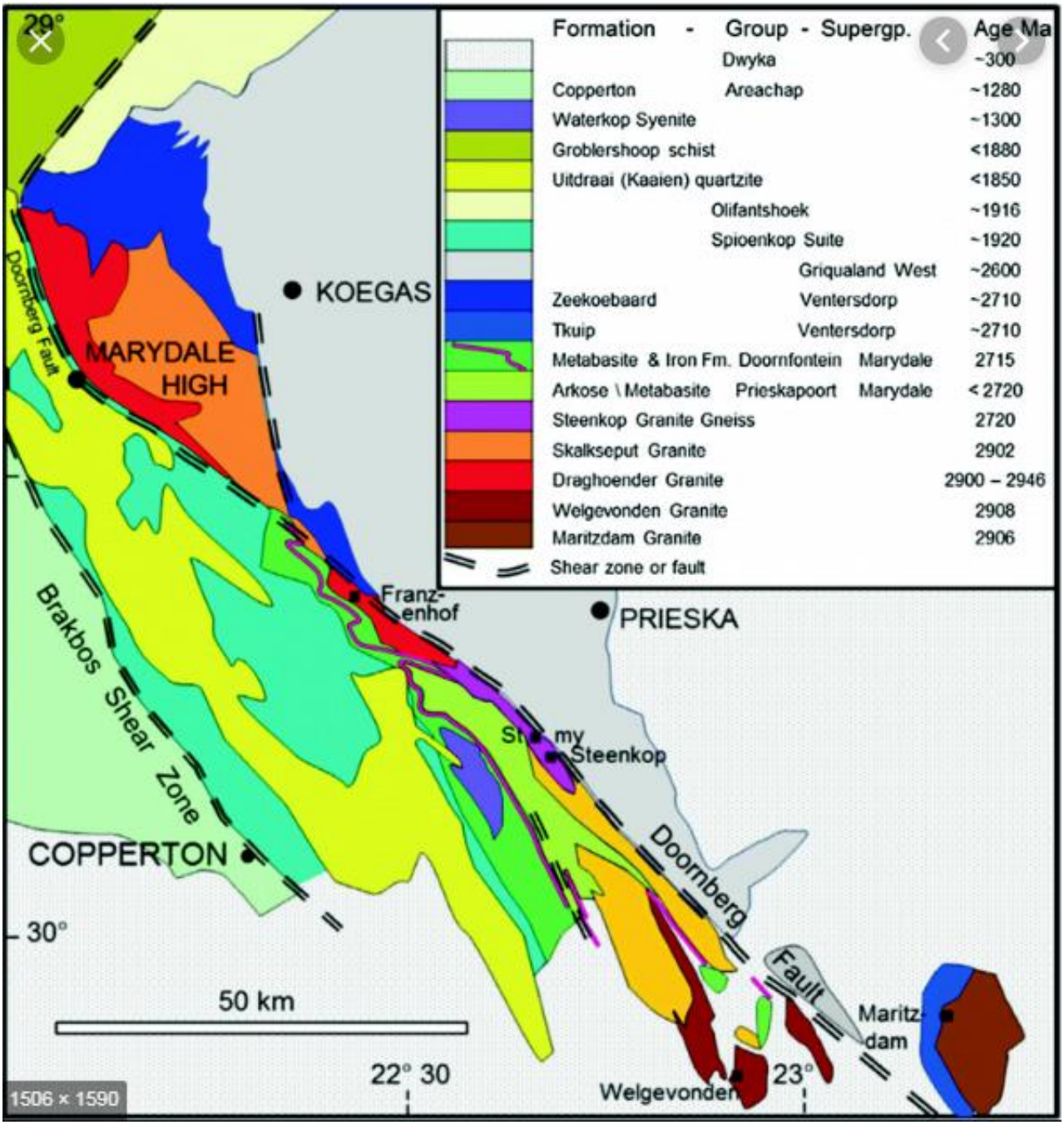



**Figure 2.8: The 2922 Prieska map illustrating the lithostratigraphy from the Maritzdam Granite to the Copperton Formation. (Modified after Anhaeusser, 2019).**

## 2.3 Exploration History

Exploration, mining history, and the research on mineral deposits within and or in close vicinity to the Prieska area are important in understanding the geochemistry and interpreting the present stream sediment data. A number of different types of deposits occur, many of which have been worked in the past.

### *2.3.1 The Economic geological work done in the study area.*

Asbestos mining in South Africa began in the 1930s, and attracted a number of large and small companies, and even individuals (Hart, 1988). The history dates back to the years between 1803 and 1806 when H. Lichtenstein who was a geologist came across the exposure of asbestos near Prieska. Years later in 1831, the mineral was re-examined by Stromeyer and Hausmann, who proposed the name crocidolite. Mining activity then took place when the Cape Asbestos Company acquired surface and mineral rights on a portion of the land at Koegas in Prieska district (Hanekom, 1966). The prospectors travelled everywhere to hunt for new promising deposits, as traces of the crocidolite are exposed from Koegas southwards to beyond Prieska and north towards Griqualand and Kuruman (Hanekom, 1966). The evidence of prospecting activities is revealed by numerous shallow pits, which today are found along the range of the Asbestos Mountains (Hanekom, 1966).

During 1907, Cheynoweth made excavations along the outcrop to up to 30 m depth, exposing friable gossan and minor malachite. The drilling did not core any massive sulphide because the drill site indicates that the holes would have passed through the leached zone. In 1914 Blenkensop evaluated the VMS deposit, but plans were interrupted by the death of Hutchings during the outbreak of war. Anglo-Transvaal Consolidated Investment commenced drilling in November 1968 (Middleton, 1976). Three holes were drilled and these intersected the leached zone ~ 100m beneath the ore body. The fourth borehole intersected massive sulphide, which assayed 1.2 % copper and 7.1 % zinc (Middleton, 1976; Theart, 1986; Wagener and Van Schalkwyk, 1986).

In the Copperton area, the Prieska zinc- copper mine exploited the massive sulphide in 1972 with reserves of 47 Mt grading at 1.74% Cu and 3.87% Zn, 8.0 gram/tonne Ag (g/t) and 0.4 g/t Au (Rossouw, 2013). Based on several authors (Middleton, 1976, Theart, 1986; Wagener and Van Schalkwyk, 1986) the massive sulphide was found to be stratabound within the Copperton Formation. The sulphide minerals included pyrite, sphalerite, pyrrhotite and galena and traces of Ag and Au (Rossouw, 2013 with references therein).

#### *2.3.1.1 The main Prieska Ore body*

The main sulphide ore body (Figure 2.9) is defined as quartz-cordierite-sillimanite-andalusite-muscovite-biotite rock that is very fine and strongly foliated (Theart *et al.,* 1989). It displays great compositional and mineralogical variation and includes some unusual rock types. A contact between the individual component lithologies and the underlying Smouspan Gneiss are gradational or massive amphibolite separates these two members (Theart, *et al.,* 1989).

The main Prieska Ore body is a tabular interstratified massive sulphide body that is 10m wide and strikes 1 800 m, which plunges at 30° to 45° southeast. It provided 47 million tons of ore to a depth of 900m (Middleton, 1976). Based on the work by Rossouw, 2013, samples were collected every 100 m along the roads and fences on 1 km line spacing with the purpose to find gahnite, a dark-green to yellow, zinc spinel. This was because gahnite had been found at the Prieska Zn-Cu mine, and was therefore believed to be a good indicator for Zn mineralization (Rossouw, 2013).

Theart et al. (1989) reported the footwall alteration zone at the Copperton deposit to be enriched in MgO, $K_2O$, V, Sc, Ni, Ba, Cu and Zn, and depleted in CaO, $Na_2O$, Sr and $SiO_2$. The two major rock types within the member were characterised by the silica and mineralogy content. The first rock type is a gedrite fels (Theart *et al.,* 1989). The gedrite fels of the Prieska Copper Mines Member is formed by synmetamorphic metasomatism and at other localities formed by syngenetic alteration prior to metamorphism, gedrite fels

may represent talc-rich precipitates (Theart *et al.,* 1989). The gedrite fels is depleted in Si, Ca, Na, Sr, and highly enriched in Al, Mg, Fe, Mn, K, Ti, V, Sc, Ni, Ba, Cu, and Zn. The second main lithotype is a quartz-perthite-sillimanite gneiss, which contains 70 - 80% silica and an abnormally high Mg content (Theart *et al.,* 1989).

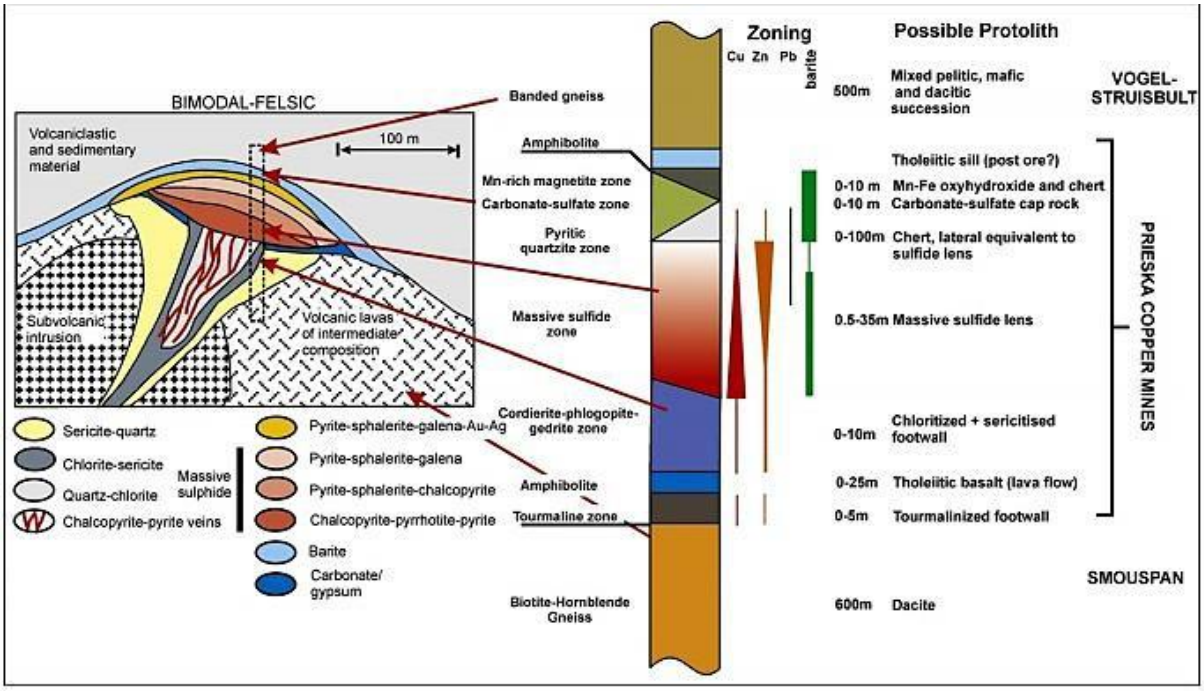



**Figure 2.9: A simplified architecture of the Copperton deposit as related to a model of a biomodal felsic type of VMS deposit. (Bailie and Gutzmer, 2011 and reference therein; Theart et al., 1989).**

Based on studies conducted by Middleton (1976) copper has the most uniform distribution through the orebody, and values rarely fall outside the 1 and 3 % range (Middleton, 1976). The southeastern margin of the orebody is copper deficient and copper is concentrated towards the centre and deeper levels (Middleton, 1976). The frequency distribution of copper shows a positively skewed shape, which is common in this type of deposit, the arithmetic mean of copper is 1.76 %, median is about 1.0 % and the spread is zero to 5.1 %. The distribution of zinc is much more unpredictable, the spread of the values is greater than for copper, varying between 2 and 6 % (Middleton, 1976). Zinc is concentrated in the south-eastern and north-western edges. Zinc distribution shows a complete skewness, with tendency toward being bimodal, the main peak lying near 0 % and another peak at 4 % (Middleton, 1976). The frequency distribution of copper-zinc weight ratios is skewed with a peak at 0 %, this distribution pattern reflects narrow spread of copper values versus the variability in zinc values and also the tendency for copper-rich zones to be zinc poor (Middleton, 1976).

Lead is concentrated near the surface towards the western part of the ore body. The lead content is about 0.20 % of the ore, it is associated with tremolite (Middleton, 1976). Tremolite occurs as a result of contact metamorphism of calcium and magnesium rich siliceous sedimentary rocks (Deer, *et al.,* 1963). Iron and sulphur are concentrated in the central and upper parts of the ore body, they occur mainly in pyrite which is composed of roughly the equal weights of iron and sulphur (Middleton, 1976).

## CHAPTER 3

## Methodology

In order to accomplish the goals and objectives set out for this study, several techniques were used to investigate stream sediment geochemical patterns of the Orange River catchment prospecting area. The methods included geological mapping and stream sediment geochemistry. A descriptive methodology is summarized in the flow chart below (Figure 3.1). The steps followed in order to achieve the objectives of this study were divided into several stages, namely; desktop study, reconnaissance survey, fieldwork, laboratory work, data analysis and interpretation, discussion, conclusions and recommendations (Figure 3.1).

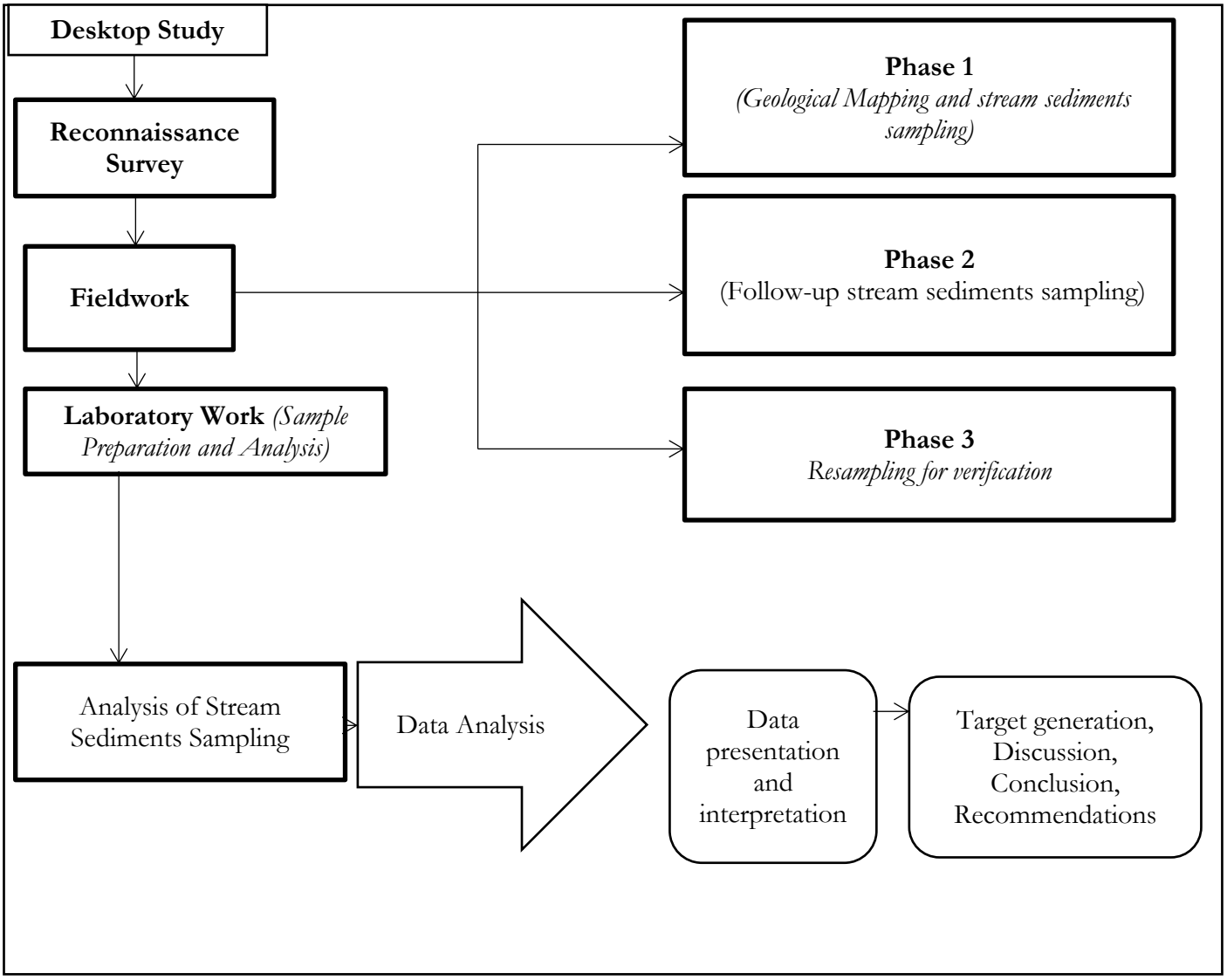



**Figure** 3.1 **Flow chart indicating methods and procedures applied during the study.**

### 3.1 Desktop Study

A desktop study was conducted prior to a field visit to acquire information from previous work on the geology, nature of mineralization and previous exploration conducted in the Orange River catchment prospect. This was conducted in order to acquire first-hand information about the study area. The various sources of information which were utilised included information from textbooks, unpublished technical reports, geological reports, topographical maps, journals and internet sources. . The distribution of streams that drain into the Orange River catchment prospect was also assessed.

### 3.2 Fieldwork

A reconnaissance survey was undertaken prior to stream sediments fieldwork. During this reconnaissance, an overview of the geology, vegetation, and accessibility of the study area was undertaken. The objective of this was to precisely locate the ground and target areas indicated by outcrops of different lithologies. The general attitudes of the lithologies, rock outcrops, and quantity of samples and duration required for later fieldwork were established. Additionally, a thorough study of topography, vegetation, pedology, drainage patterns and characteristics of rocks was also to gather as much information as possible in the study area.

#### *3.2.1 Stream Sediment sampling*

A Bell Jet Ranger Helicopter and 4X4 support field vehicles were used during stream sediment sampling. The sampling took place in 1986 under the supervision of geologist Schalk Strauss. Sampling was carried-out by using aerial photographs with preselected sample positions, the sample selection was based on first order streams draining on a km2 grid system. Sample positions were selected on a 1:50 000 scale topographic sheet. The aerial photographs were used for navigation as GPS were not commercially available at the time. The preselected stream sample positions were sampled. The final sample positions were digitized and saved in a spreadsheet with the map code and sample number. Once analytical data was available the coordinates were merged into a single data set. The samples were analysed in April, during October and November 2014, and during the period September to November 2015 at the Council for Geoscience laboratory supervised by HCCC Cloete and S Burger.

### 3.3 Laboratory Work

All samples collected from the field were transported to the Council for Geoscience laboratory in Pretoria. This section describes the methods used to prepare stream sediments samples collected from the Orange River catchment prospect for laboratory analysis and the sample analysis

#### *3.3.1 Drying and Milling*

Sieve shaker, and drying oven were used for sample preparation. Samples were sorted and oven dried at 105-110 °C. Once completely dry, samples were first sieved through a 2 mm sieve to remove gravels and organic materials and subsequently sieved through a -125 µm fraction size and milled to 85% -75 µm. The milled samples were placed in labelled sample bags ready for analysis.

#### *3.3.2 Sample Analysis*

The prime requirement for mineral exploration survey is the availability of analytical procedures capable of high precision, low detection limit and acceptable accuracy.

#### *3.3.2.1 Stream Sediments Geochemical Analysis using XRF*

Geochemical analysis of stream sediments was carried out using a PANanalytical-Axios XRF at the Council for Geoscience. The milled samples were roasted at 1000°C for at least three hours to oxidise Fe2+ and S and to determine loss of ignition (LOI). Glass disks for XRF analysis were prepared by fusing 1 g sample and 8 g of flux (35% $LiBO_2$ and 64.71% $Li_2B_4O_7$) at 1050°C for major element analysis. Major element oxides ($SiO_2$, $TiO_2$, $Al_2O_3$, $Fe_2O_3t$, MnO, MgO, CaO, $Na_2O$, $K_2O$, $P_2O_5$ and $Cr_2O_3$) and trace element (Ni, Cu, Co, As, Zn, Pb, Cr, Ba, Sc, Sr, V, Th, U, Y, and Zr) were analysed.

Trace element analysis was achieved by mixing 12 g milled sample and a 3 g Hoechst wax and then pressing into a powder briquette by a hydraulic press with the applied pressure at 25 ton. The glass disks and wax pellets were analysed by PANalytical Axios XRF.

The XRF was calibrated by identification of optimum conditions of several variable factors for each element, like identifying correct elemental peak and background, pulse height, collimator mask, counting time, dead time, followed by matrix and inter-element interference corrections (Elsenbroek, 1995). This was achieved by repeated analysis of certified reference material and correcting the variables to yield elemental concentration close to known values. The weighted inverse distance interpolation (IDW) method was used to convert point XRF data into continuous geochemical maps using ArcGIS, the IDW parameters used were: power = 2, maximum neighbours= 15, minimum neighbours = 10, cell Size = Maximum of Inputs.

### *3.3.3 Quality Control and Quality Assurance*

It is vitally important that an analysis is precise but the accuracy is not generally so crucial, although some indication of accuracy is needed for most purposes in mineral exploration (Moon, 2006). A quality assurance program should aim to assess the quality and accuracy at all stages of measurement process, from site selection and sampling through sample handling, preparation and analysis. Subsequently, a quality control/quality assurance program such as in-house reference materials which check the accuracy and precision of the analytical method was incorporated during the analysis of samples. The results of the reference material and lower limit of detection for each element are shown in Table 3.1. The glass disk R422 was analysed firstly with the calibration standards and then every 12 hours during analysis of the sample. The three sediment reference material GSD-9, GSD-11 and GSD-14 were repeatedly analysed every 30 samples to evaluate the precision of the analysis.

The statistical tests of standard sample analysis repeatability can be based on replicate assays of a certified standard in one laboratory or, conversely, inter laboratory analyses. Blank samples for materials that have very low grade of a metal of interest are usually inserted in a batch of samples being processed. The main purpose of using blanks is to monitor the laboratory for a possible contamination of samples, which are mainly caused by poor housekeeping, and insufficient thorough cleaning of equipment.

Table 3.1. The lower limit of detection (LLD) of each element and the reference material obtained results.

| | | GSD-9 | | | | GSD-11 | | | | GSD-14 | | | |
|---|---|---|---|---|---|---|---|---|---|---|---|---|---|
| Oxide (wt %) | Lower level of | N=391 | | | | N= 525 | | | | N=435 | | | |
| Element (ppm) | determination | Certified | Average | Standard | %RMS | Certified | Average | Standard | %RMS | Certified | Average | Standard | %RMS |
| $SiO_2$ | 0.01 | 64.89 | 68.20 | 3.20 | 4.70 | 7 6.25 | 77.29 | 3.17 | 4.10 | 57.25 | 53.43 | 2.51 | 4.69 |
| $TiO_2$ | 0.01 | 0.92 | 0.94 | 0.01 | 1.34 | 0.35 | 0.35 | 0.00 | 1.02 | 2.40 | 2.29 | 0.04 | 1.84 |
| $Al_2O_3$ | 0.01 | 10.58 | 11.30 | 0.72 | 6.40 | 10.37 | 10.41 | 0.56 | 5.39 | 13.39 | 11.75 | 0.77 | 6.56 |
| $Fe_2O_3$ | 0.01 | 4.86 | 4.82 | 0.13 | 2.63 | 4.39 | 4.15 | 0.08 | 1.96 | 9.50 | 9.75 | 0.17 | 1.77 |
| MnO | 0.00 | 0.08 | 0.08 | 0.00 | 2.91 | 0.32 | 0.31 | 0.01 | 3.10 | 0.16 | 0.17 | 0.00 | 2.52 |
| MgO | 0.01 | 2.39 | 2.57 | 0.15 | 5.64 | 0.62 | 0.64 | 0.06 | 8.68 | 3.40 | 3.27 | 0.17 | 5.10 |
| CaO | 0.01 | 5.35 | 5.99 | 0.26 | 4.31 | 0.47 | 0.45 | 0.02 | 4.70 | 3.50 | 3.17 | 0.15 | 4.60 |
| $Na_2O$ | 0.01 | 1.44 | 1.68 | 0.17 | 10.15 | 0.46 | 0.52 | 0.06 | 11.73 | 2.00 | 2.03 | 0.17 | 8.21 |
| $K_2O$ | 0.01 | 1.99 | 2.18 | 0.03 | 1.29 | 3.28 | 3.43 | 0.05 | 1.43 | 2.30 | 2.28 | 0.04 | 1.60 |
| $P_2O_5$ | 0.00 | 0.15 | 0.17 | 0.01 | 4.56 | 0.06 | 0.07 | 0.01 | 8.32 | 0.23 | 0.22 | 0.01 | 5.86 |
| Ag | 4.00 | | 5.00 | 1.00 | 19.20 | | | | | | | | |
| As | 4.00 | 8.40 | 13.00 | 4.90 | 38.00 | 188.00 | 195.00 | 3.00 | 1.60 | 18.00 | 11.00 | 8.00 | 71.40 |
| Ba | 5.00 | 430.00 | 430.00 | 9.70 | 2.30 | 260.00 | 258.00 | 7.40 | 2.90 | 760.00 | 810.00 | 18.10 | 2.20 |
| Ce | 10.00 | 78.00 | 79.00 | 12.20 | 15.40 | 58.00 | 59.00 | 8.70 | 14.70 | 10.00 | 107.00 | 11.50 | 10.80 |
| Co | 4.00 | 14.40 | 13.00 | 0.20 | 1.90 | 8.50 | 8.00 | 0.50 | 6.70 | 28.00 | 28.00 | 0.60 | 2.30 |
| Cr | 4.00 | 85.00 | 89.00 | 2.60 | 2.90 | 40.00 | 36.00 | 2.70 | 7.50 | 243.00 | 244.00 | 7.50 | 3.10 |
| Cu | 2.00 | 32.10 | 33.00 | 1.40 | 4.10 | 78.60 | 78.00 | 2.00 | 2.60 | 66.00 | 72.00 | 2.50 | 3.50 |
| Ga | 2.00 | 14.00 | 18.00 | 3.00 | 16.90 | 18.50 | 19.00 | 3.40 | 17.20 | 25.00 | 30.00 | 4.00 | 13.70 |
| Hf | 5.00 | 9.70 | 11.00 | 0.70 | 6.90 | 5.40 | 6.00 | 0.80 | 14.70 | 13.00 | 15.00 | 1.20 | 8.00 |
| Mo | 2.00 | 0.64 | | | | 5.90 | 7.00 | 0.50 | 7.70 | 2.70 | 4.00 | 0.50 | 13.90 |
| Nb | 3.00 | 17.70 | 22.00 | 2.90 | 13.20 | 25.00 | 29.00 | 2.80 | 9.70 | 72.00 | 86.00 | 4.90 | 5.70 |
| Nd | 3.00 | 34.00 | 37.00 | 7.80 | 20.09 | 27.00 | 23.00 | 6.40 | 27.80 | 45.00 | 51.00 | 10.10 | 19.70 |
| Ni | 2.00 | 32.30 | 34.00 | 1.00 | 2.80 | 14.40 | 18.00 | 1.20 | 7.10 | 87.00 | 100.00 | 3.70 | 3.70 |
| Pb | 2.00 | 23.00 | 23.00 | 0.90 | 8.10 | 636.00 | 627.00 | 14.70 | 2.30 | 66.00 | 68.00 | 3.20 | 4.70 |
| Rb | 2.00 | 80.00 | 84.00 | 2.20 | 2.60 | 408.00 | 417.00 | 10.50 | 2.50 | 87.00 | 92.00 | 3.40 | 3.70 |
| S | 3.00 | 150.00 | 217.00 | 6.70 | 3.10 | 170.00 | 178.00 | 14.50 | 8.10 | | 175.00 | 16.10 | 9.20 |
| Sb | 3.00 | 0.80 | | | | 14.90 | 11.00 | 1.30 | 11.60 | 2.70 | 4.00 | 0.70 | 18.70 |
| Sc | 3.00 | 11.10 | 16.00 | 4.30 | 26.90 | 7.40 | 8.00 | 3.80 | 45.20 | 18.00 | 21.00 | 4.30 | 20.50 |
| Sn | 3.00 | 2.60 | 5.00 | 2.10 | 42.30 | 370.00 | 400.00 | 7.90 | 2.00 | 9.50 | 8.00 | 3.90 | 47.70 |
| Sr | 2.00 | 166.00 | 168.00 | 1.90 | 1.10 | 29.00 | 34.00 | 1.10 | 3.30 | 216.00 | 327.00 | 5.40 | 2.30 |
| Ta | 3.00 | 1.30 | | | | 5.70 | 5.00 | 1.40 | 24.80 | 5.00 | 4.00 | 0.80 | 19.60 |
| Th | 3.00 | 12.40 | 11.00 | 1.90 | 17.00 | 23.30 | 48.00 | 2.10 | 4.30 | 12.40 | 12.00 | 2.20 | 17.40 |
| U | 3.00 | 2.60 | 4.00 | 0.80 | 20.60 | 9.10 | 8.00 | 1.20 | 15.20 | 3.00 | 4.00 | 1.50 | 37.20 |
| V | 4.00 | 97.00 | 105.00 | 5.40 | 2.50 | 46.80 | 39.00 | 3.60 | 9.20 | 190.00 | 230.00 | 20.30 | 8.80 |
| W | 3.00 | 1.76 | | | | 126.00 | 97.00 | 3.80 | 3.90 | 5.60 | 5.00 | 0.90 | 18.10 |
| Y | 3.00 | 26.50 | 25.00 | 0.60 | 2.30 | 42.70 | 37.00 | 2.00 | 5.50 | 3.40 | 34.00 | 1.50 | 5.30 |
| Zn | 3.00 | 78.00 | 72.00 | 0.60 | 0.90 | 373.00 | 368.00 | 9.50 | 2.60 | 165.00 | 183.00 | 5.20 | 2.80 |
| Zr | 3.00 | 370.00 | 391.00 | 9.00 | 2.30 | 152.00 | 156.00 | 5.60 | 3.60 | 524.00 | 560.00 | 17.40 | 3.10 |

### 3.4 Data Processing and Evaluation

Analytical data processing aims, firstly, at reducing random and/or systematic errors resulting from field survey and/or laboratory analysis, and secondly, at identifying whether the data contain some useful information indicating the source, pathway and trap of VMS deposit in the study area.

#### *3.4.1 Statistical Data Analysis*

Statistical methods have been widely applied to interpret analytical data sets and define anomalies (McQueen, 2008). However, such methods need to be used cautiously since the data are typically and spatially dependent on each sample site and a range of different processes that may have influenced the element abundance measured. The data are also imprecise because of unavoidable variability in sampling methods and media and the level of analytical precision. Moon (2006) indicated that the aim of mineral exploration is to define significant anomalies. Anomalies are defined by statistically grouping data and comparing these with geology and sampling information. Strong anomalies detected may be for instance due to a combination of factors such as sampling and analytical errors, or contaminations which do not represent mineralization. The absence of an anomaly on the other hand may not necessarily mean the absence of mineralization in the area of study. Such absence may be due to low rate of weathering in the area, solubility of an element, buried or blind mineralization, or dilution between source and sample site (Carranza, 1994).

The use of descriptive statistics helps in the simplification of large amounts of data into a simpler summary. Numerical and graphical methods are the two commonly used methods. Numerical method enables to the computation of statistics such as mean and standard deviation while, graphical methods are better suited for identifying patterns in the data sets. The numerical and graphical methods complement each other and it is therefore wise to use both. Consequently, histograms, and summary statistical information were used in this study to identify patterns in data sets. According to Riemann et al. (2005), a graphical inspection of analytical data is necessary as the first step in data analysis. The best means of statistical grouping data is graphical examination using histograms and box plots (Howarth, 1984; Garret, 1989).

##### *3.4.1.1 Histogram Plots*

Histograms were used in this study to assist in the visual evaluation of data and to determine whether the data is distributed symmetrically (normal Gaussian) or whether the distribution is asymmetrical and skewed. When the distribution is not normal, it cannot accurately be described by mean and standard deviation, but instead the median, mode, quartiles and percentiles should be used. Histograms also clearly indicate multi-modal distribution (if it exists). For example, if the data indicate bimodal distribution, it may suggest that the samples are not homogeneous and may possibly originate from two different populations, each more or less normal distributed.

##### *3.4.1.2 Box and Whisker Plots*

Univariate statistical methods, involves observations with only one variable that can be used to organise and extract information from data set of values for a single element. This type of plot shows the median (middle of box plot) – Q2, upper and lower hinges (or limits) defined by $25^{th}$ and $75^{th}$ percentile values respectively (Q1 and Q3) and, inner fence defined as 1.5 times the length of the box (the interquartile range –IQR) towards maximum and minimum values (Tukey, 1977).

The central box will contain 50% of the data and values below or above the whiskers are considered outliers and values of more than 3 times the interquartile range (length of the box) from the box hinges which are referred to as extremes. Outliers are outlying observations that appears to deviate markedly from another members of the sample in which it occurs, while extremes are any data values which lie more than 3.0 times the inter quartile range (IQR), range below the first quartile or above the third quartile (Grubbs, 1969).

#### *3.4.1.3 Determination of Threshold Values*

In exploration geology, definition of background and anomalous values is a fundamental issue (McQueen, 2008). In early geochemical surveys applied to mineral prospecting, a threshold value was the concentration of a particular element that separated 'high and low data values of fundamentally different character. This value identify anomalously high values indicating mineralization or low values reflecting alteration (McIlwaine et al., 2016). The traditional statistical methods assumed in the past that the concentration of chemical elements in the crust follows a normal or log-normal distribution (Rose et al., 1979; Chork and Mazzuchelli, 1989; Stanley, 2003). A geochemical anomaly is defined as a region where the concentration of element of interest is greater than certain threshold value, and the latter is determined based on statistical parameters, such as mean, median, and standard deviations (α) above the mean (x) value (Rose et al., 1979; Ciftci et al., 2005). Different approaches are applied in determining the threshold values; the upper limit of the upper whisker line (ULBL) method is mostly used European countries (McIlwaine et al., 2016).

$ULBL = P75 + 1.5 \times (P75 - P25)$……. Equation 2

Where P75 and P25 are the 75th and 25th percentiles of the element concentrations respectively. Another method that researchers use is called normal background concentrations (NBCs) (McIlwaine et al., 2016). In this study the geochemical threshold (Th) of the raw data is defined as:

$Th = x + 2\alpha$…… Equation 3.

ArcGis and Excel Microsoft were used in calculating the threshold values. A geostatistical analysis arc tool was used to calculate statistics of each element (Appendix 3) which was then exported to the Excel file. Where a threshold formula (Equation 3) was used to calculate the threshold values, these values were used in chapter 5 for understanding and discussing anomalies or generating targets. The crustal abundance of more relevant elements is tabulated in Table 3.2.

Table 3.2.The Average abundance of relevant element in the continental crust

| Element | Average abundance in the continental crust (McLennan and Taylor, 1996) | Average abundance in the continental crust (Taylor, 1964) |
|---|---|---|
| Na, wt % | 2.89 | 2.36 |
| Mg, wt % | 1.33 | 2.33 |
| Al, wt % | 8.04 | 8.23 |
| Si, wt % | 30.8 | 28.15 |
| P, ppm | 700 | 1050 |
| K, wt % | 2.8 | 2.09 |
| Ca, wt % | 3 | 4.15 |
| V, ppm | 107 | 135 |
| Cr, ppm | 83 | 100 |
| Mn, ppm | 600 | 950 |
| Fe, wt % | 3.5 | 5.63 |
| Co, ppm | 17 | 25 |
| Ni, ppm | 44 | 75 |
| Cu, ppm | 25 | 55 |
| Zn, ppm | 71 | 70 |
| Ga, ppm | 17 | 15 |
| Ge, ppm | 1.6 | 1.5 |
| As, ppm | 1.5 | 1.8 |
| Se, ppm | 50 | 0.05 |
| Rb, ppm | 112 | 90 |
| Sr, ppm | 350 | 375 |
| Y, ppm | 22 | 33 |
| Zr, ppm | 190 | 165 |
| Nb, ppm | 12 | 20 |
| Mo, ppm | 1.5 | 1.5 |

#### *3.4.1.4 Correlation and Correlation Coefficient (r)*

The use of scatter plots alongside a correlation coefficient is strongly advised as scatter plots aid in the visualization of the correlation among the elements (Fifield and Haines, 1995). Correlation coefficients measure the strength of association between elements pairs. The most common correlation coefficient, called the Pearson product-moment correlation coefficient, measures the strength of linear association between variables. A set of bivariate data, expressed graphically as an X-Y plot, is fitted to a straight line that may or may not pass through the origin. This line represents the best estimate of the relationship between what is termed dependent variable (which is normally plotted on y-axis) and independent variable (x- axis). The output is the degree of similarity between two datasets given by the following expression:

$$r = \frac{\in xy - \in x \in y \div N}{\sqrt{(\in x2 - (\in x2 \div N)\,(\in y2 - \in y2 \div N)}}$$

The result of the calculation, (r), is the measure of the linear association between X and Y as it exists in any given set of data pairs. Excel Microsoft is a significant tool used in this study, to explore the data and help in the calculation of correlation coefficient (Table 3.3)

Table 3.3. The Correlation matrix showing the correlation between elements from negative correlation to very strong positive correlation.

| | Ag | As_ | Ba | Ce | Co | Cr | Cu | Ga | Hf | Mo | Nb | Nd | Ni | Pb |
|---|---|---|---|---|---|---|---|---|---|---|---|---|---|---|
| Ag | 1.0000 | | | | | | | | | | | | | |
| As_ | 0.1552 | 1.0000 | | | | | | | | | | | | |
| Ba | 0.0520 | -0.0555 | 1.0000 | | | | | | | | | | | |
| Ce | 0.0956 | 0.5085 | -0.0218 | 1.0000 | | | | | | | | | | |
| Co | 0.1271 | 0.0562 | 0.0767 | 0.0064 | 1.0000 | | | | | | | | | |
| Cr | 0.1998 | 0.4000 | -0.0958 | 0.2664 | 0.5850 | 1.0000 | | | | | | | | |
| Cu | 0.0738 | -0.0106 | 0.5897 | -0.0222 | 0.2059 | 0.0606 | 1.0000 | | | | | | | |
| Ga | 0.1201 | 0.1445 | 0.3487 | -0.0953 | 0.1985 | 0.0926 | 0.1297 | 1.0000 | | | | | | |
| Hf | 0.1611 | 0.8199 | -0.0435 | 0.6219 | 0.0443 | 0.4811 | -0.0134 | 0.1140 | 1.0000 | | | | | |
| Mo | 0.1508 | 0.4587 | 0.1155 | 0.4859 | 0.1453 | 0.3451 | 0.2328 | -0.0075 | 0.4829 | 1.0000 | | | | |
| Nb | 0.4435 | 0.6413 | 0.1369 | 0.4409 | 0.0939 | 0.4380 | 0.0356 | 0.3268 | 0.8157 | 0.4147 | 1.0000 | | | |
| Nd | 0.1358 | 0.5690 | -0.0068 | 0.8967 | -0.0168 | 0.3239 | -0.0245 | -0.0169 | 0.7506 | 0.3212 | 0.5731 | 1.0000 | | |
| Ni | 0.1609 | -0.0154 | 0.0303 | -0.0828 | 0.7213 | 0.5889 | 0.1484 | 0.2066 | 0.0004 | 0.0565 | 0.0926 | -0.0727 | 1.0000 | |
| Pb | 0.2079 | 0.0909 | 0.5272 | 0.1199 | 0.0348 | 0.0140 | 0.3975 | 0.3629 | 0.1723 | 0.1611 | 0.3920 | 0.1846 | 0.0470 | 1.0000 |
| Rb | 0.0999 | 0.0098 | 0.4749 | 0.0740 | -0.1606 | -0.2758 | 0.0678 | 0.5134 | 0.0385 | -0.0054 | 0.2702 | 0.0929 | -0.0889 | 0.4933 |
| S | -0.0072 | -0.0354 | 0.2343 | 0.0001 | -0.0166 | -0.0475 | 0.1906 | -0.0291 | -0.0377 | 0.0375 | -0.0501 | -0.0048 | -0.0014 | 0.0529 |
| Sb | -0.0034 | 0.0161 | 0.0213 | 0.0036 | -0.0242 | -0.0089 | 0.0064 | 0.0041 | -0.0144 | -0.0094 | -0.0080 | 0.0031 | -0.0122 | -0.0098 |
| Sc | 0.2047 | -0.0250 | 0.0318 | -0.1328 | 0.4429 | 0.2516 | 0.0639 | 0.2282 | -0.0301 | 0.0183 | 0.1180 | -0.1172 | 0.2640 | 0.0207 |
| Sn | 0.0304 | 0.0776 | 0.0155 | 0.0503 | 0.0261 | 0.0482 | 0.0054 | 0.0062 | 0.0402 | 0.0568 | 0.0500 | 0.0601 | 0.0250 | 0.5404 |
| Sr | 0.0695 | -0.0067 | 0.1634 | 0.0728 | 0.1555 | 0.1554 | 0.0720 | 0.1295 | -0.0078 | 0.0549 | 0.0924 | 0.0699 | 0.0793 | 0.0682 |
| Ta | 0.1991 | 0.8914 | -0.0058 | 0.4447 | 0.1062 | 0.4401 | 0.0028 | 0.3407 | 0.8254 | 0.3844 | 0.7192 | 0.5675 | 0.0819 | 0.1960 |
| Th | 0.2442 | 0.6040 | 0.1355 | 0.4527 | 0.0881 | 0.3830 | 0.0042 | 0.3247 | 0.7713 | 0.3685 | 0.8119 | 0.5952 | 0.0532 | 0.3880 |
| U | 0.4857 | 0.6433 | 0.0206 | 0.4750 | 0.1511 | 0.4374 | 0.0340 | 0.0623 | 0.7311 | 0.4912 | 0.7532 | 0.5298 | 0.0777 | 0.2401 |
| V | 0.2149 | 0.4729 | 0.1704 | 0.3644 | 0.4582 | 0.6379 | 0.1149 | 0.4151 | 0.6194 | 0.2823 | 0.6647 | 0.5072 | 0.3049 | 0.2850 |
| W | 0.1762 | 0.7146 | -0.0475 | 0.4144 | 0.0653 | 0.3628 | 0.0655 | 0.2838 | 0.6472 | 0.3569 | 0.5250 | 0.4742 | 0.1001 | 0.1219 |
| Y | 0.0760 | 0.6130 | 0.1944 | 0.4462 | 0.0596 | 0.2291 | 0.0368 | 0.1847 | 0.6366 | 0.3524 | 0.6057 | 0.4921 | -0.0679 | 0.2747 |
| Zn | 0.0507 | -0.0406 | 0.6355 | -0.0231 | 0.1166 | 0.0117 | 0.9713 | 0.1624 | -0.0329 | 0.2150 | 0.0267 | -0.0194 | 0.0852 | 0.4360 |
| Zr | 0.1553 | 0.8292 | -0.0691 | 0.6256 | 0.0378 | 0.4734 | -0.0244 | 0.0292 | 0.9865 | 0.5239 | 0.7904 | 0.7298 | -0.0231 | 0.1445 |

| | Rb | S | Sb | Sc | Sn | Sr | Ta | Th | U | V | W | Y | Zn | Zr |
|---|---|---|---|---|---|---|---|---|---|---|---|---|---|---|
| Rb | 1.0000 | | | | | | | | | | | | | |
| S | -0.0482 | 1.0000 | | | | | | | | | | | | |
| Sb | 0.0573 | -0.0063 | 1.0000 | | | | | | | | | | | |
| Sc | 0.0119 | -0.0715 | 0.0271 | 1.0000 | | | | | | | | | | |
| Sn | 0.0168 | -0.0106 | 0.0187 | -0.0079 | 1.0000 | | | | | | | | | |
| Sr | -0.0083 | 0.2750 | 0.0156 | 0.0796 | -0.0029 | 1.0000 | | | | | | | | |
| Ta | 0.0602 | -0.0345 | -0.0151 | -0.0390 | 0.0562 | 0.0001 | 1.0000 | | | | | | | |
| Th | 0.3286 | -0.0708 | -0.0072 | 0.0508 | 0.0870 | 0.0994 | 0.5251 | 1.0000 | | | | | | |
| U | 0.1082 | -0.0399 | -0.0052 | 0.1456 | 0.0738 | 0.0748 | 0.4471 | 0.7255 | 1.0000 | | | | | |
| V | 0.1388 | -0.0441 | 0.0091 | 0.2151 | 0.0459 | 0.2889 | 0.4409 | 0.7084 | 0.5656 | 1.0000 | | | | |
| W | -0.0574 | 0.0089 | -0.0233 | -0.1385 | 0.0592 | -0.0880 | 0.6536 | 0.4426 | 0.3475 | 0.3731 | 1.0000 | | | |
| Y | 0.3773 | -0.0808 | 0.0349 | 0.1034 | 0.0384 | 0.1085 | 0.3644 | 0.6741 | 0.6577 | 0.5464 | 0.0729 | 1.0000 | | |
| Zn | 0.1348 | 0.1933 | 0.0016 | 0.0126 | -0.0011 | 0.0920 | -0.0125 | 0.0093 | 0.0037 | 0.1061 | 0.0443 | 0.0403 | 1.0000 | |
| Zr | 0.0038 | -0.0438 | -0.0143 | -0.0294 | 0.0488 | -0.0256 | 0.6015 | 0.7498 | 0.7594 | 0.5776 | 0.5925 | 0.6669 | -0.0501 | 1.0000 |

| | |
|---|---|
| | Very Strong Correlation |
| | Moderate to strong correlation |
| | Moderate Correlation |

The groupings of correlations are assigned ratings of very strong (0.7+), moderate to strong (0.5-0.69), and moderate (0.25-0.49). Before interpreting the individual elemental data an examination of the elemental associations within these groupings draws attention to any geological environments having possible economic interest. These elemental associations of interest are:-

| | | |
|---|---|---|
| Very Strong Correlation | Cu -Zn | Possible volcanogenic, sedimentary ore types. |
| | Ni - Co -Cr | Possible Cr-Ni ore in ultramafic mafic rock types Zr_ Nb – U –Th Felsic index, Heavy mineral index |

| | | |
|---|---|---|
| | Zr –Hf | Possible potential of rare-metal granites, commonly associated with heavy mineral deposits |
| Moderate to strong Correlation | | |
| | U – Ag | |
| | V – Mo | Uranium mineralization |
| | Ce – Th- U | pegmatite-type thorium-uranium deposit |
| Moderate correlation | | |
| | S – Sr –Cu-Zn-Ba | possible volcanogenic ore type |

# CHAPTER 4

## Data presentation and interpretation

### 4.1 Univariate Stream Sediment Geochemistry

The geochemical data was transformed into a raster data with a cell size of 1 km using weighted inverse distance interpolation method. A maximum of four points were used to calculate a value for each cell location. First, the raster maps of the uni-elements were visualized in ArcGIS and compared to the underlying geology and known base metal occurrences. Univariate statistical methods were used to extract information from a data set of values for a single element. Frequency histograms were created using a GIS geostastical analyst tool, in order to examine the frequency distribution and identify the type of distribution. When dealing with a large dataset, the lognormal distribution pattern appears to be the one most applicate to the results of most geochemical surveys (Lepeltier, 1969).

The only elements that correlate (Table 3.3) importantly with the known base metal occurrences in the Prieska area as discussed in section 2.2 are presented below, Based on Ghavami-Riabi (2006), the indicator elements for base metal mineralization includes Cu, Zn, Pb, Mo, Fe, Ba and Co. The copper, lead, zinc, gold and silver minerals are historically known to be associated with Volcanogenic Massive Sulphide (VMS) deposits. The Prieska area is underlain by the Areachap Terrane, known to host VMS and SEDEX deposits, including the mined out Copperton deposit, approximately 10km southwest of the town of Prieska. Within the project area the Areachap terrane is overlain by up to 100m of Karoo sediments that limited historical exploration within this highly prospective extension.

The elemental distribution maps are plotted using the Jenks natural classification system. The elemental population is classified into five break points; the first break is minimum to mean value, and second break is from mean to (mean plus standard deviation) value, the first two break are regarded as a background value, values above the threshold calculated in Appendix 3 are anomalous, From the threshold to the mean + 3*standard deviation value is highly anomalous and the fifth break is the value from the mean + 3*standard deviation value to the maximum value.

#### *4.1.1 Barium (Ba)*

The Barium (Ba) anomaly (Figure 4.1.1b) is prominent over the Kalahari Group and Dwyka Group to the south of the Prieska area and to a lesser extent over the Spioenkop, Ghaap Group, and Uitdraai Formation, the other lithostratigraphic units within the study area are poorly enriched in Ba (ppm). The break points are 410.6 ppm, 564.1 ppm and 640 ppm, these break points are mean, threshold and mean + 3X Standard Deviation respectively. Barium has a moderate to strongly correlation with copper and zinc.

The Barium anomaly corresponds to the known Cu-Zn Prieska Copperton deposit, the Prieska Copperton deposit is situated within the Areachap Terrane. The frequency distribution plot of the Ba indicates that the frequency of Ba is positively skewed and the kurtosis is positive (Figure 4.1.1a) (Table 3.3). The tails of the histogram is towards high values which implies that the data is positively skewed.

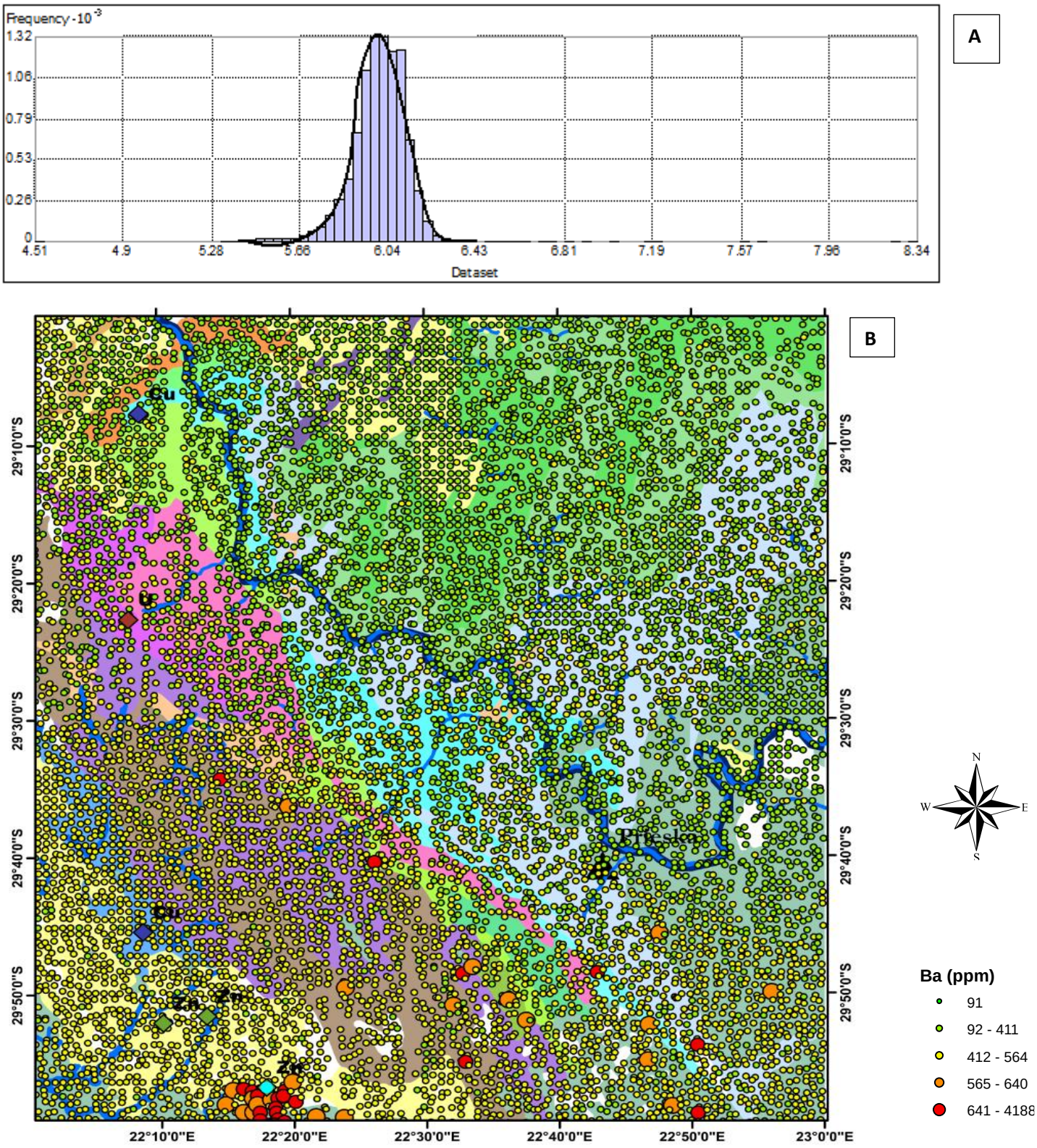



**Figure 4.1.1 a) Histogram frequency distribution showing the skewness and Kurtosis of Ba (ppm) dataset, b) The Regional geochemical distribution map illustrating the location of Ba (ppm) anomalies.**

### *4.1.2 Cobalt (Co)*

Cobalt concentrations are elevated on the Dwyka Group to the east of Prieska town in close vicinity to the Orange River catchment. They are also highly anomalous on the Ongeluk Formation. Figure 4.1.2b indicates the strong correlation of Co with the known Cu occurrence on the Zeekoebart Formation and the Matsap Subgroup. Cobalt is a pathfinder for Ni-Cu massive sulphides, Cu in shales, U (vein type) and certain Ag and Au deposits (Levinson, 1974). From the calculated correlations of elements (Table 3.3), Co indicates a strong correlation with Ni therefore there is a possibility of the occurrences of Ni-Cu massive sulphides or ultramafic Ni- Cr (±Cu) in the Prieska area.

The lognormal histogram frequency distribution display the skewness that is close to zero and the kurtosis is at 6.9 (Figure 4.1.2a). This histogram exhibit the characteristics of the normal distribution histograms, it unimodal bell shaped curve.

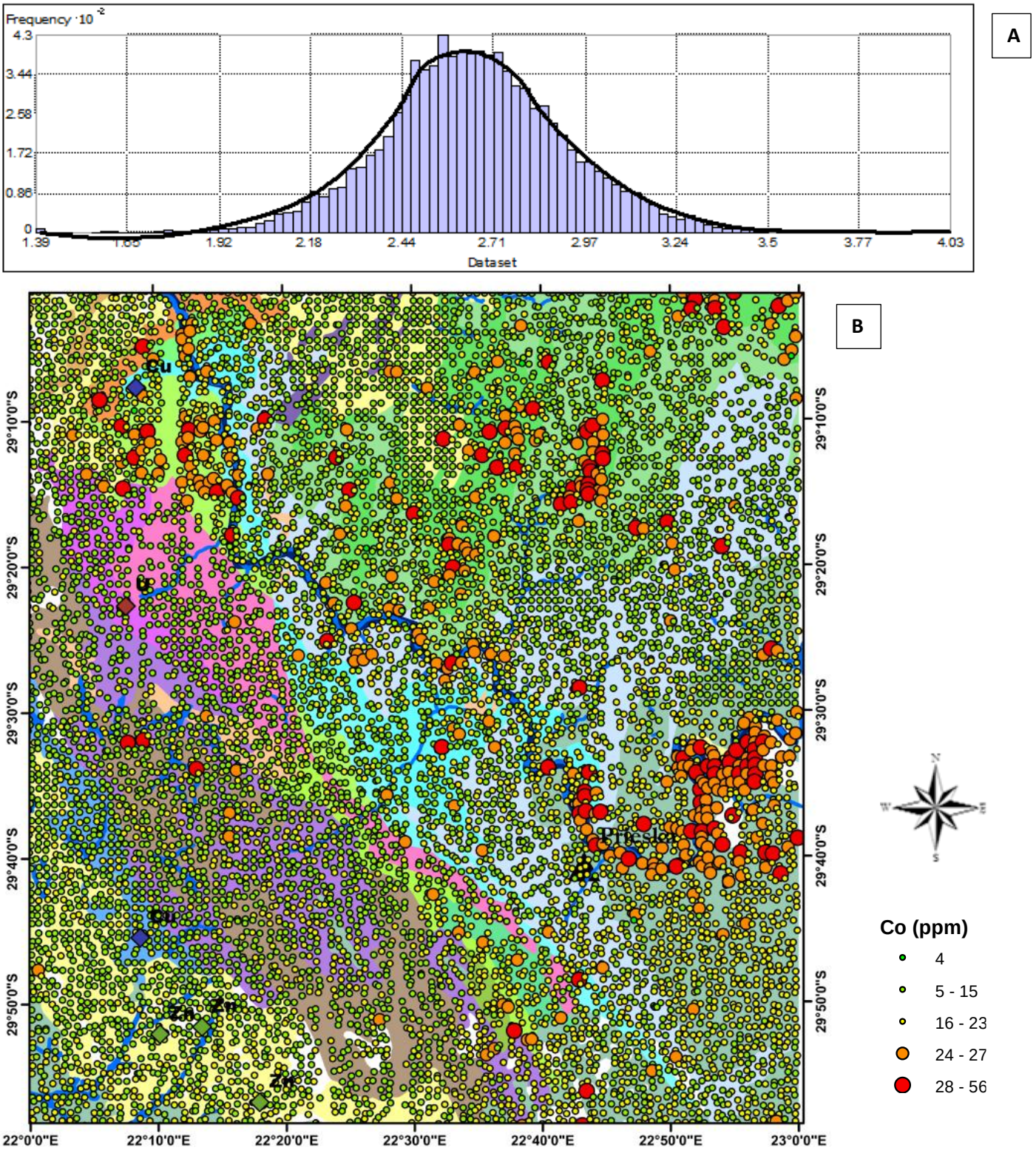



**Figure 4.1.2 a) Histogram frequency distribution showing the skewness and Kurtosis of Co (ppm) dataset, b) The Regional geochemical distribution map illustrating the location of Co (ppm) anomalies.**

### *4.1.3 Copper (Cu)*

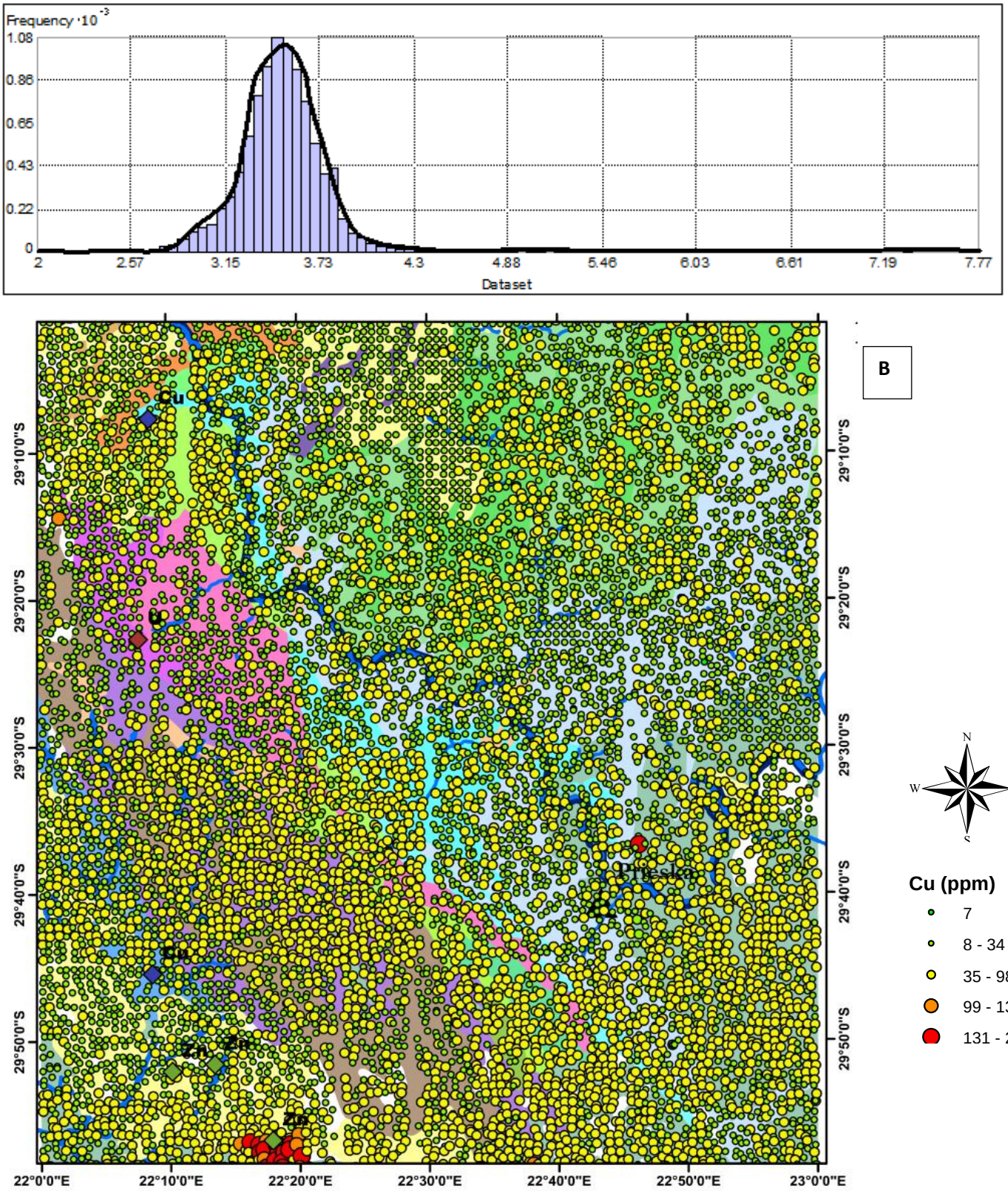



**Figure 4.1.3 a) Histogram frequency distribution showing the skewness and Kurtosis of Cu (ppm) dataset, b) The Regional geochemical distribution map illustrating the location of Cu (ppm) anomalies.**

The Copper break points are 34.48 ppm, 98.2 ppm and 130 ppm, this break points are mean, threshold and mean + 3X Standard Deviation respectively. Cu strongly correlate with the known occurrence of Zinc, and the calculated correlation coefficient in Table 3.3 also indicate a very strong correlation between Cu and Zn. Moderately correlates with Ba and Pb. Cu is extremely anomalous on Kalahari Group and Dwyka Group to the south of Prieska area. The Cu concentration on the other lithostratigraphy are above Cu mean values (Figure 4.1.3b).

The very strong correlation of Copper, Lead and Zinc in the south of the study area may indicate the possibility volcanogenic, sedimentary deposit ore types, the concentration of Cu are at peak on this area, at the range of 130 ppm to 2357ppm. The Frequency distribution is positively skewed and heavy tailed relative to normal distribution and therefore the data set is normalised to or log transformation to exhibit the normal distribution (Figure 4.1.3a). The lognormal distribution curve (Figure 4.1.3a) is perfectly bell shaped.

### *4.1.4 Molydenum (Mo)*

The most extensive high Mo anomaly is present to the west of the known Cu occurrence area to the north of the study area. The lithostratigraphy on this area is the Kalahari Group, Globershoop Formation, Matsap Subgroup and Zeekoebaart Formation. Another anomaly where Mo is extensively high anomalous is observed (Figure 4.1.4b) on the Dwyka Group and Kalahari Group to the east of the Prieska town. The anomaly is less extends on the Koegas Subgroup and Asbestos Hills. The Mo correlates moderately to very strongly with Ta, Th, Cr, V, W, Cu and Ce, therefore there is a possibility of diverse mineralisation example Ta, Ta-Cu, Z n, Cr and asbestos.

The break points are 2.1 ppm, 3.3 ppm and 3.8 ppm, this break points are mean, threshold and mean + 3X Standard Deviation respectively. The lognormal frequency distribution is positively skewed and highly heavy tailed than expected under normal distribution population (Figure 4.1.4

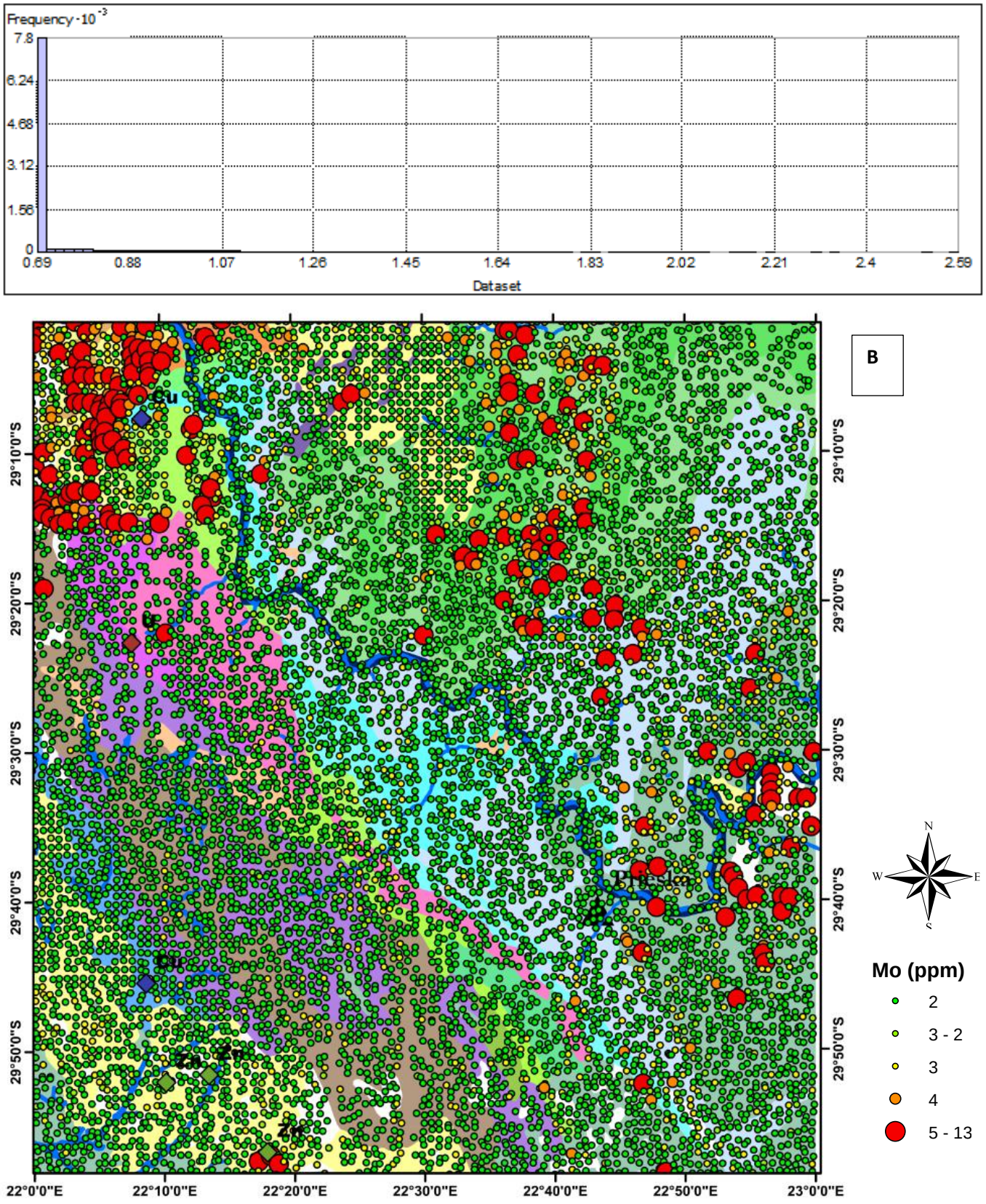
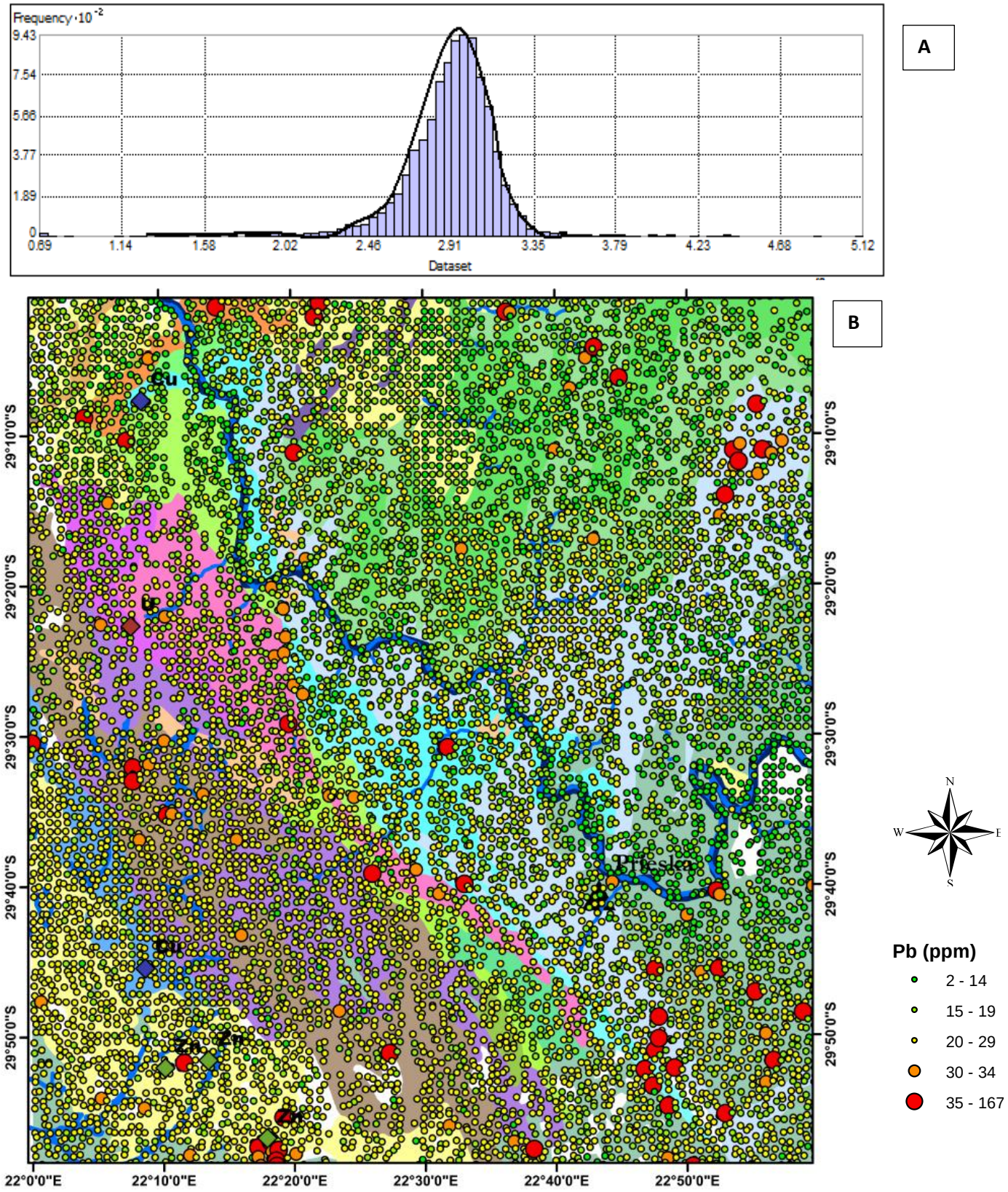



**Figure 4.1.4 a) Histogram frequency distribution showing the skewness and Kurtosis of Mo (ppm) dataset, b) The Regional geochemical distribution map illustrating the location of Mo (ppm) anomalies.**

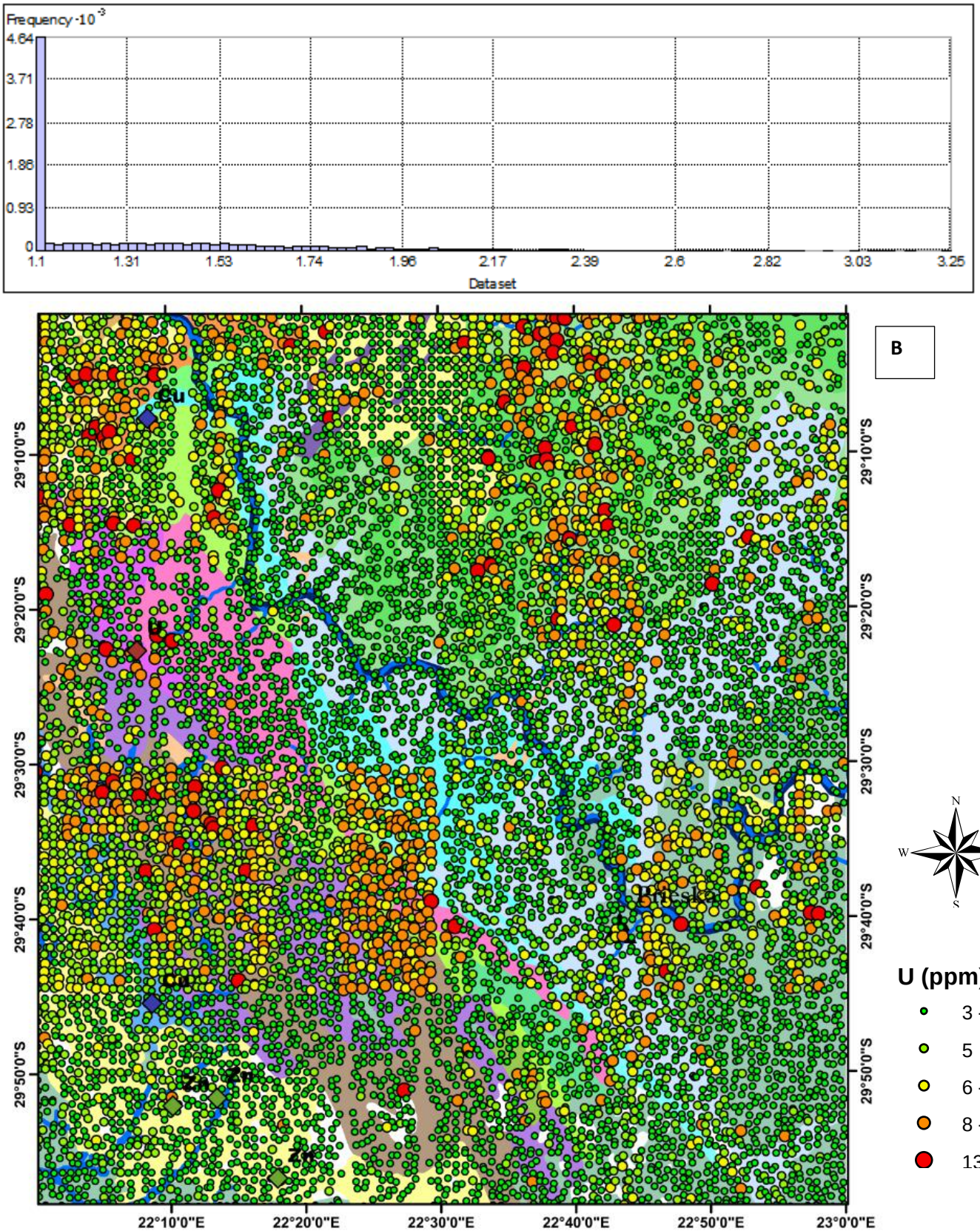
### *4.1.5 Lead (Pb)*

The most prominent lead patterns are found over majority of the Lithostratigraphy observed within the study area of this research. The extreme anomalies are found on the Matsap Subgroup occurring in the north in close vicinity with the known Cu occurrence, to the east of the study area on the Asbestos hill and Koegas Supergroup, and on the Dwyka and Kalahari Group to the south. Lead moderately correlates with Th, V, Y and Zn (Table 3.3). The anomaly pattern distribution of Pb (Figure 4.1.5b) indicate a strong correlation between Zn and Pb over Dwyka and Kalahari Group.

The break points are 18.77 ppm, 28.84 ppm and 33.88 ppm, this break points are mean, threshold and mean + 3X Standard Deviation respectively. The Frequency distribution (Figure 4.1.5a) is positively skewed and heavy tailed relative to normal distribution, the skeweness is 8 and kurtosis is 192


A
Frequency·10⁻²
9.43
7.54
5.66
3.77
1.89
0
0.69
1.14
1.58
2.02
2.46
2.91
3.35
3.79
4.23
4.68
5.12
Dataset
B
Cu
Pb
Zn
Pb
Pb
Pb

### *4.1.6 Uranium*


A
Frequency·10⁻³
4.64
3.71
2.78
1.86
0.93
0
1.1
1.31
1.53
1.74
1.96
2.17
2.39
2.6
2.82
3.03
3.25
Dataset
B
Cu
Pb
Zn
Pb
Zn
Zn
Pb
Pb
Pb

Uranium is extremely high anomalous on the Matsap Subgroup, Kalahari Group, and Zeekoebaart Formation to the north –west of the study area at the known Copper occurrence area, another extreme anomarly is observed on the Draghoender Granite, Jacomyns pan, Uitdraai Formation and Skalkseput granite at the known Uranium occurrence area. The last extreme anomaly is on the Koegas Subgroup and Ongeluk Lava Formation (Figure 4.1.6b). Uranium correlates with Vanadiun, moderate correlates with Ce, and Th which may indicate the pegmatite-type thorium-uranium deposit. The Skeweness of the frequency distribution histogram is 3.5 and the kurtosis is 22.3 therefore the Histogram is positively skewed and heavly-tailed relation to the normal distribution (Figure 4.1.6a).

### *4.1.7 Vanadium (V)*

The Vanadium distribution anomaly pattern (Figure 4.1.7b) is similar to the Co distribution discussed in Figure 4.1.2b. Vanadium has a moderate to strong correlation with Cr, U and Co and moderately correlates to Ce, Mo, Ni, Pb, Sr, and Th. The high V concentration are equally distributed on the Uitdraai Formation, Draghoender granite, Skalkseput granite and Spioenkop Formation, the positive correlation between Molybdenum and Vanadium indicates the possibility of Uranium mineralization.

The V break points are 126.5 ppm, 194.2 ppm and 227.9 ppm which are mean, threshold and mean + 3X Standard Deviation respectively. The Histogram is slightly positively skewed, this histogram exhibit the characteristics of the normal distribution histograms, it more dense to the centre and less dense to its trails. The Skeweness is at 3 and the kurtosis is 4.5. The V dataset does not require normalization.

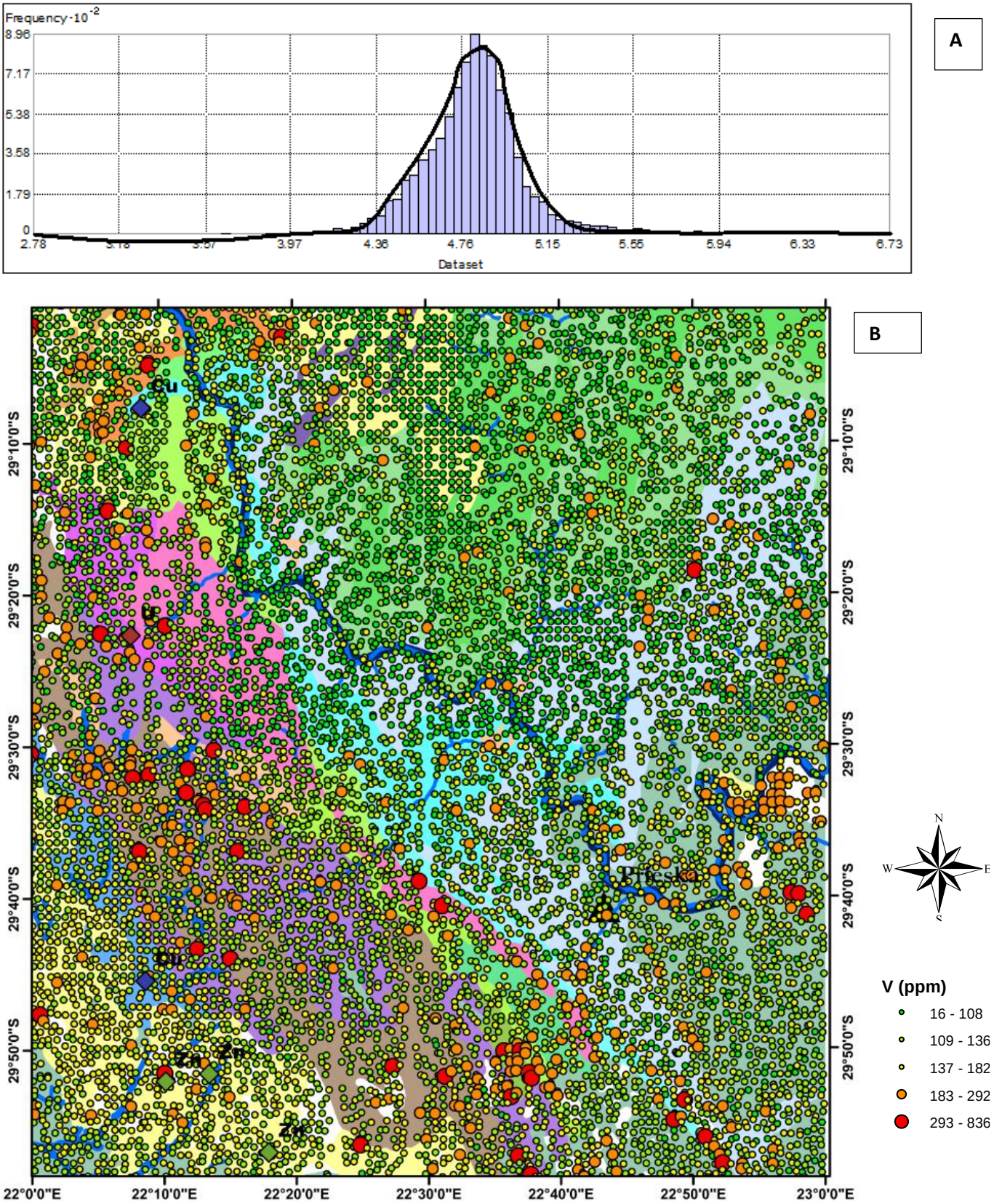
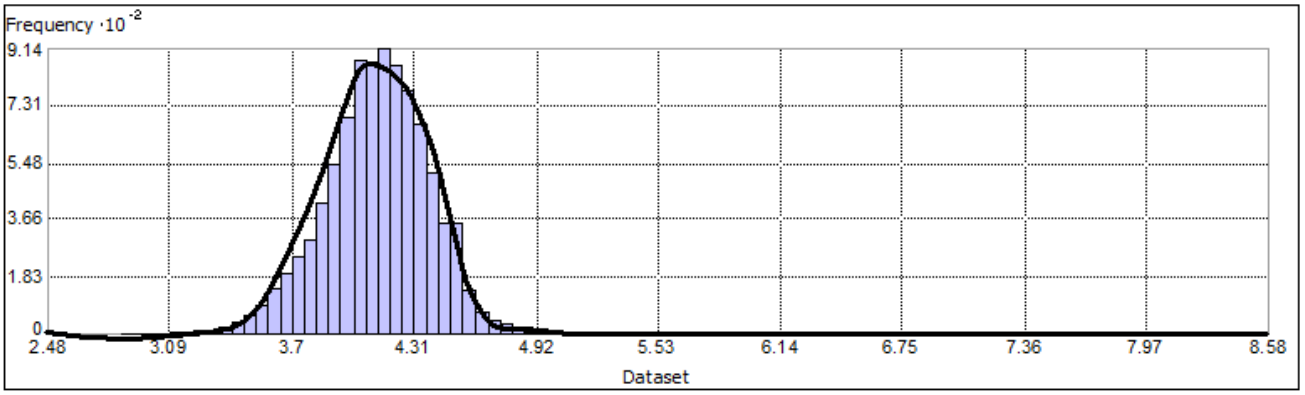



**Figure 4.1.7 a) Histogram frequency distribution showing the skewness and Kurtosis of V (ppm) dataset, b) The Regional geochemical distribution map illustrating the location of V (ppm) anomalies.**

### *4.1.8 Zinc (Zn)*



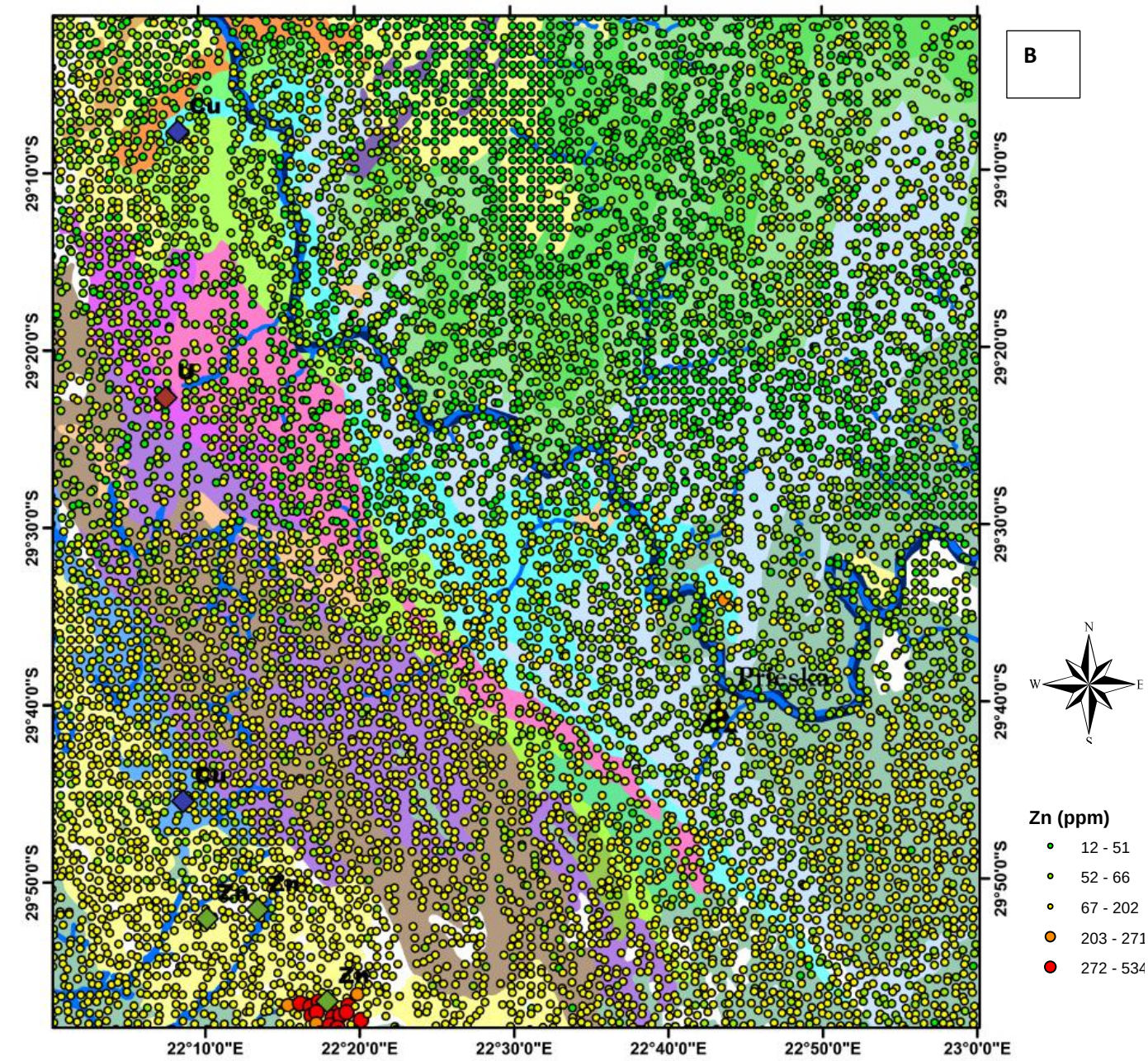




**Figure 4.1.8 a) Histogram frequency distribution showing the skewness and Kurtosis of Zn (ppm) dataset, b) The Regional geochemical distribution map illustrating the location of Zn (ppm) anomalies.**

The most prominent Zn patterns are present in the south portion in close vicinity to the known Zn mine. Generally Zn of less than 66 ppm covers the whole Prieska area except around the known Zn occurrence. Zinc strongly correlates with Copper, Barium and Lead this indicates the possibility of the possibility volcanogenic, sedimentary deposit ore types, Cu mineralization and Zn mineralization.

The V break points are 66 ppm, 202 ppm and 271.3 ppm which are mean, threshold and mean + 3X Standard Deviation respectively. The frequency distribution is skewed to the right and the kurtosis is positive, the histogram is asymmetrical, none transformation must be changed to Box-cox or log transformation to normalise the frequency distribution histogram.

### *4.1.9 Sulphur(S)*

The S concentration is elevated at the Copperton mine, on the Dwyka and Kalahari Group. Sulphur is associated with the known Zn metal occurrence. S is moderately correlates with Cu, Zn, Ba, and Sr (Table 3.3), positevley correlates with Ce, MO and Pb. The values of S appear on the Uitdraai Formation and Spioenkop Formation, also elevated on the Dwyka Group sediments east of Prieska town. The correlation between the Pb and S (Table 3.3) is proven by the anomaly to the east of the study area (Figure 4.1.9b) whereby S concentrations are elevated on the Asbestos Hills Formation exactly where Pb and Fe anomalies are visible (Figure 4.1.5b and Figure 4.1.11b).

The Sulphur break points are 233 ppm, 1177 ppm and 1648 ppm, this break points are mean, threshold and mean + 3X Standard Deviation respectively. The Histogram of S frequency distribution (Figure 4.1.9a) is positively skewed, the kurtosis is at 3037. The S data set is heavy tailed relative to normal distribution and the standard deviation is 472ppm.

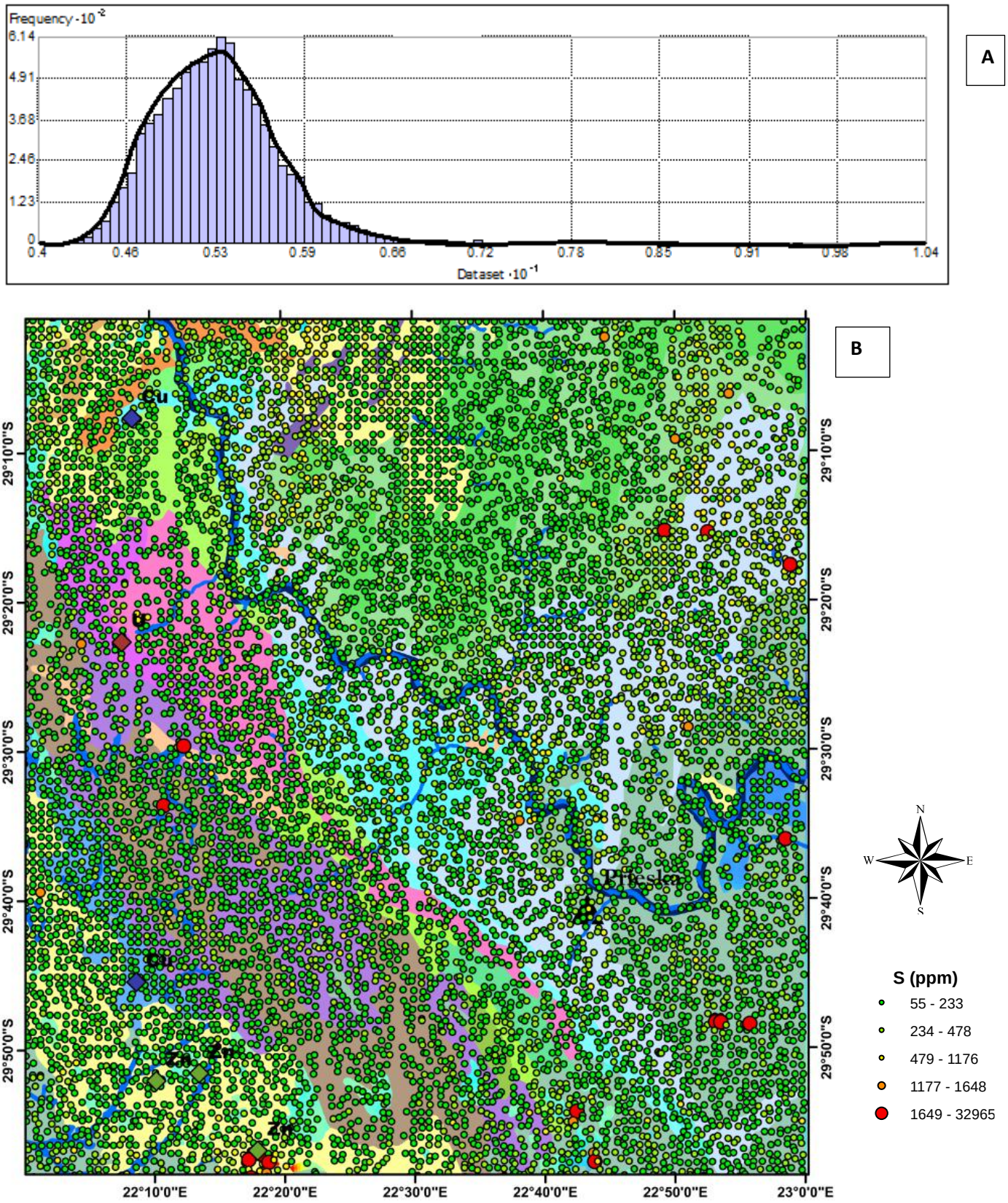
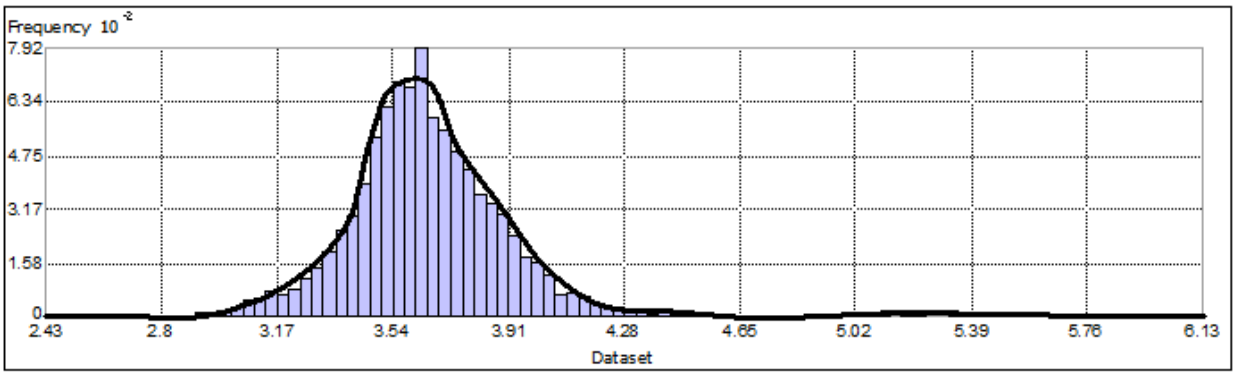



**Figure 4.1.9 a) Histogram frequency distribution showing the skewness and Kurtosis of S (ppm) dataset, b) The Regional geochemical distribution map illustrating the location of S (ppm) anomalies.**

### *4.1.10 Nickel (Ni)*




A

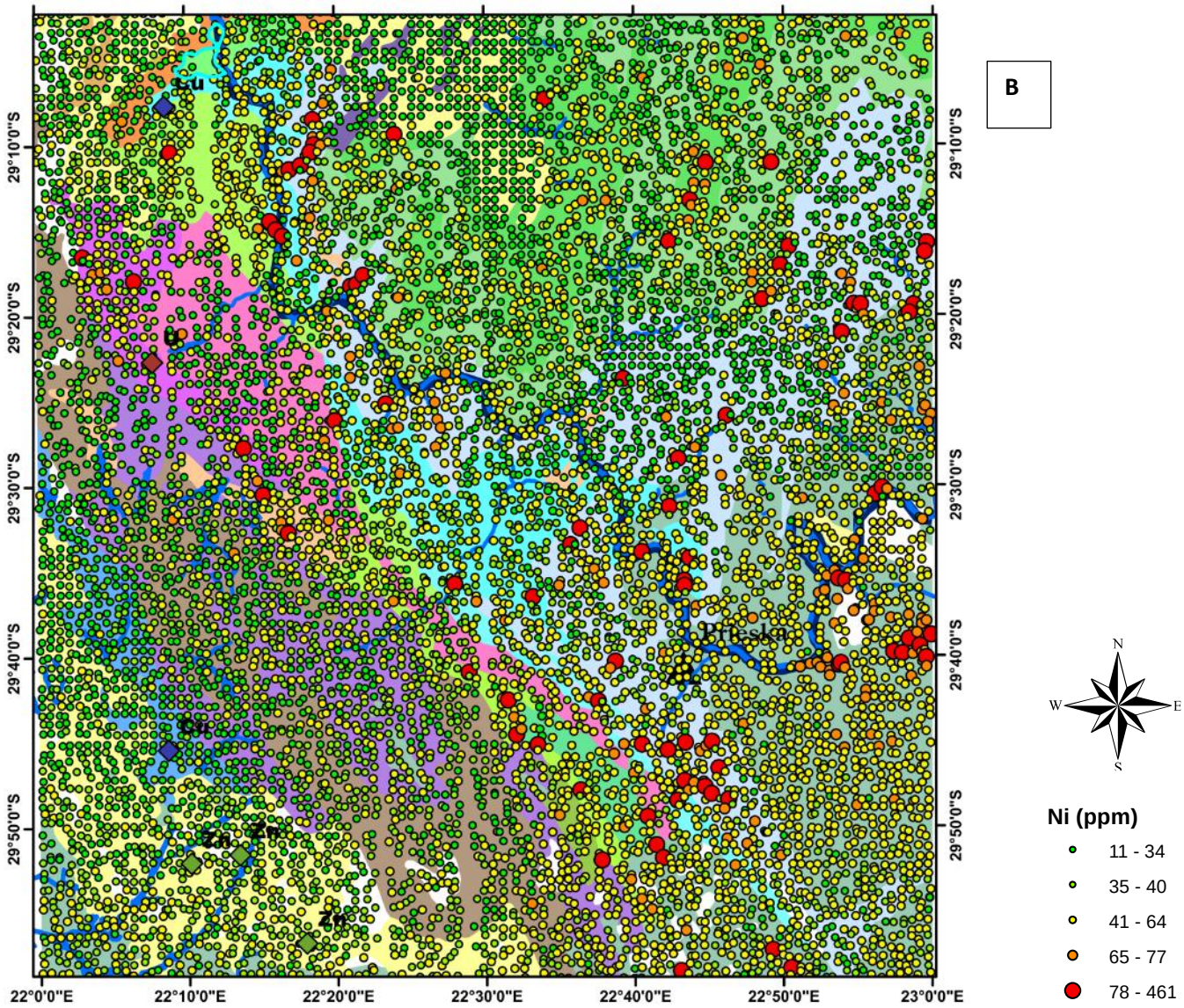



**Figure 4.1.10 a) Histogram frequency distribution showing the skewness and Kurtosis of Ni (ppm) dataset, b) The Regional geochemical distribution map illustrating the location of Ni (ppm) anomalies.**

The elevated concentrations of Nickel are associated with the Asbestos Hill Subgroup. The anomaly is distributed across the Asbestos Hill Subgroup. Asbestos Hill Subgroup underlying rocks includes banded Iron-Formation, jaspelite and amphibolite. The Ni is anomalous in the western contact of the Draghoender granite; this anomaly is associated with the known occurring U metal. Ni positively correlates with Co, both concentration are elevated to the east of the study area in association with Ongeluk Lava Formation, the underlying rock is andesite and basalt.

Figure 18, indicates the strong correlation of Ni and Dwyka Group sediments to the east of Prieska town. The break points are 40ppm, 64 ppm and 77 ppm, this break points are mean, threshold and mean + 3X Standard Deviation respectively. The Frequency distribution is positively skewed and heavy tailed relative to normal distribution, the skeweness is 7.9 and kurtosis is 192.6

#### *4.1.11 $Fe_2O_3$ (%)*

The high Fe2O3 concentrations are distributed across the Asbestos Hill Subgroup of the Ghaap Group, the underlying rocks includes banded-iron formation, jaspelite, riebeckite and amphibolite (Figure 4.1.11b). Iron content of the BIF's is typically 25-35% Fe. The highest Fe concentration of this report dataset is 27% (Figure 4.1.11b) in the South-west of Prieska in close vicinity with the Copperton, Fe concentration are minimum, they range from 3 to 8 %.

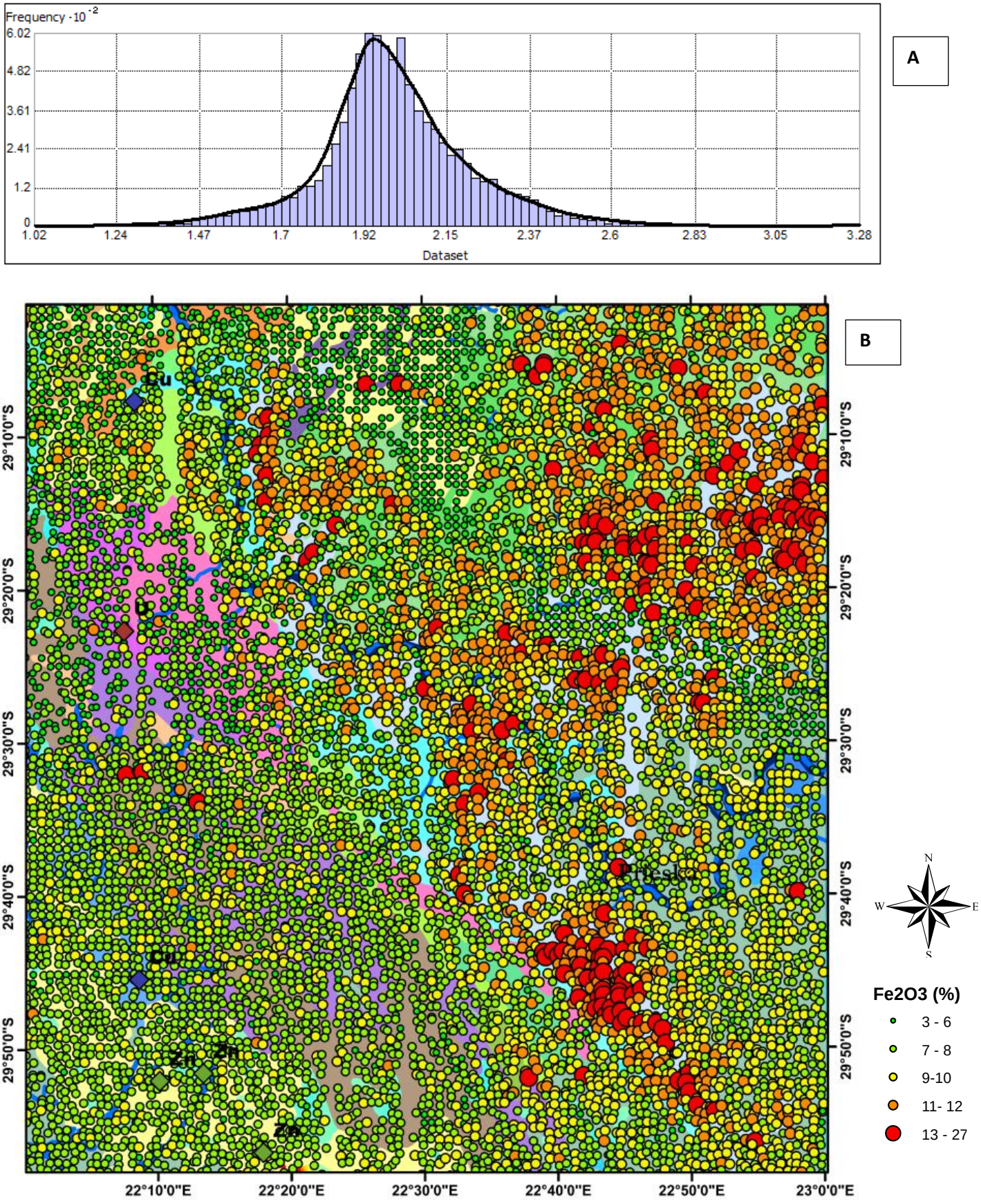



**Figure 4.1.11 a) Histogram frequency distribution showing the skewness and Kurtosis of Fe2O3 (ppm) dataset, b) The Regional geochemical distribution map illustrating the location of Fe2O3 (ppm) anomalies**

## 4.2 Normal Quantile-Quantile plots

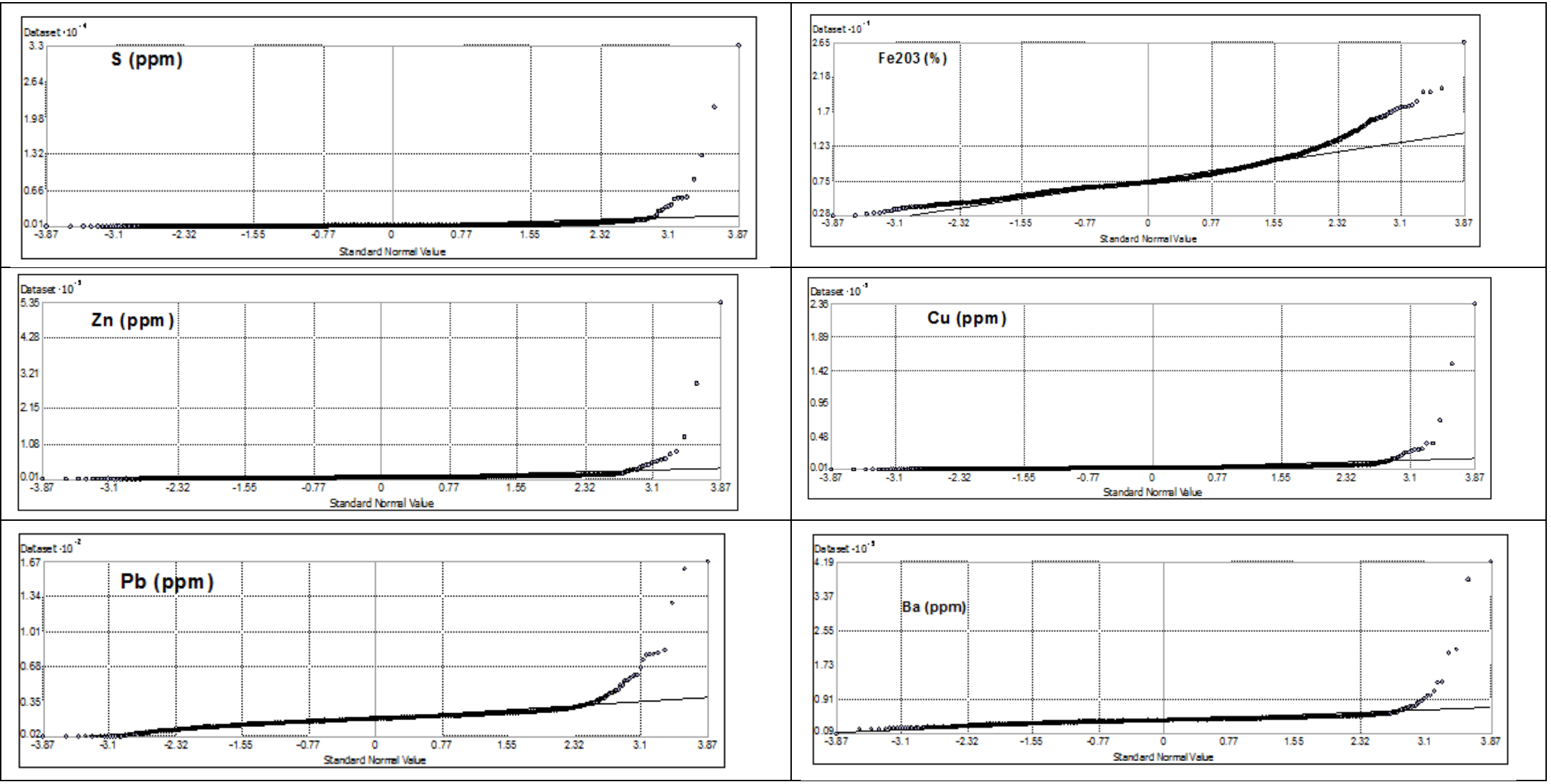



**Figure 4.2: Normal Q-Q plots for data after none transformation, in order to preserve symmetry for the expected values (y-axis) negative values (observed values) on the x-axis are included.**

Most base metal indicators discussed have high values, which are not well reflected in the histograms because extreme values form only a part of the highest concentration bins. However, the extreme values are well visualized on the normal Q–Q plots (Figure 4.2). Normal Q-Q plots for S, Zn, Pb, and Ba have similar trends. The characteristics of these plots includes the following facts; the sample points form a straight line following the diagonal line and curves upwards at the largest values, the plots show a slight positive skewness, this is also be observed on the elements histograms, the outliers are visible on the plot whereby the larger values are much larger than expected and smaller values are not as extreme as would be expected under sampling normal distribution population. Fe normal Q-Q plots is strongly positively skewed, the outlier largest values are much larger than expected on the normal distribution population, consists of the heavy right tail and left tail with values above the straight line.

**4.3 Stream Sediment Exploration Target generation: Geology and Economic geology synthesis Map of Prieska area.**

The primary aim of the exploration target generation is twofold; to generate new areas for exploration activity where favourable geology and no mineral occurrences are coincident, and secondly a rethink in areas of known mineralisation on the possibilities of other styles or models of mineralisation. The geology of Prieska area and the geochemistry was joined using the Analysis tool spatial joint, the aim is to calculate the mean values of Uni-element of the lithostratigraphic unit.

A multi-element technique was applied to delineate the individual geological units present in the study area. The technique was based on the litho-statistics consisting of the highest mean values of elements in each geological unit. Various indices were then derived for each geological unit, consisting of the elements with highest mean values in comparison to other geological units (Appendix 2). It is expected that these indices are suited to best outline these geological units in principle. The indices determined for each geological unit in the Prieska map area are as recorded in Table 4.3.

Table 4.3: Elements relative or in association to the lithostratigraphic unit

| **Geology** | **Index** |
|---|---|
| Zeekoebraat Formation | W, Fe |
| Spioenkop Formation | Cu, Ga, Rb, Zn, S |
| Uitdraai Formation | V, Ni, Cr |
| Waterkop | Ba |
| Ongeluk lava Formation | Co, Ni, |
| Prieskaspoort | Cr, S, Sr, Mg |
| Koegas Group | Nd, Pb, Th |
| Jacomyns Pan | Ag |
| Kalahari Group | Sn |
| Brulsand | Hf, Mo, Nb, Sc, Ta, U |
| Boegoeberg Dam | Zr, As |
| Asbestos Hill | Ce, Fe |

Based on An et al. (1991) the five Fuzzy operators are useful for combining exploration datasets, Fuzzy AND, OR, Algebraic product, algebraic sum and γ-operator. In this study Fuzzy OR operation was applied to combine maps of relevant elements associated with the geology (Table 4.3) and the combination of elements associated with specific geology are the related to the possible mineralisation discussed in chapter 3 determined by the strength of their correlation coefficients.

### *4.3.1 Spioenkop Formation*

The elements of the highest mean averages associated with the Spioenkop Formation is the Cu, Ga, Zn and Rb. Cu and Zn correlates very strong at the correlation coefficient of 0.97. As discussed in section 4.1, the Cu and Zn distribution map indicates that this two elements strongly correlated with the known VMS Copperton deposit.

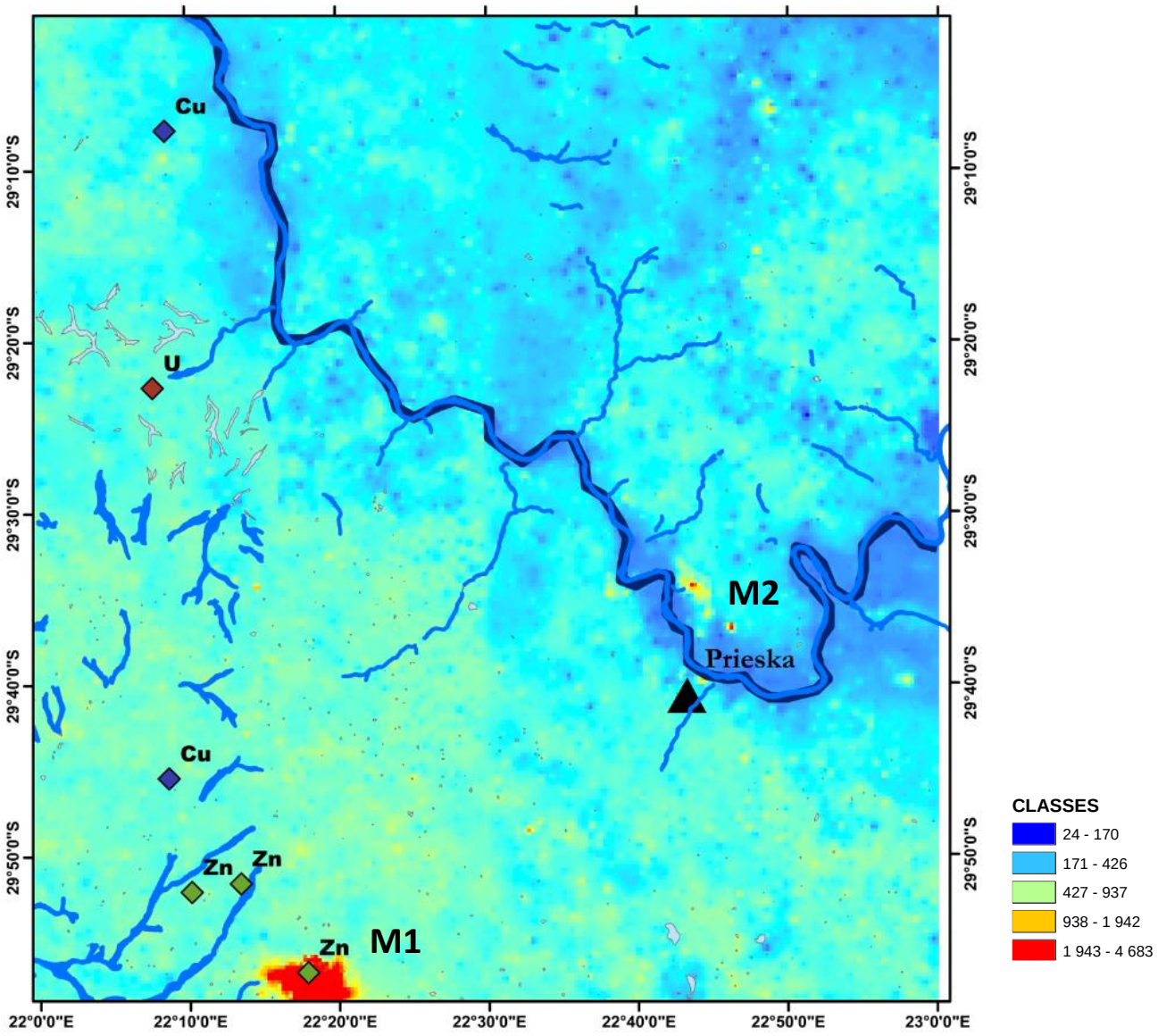



**Figure 4.3.1: Fuzzy OR overlay multi-element map index of Cu, Ga, Zn, and Rb**

Figure 4.3.1 displays a Fuzzy OR overlap multi-element map of Cu, Ga, Zn and Rb. The map index poorly delineate Spioenkop Formation, the second dispersion occur in Uitdraai Formation, Jacomyns pan Formation, Globershoop, and Spioenkop Formation. The observed mineralisation potential areas are labelled (M1 and M2) The M1 anomaly is associated with the known mine area named Copperton Deposit, Prieska mine, the M1 anomaly is overlaying the Kalahari and Dwyka Group The Prieska Cu_Zn is known as the VMS deposit, the most common commodities or minerals exploited in this area are the Zinc, Copper and Sphalerite. The Mine is recorded in the literature as a medium scale abandoned mine. The M2 anomaly is in close vicinity to the Orange River catchment, the anomaly is overlaying the Campbellrand subgroup. Campbell Rand Subgroup belongs to the Ghaap Group. The base mineralisation have been recorded in Ghaap Group is Pering deposit

far northeast about 150km from the study area. The Host rocks to Zn–Pb mineralisation on the Ghaap Plateau are stromatolitic dolomites, with minor oolitic dolomites, chert and carbonaceous shale beds of the Campbell Rand Subgroup (Gutzmer, 2006). The occurrence of the M2 potential mineralisation zones requires follow-up studies.

### *4.3.2 Ongeluk lava Formation*

There is a very strong correlation between the Co and Ni, and moderate to strong correlation between Co and Cr indicator elements. The correlations of Co-Ni-Cr are the indicator of mafic- ultramafic geological index. The strong correlation between Co and Ni can also indicate the base metal mineraization. The Ni-Co covers the sulphides and oxides of interest (Co-Ni-Cr) in ultramafic rocks. Co-Ni is a pathfinder of Ni-Cu.

The Co-Ni anomalies are high values are presented by anomaly M3 – M7 (Figure 4.3.2). The M3 potential mineralisation area to the west of Prieska town covers the Dwyka Group, this mineralisation is identified at the very close vicinity to the Orange River catchment (primary stream) dominant mostly to the south of the catchment. The Co-Ni anomaly (M3) to the north of the Catchment is similar to the Cu-Ga-Zn-Rb anomaly M2 which also cover the Campbellrand Subgroup at the same area, therefore this outline the new potential of base metal mineralisation The M4 anomaly overlay the Dwyka Group, Asbestos Hills and the Skalkseput Granite. The M4 anomaly trends to the north-west following the Skalkseput Granite lithology, at the M7 the Co-Ni anomaly covers the Skalkseput Granite and is associated with the known occurring Uranium commodity, the status of the known Uranium deposit is that the deposit is never exploited.

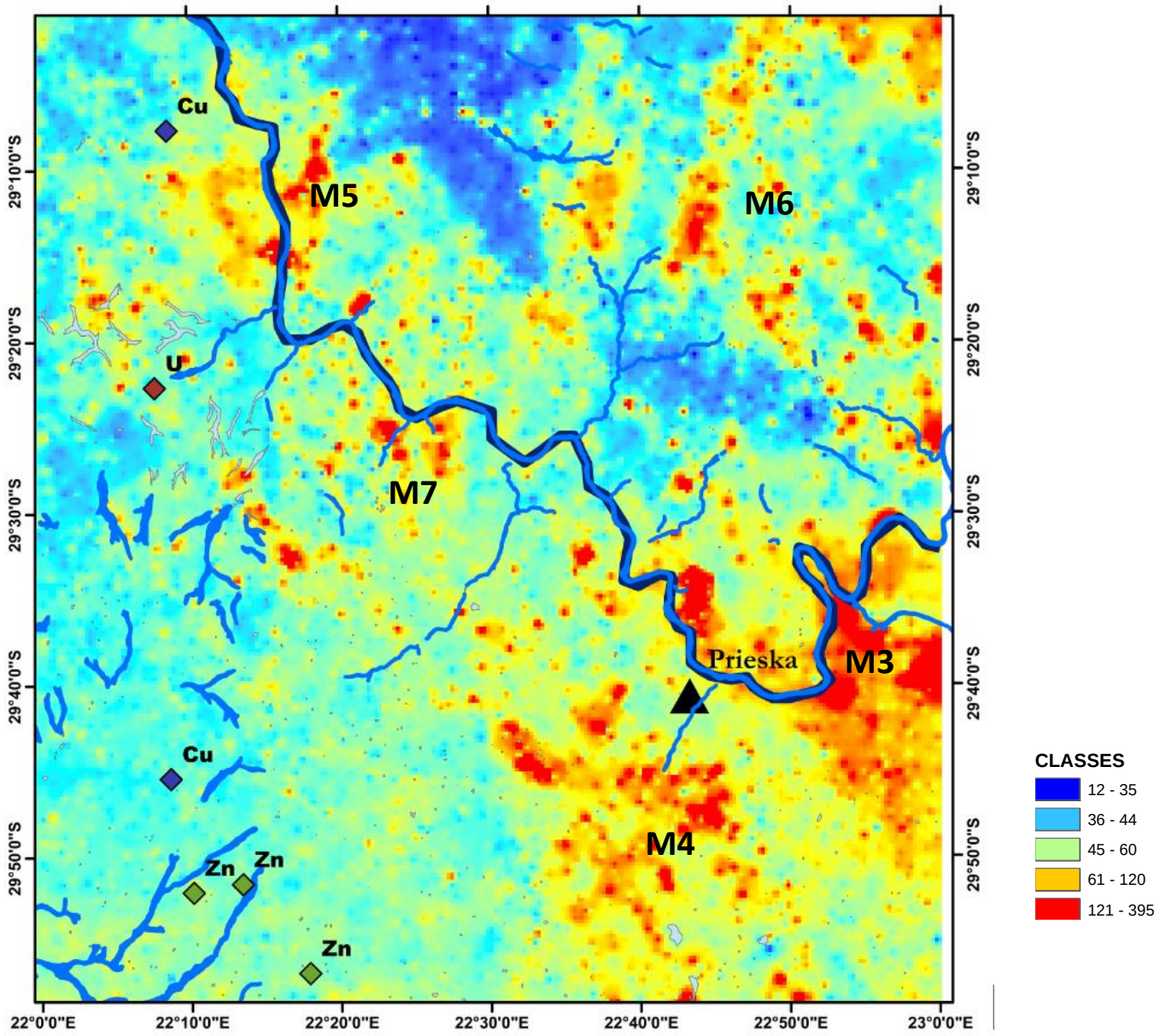



**Figure 4.3.2: the Fuzzy OR overlay multi-element map index of Co and Ni**

The M5 Co-Ni anomaly is in close vicinity with the known small Copper occurrence and the anomaly is evident in and around the Orange River Catchment, this will require follow up study to confirm the parent source of the anomaly, because of its close vicinity with the known Cu occurrence the Co-Ni correlation may possibly indicate the Base (Cu_Zn) mineralisation. Unlike the M7 anomaly associated with Spioenkop Formation and Ongeluk lava Formation. The M6 anomaly overlay the Ongeluk Lava Formation, and Asbestos Hill.

### *4.3.3 Brulsand*

The elements of the highest mean averages associated with the Brulsand are the Hf, Mo, Nb, Sc, Ta, and U. The Hf, Sc, Mo, Nb, and Ta are transition elements and most of are typically treated as being immobile during metamorphic processes and therefore can be useful in understanding the effects of metamorphism. U strongly correlates with Hf, Ta and Nb, and moderately correlates with Mo.

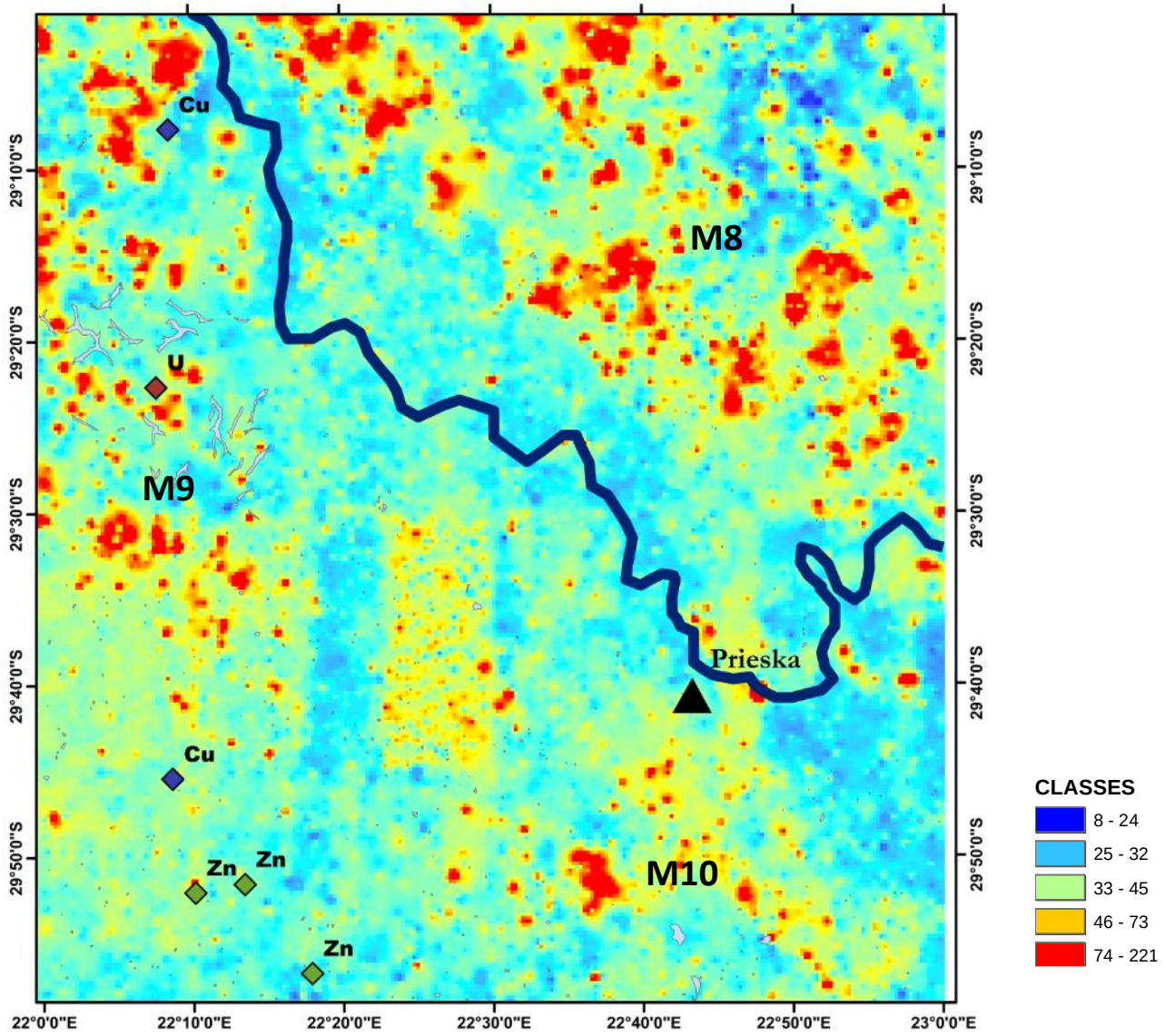



**Figure 4.3.3: the Fuzzy OR overlay of Mo, Nb, Sc, Ta, and U**

The M8 potential mineralisation (Figure 4.3.3) consist of isolated cluster of potential mineralisation zones overlying the Asbestos Hills Subgroup, Koegas Group, Kalahari group, Olifantshoek Supergroup. M9 is associated with known metals occurrences; Cu and U, the isolated cluster of anomalies towards the know Prieska Copperton mine. The M9 potential mineralisation zones on the west of Orange River catchment overlies the Draghoender granite/gneiss, Skalkseput granite, Uitdraai Formation and Zeekoebaart Formation. Granitic rocks rich in pyrochlore, euxenite, brannerite, thorite yield soils rich in Nb, Ta, Ti, rare earths, Sc and Zr, such soils are enriched in dark heavy minerals of which the radioactive species originally contained in the parent rocks form a major fraction (Boyle, 1982). The Sc, U, Nb, and Ta are indicators of uranium-bearing minerals in granitic, syenitic, magmatitic, pegmatitic and aplitic bodies and complexes. Strauss and Elsenbroek (2006) found in a study on South African alkali and carbonatite complexes that Nb is by far the strongest and most common indicator for these complexes in soils followed by Zr.

### 4.4 Stream Sediment Exploration Target generation: Economic geology synthesis Map of Prieska area

The following geochemical indices are regarded as potential target generators for the Prieska area based on the predominant geology in the area coupled with the single element distribution patterns. The Cu_Zn for VMS Zn_Cu deposit, Ni_Co_Cr ultramafic Ni_Cr (±Cu) deposit and Zr_Nb_U_Th_Hf_Ta for the heavy mineral placer deposits. First the inverse distance weighted interpolation (IDW) was applied to create new raster files for each index element. Then the indices were calculated using the fuzzy overlay OR function from ARCGIS, the advantage of using fuzzy OR overlay is generally provides a better result in cases where the indicator elements are not always associated and is better suited for the secondary dispersion where associated elements in the primary environment are likely to be separated.

#### *4.4.1 Cu_Zn index for VMS deposit*

The anomaly (Figure 4.4.1) delineates the known Copperton mine in Prieska area, the Copperton ore body occurs in a series of quartz-feldspar rocks quartz-biotite gneisses and quartz- plagioclase-amphibole gneisses, which are called Copperton Volcanic Pile.

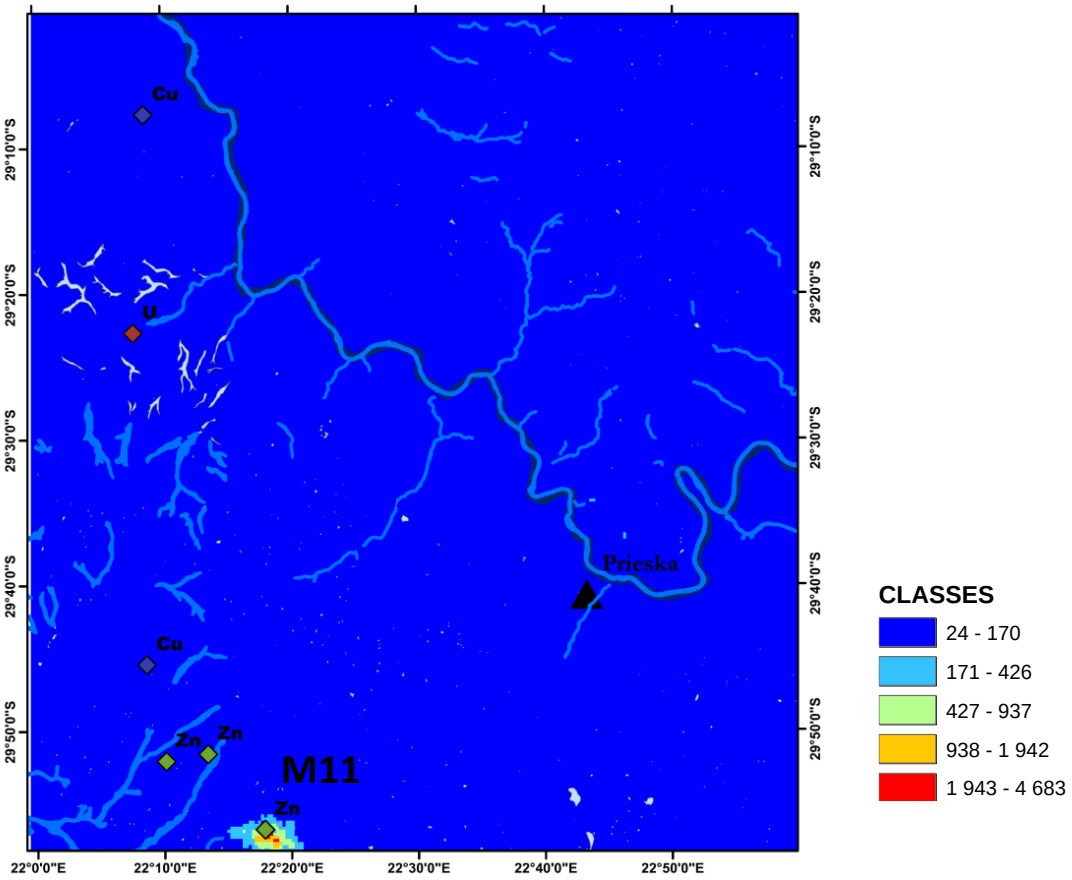



**Figure 4.4.1: the Fuzzy OR overlay map for Cu_Zn index.**

### *4.4.2 Ni_Co_Cr for the ultramafic Ni_Cr (±Cu) deposit*

The anomaly M12 associated with Koegas Group, Ongeluk lava Formation and Asbestos Hill Subgroup (Figure 4.4.2) is a preferred potential target for ultramafic Ni_ Cr (±Cu) deposit. The anomaly overlies the banded Iron Formation of the Asbestos Hill Subgroup, the Asbestos Hill Subgroup is Fe-rich. The anomaly M14 is associated with the known Cu occurrence straddles the Campbell Rand Subgroup, and Zeekoebaart Formation is identified as the secondary target. Anomaly M13 is also identified as the secondary potential target for ultramafic Ni_Cr (±Cu), it is associated with Dwyka Group.

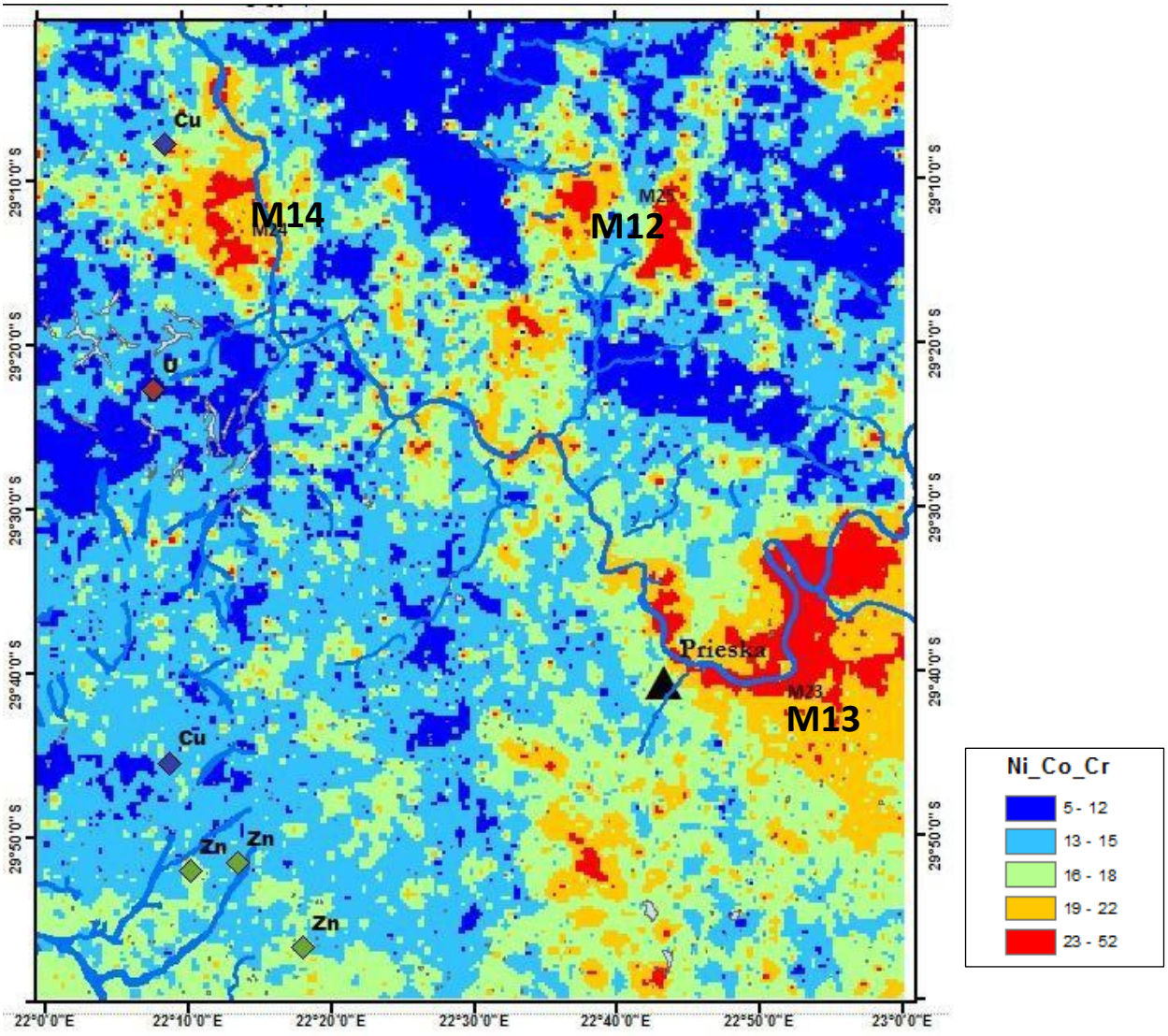



**Figure 4.4.2: the Fuzzy OR overlay map for Ni, Co and Cr index.**

### *4.4.3 Zr_Nb_U_Th_Hf_Ta for the heavy mineral deposits*

Zr_Nb_U_Th_Hf_Ta are high field strength elements associated with the carbonatites deposits and alkaline magmatic complexes, however the carbonatites deposits around the Prieska area are not discovered. The high field strength elements are primary indicators of the REE deposit. These elements are associated as incompatible ions, within alkaline igneous melts, which by their emplacement is controlled by the failed rift zone or deep seated suture.

The anomalies of the Zr_Nb_U_Th_Hf_Ta (Figure 4.4.3) may be due to thorium in waste rock or sediment; dust from mining activities in the surrounding, and possible water contamination from spillage or leakage of chemical solutions used to leach and process ore. Asbestiform amphiboles that are present in waste dumps. The correlation of the Cu-Pb-Zn anomaly with alkali elements (Nb, Zr, Th, and U) and REEs (in Table 3.3), suggests there is a possibility that the M26 –M29 anomaly are alkali-granitic genetic origin. The anomaly could therefore indicate the presence of Cu, Pb, Zn and As sulphides associated with alkali elements and REEs, which makes it a very promising target however the map (Figure 4.4.3) display a batch effect specifically anomaly M26 and 27, and therefore it is not suitable for interpretation.

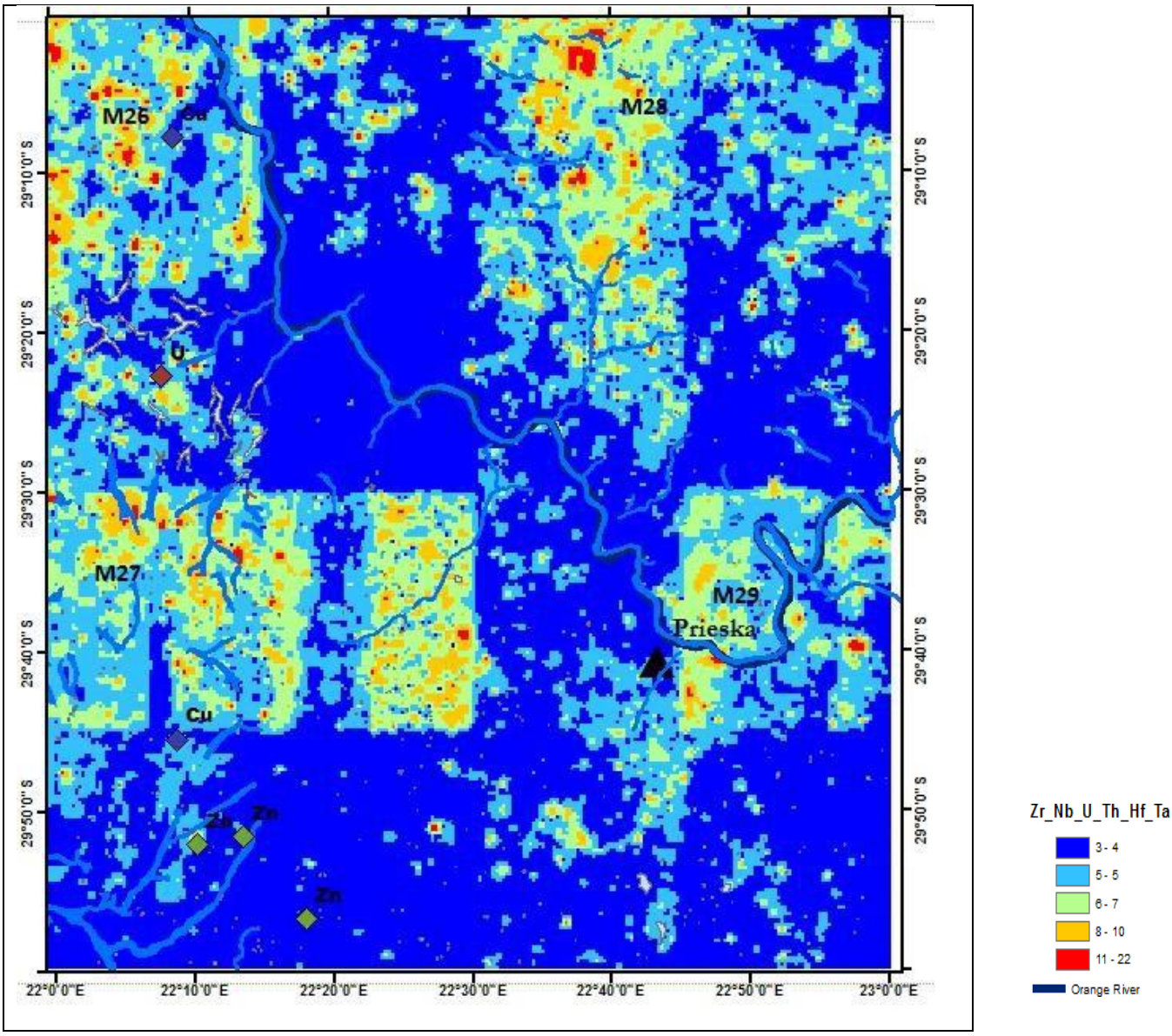



**Figure 4.4.3: the Fuzzy OR overlay of Zr_Nb_U_Th_Hf_Ta**

# CHAPTER 5

## Conclusions and Recommendations

Prieska study area generally forms part of the Namaqua Metamorphic Province and the Griqualand-West Basin. The Kalahari Aeolian sand covers the geology on the area around Prieska Cu-Zn mine. The host sequence in the Copperton district is, from the base: Smouspan Gneiss Member, Prieska Copper Mines Member, and Vogelstruisbult Member (Figure 2.9 and Figure 2.3) (Bailie and Gutzmer, 2011; Theart *et al.,* 1989). The study area is extensively covered by aeolian sand, secondary dispersion patterns of the elements in the stream sediment may also destroy the primary association of elements. To overcome this difficulty, a Fuzzy OR overlay of indicator was produced. Fuzzy OR generally provides a better result in cases where the indicator elements are not always associated and is better suited for the secondary dispersion where associated elements in the primary environment are likely to be separated.

The statistics of the univariate elements analysed from Prieska sediments area presented in Appendix 3, the dataset was used in detection of anomalies. The descriptive statistics (Appendix 3) results shows that the Ag, Co, Ga, Mo, Nb, Pb, Sb, Sn, Sc, Ta, Th, U, and W concentrations exhibited generally low standard deviation and coefficient of variation values , suggesting a homogenous spatial distribution. In contrast As, Ba, Ce, Cr, Cu, Hf, Nd, Ni, Rb, Sr, S, V, Zr and Zn contents showed a heterogeneous spatial distribution, reflected by high coefficient of variation and large standard deviation. The difference between the median and mean values of high coefficient of variation of the As, Ba, Ce, Cr, Cu, Hf, Nd, Ni, Rb, Sr, S, V, Zr and Zn may be attributed to the extremely high values of these trace elements (their maximum values, refer to Appendix 2 and Appendix 3). Based on the box plots (Appendix 4) and the normal Q-Q plots (Figure 4.2) the outliers are observed of the high coefficient of variations which might be sourced from the mine wastes.

The Fuzzy OR maps give a summary of the potential targets for mineralisation within the study area. Anomaly M1 and M2 associated with Spioenkop Formation though the anomaly does not delineate the Spioenkop Formation but Dwyka Group Sediments, Kalahari Group and Campbell Rand Subgroup. This anomaly signatures are characterised by the one or more of these elements Cu, Ga, Zn, Rb, Pb, Mo, and Ba. Barium is a powerful indicator tool of gossan and also be used as an indicator for Zn–Pb deposits, the dataset shows a significant relationship between the Ba and Zn. The relationship between these elements therefore delineate M1 and M2 as potential target for VMS deposit.

The anomaly M2 in close vicinity to the Orange River Catchment should be further studied, a follow-up study is therefore recommended. The Cu and Zn are generally interpreted as pollution related or may be as a result of metal dispersion from the mine waste. The Zn and Cu high concentrations are not distributed across the Prieska area, the Fuzzy OR overlay of these elements are only elevated in the known Copperton mine area and on the M2 potential VMS mineralisation target area. The anomaly M2 associated with Campbell Rand Subgroup may be as a result of metal dispersion or sourced from the parent underlying rocks.

The Pb and S are also elevated on the known Copperton mine, these elements strongly correlates with the Zn. The Pb and S are likely to be associated with the generic anthropogenic source including sewage discharge, agricultural practises and various kinds of industrial activities. M11 is definitely a VMS mineralisation target, the anomaly overlies the Copperton mine. The high Cu, Zn and Pb are derived from the ore minerals related VMS deposits. The Fe elevated concentration ( Figure 4.1.11) are derived from both primary minerals which are not directly related to the VMS or Co_Ni (±Cu) (illustrated in Figure 4.3.1 and Figure 4.3.2) mineralisation within the study area or from ore related minerals of deposits hosted in Banded Iron formation of the Asbestos Hills Subgroup.

The Cr, Ni reflect ultramafic fraction of the stream sediments. The Ni and Cr originate from direct ophiolitic sequences erosion and the recycling of the rocks enriched in ultramafic debris. The M13 and M14 anomaly are traced along the Orange river Catchment, on the Ghaap group which occurs NW to SE of the study area and north of the Orange River Catchment. Ghaap Group consists of shale, sandstone, andesite, and dolomite, and comprised of the magnesium, carbonate-rich Formation such as Vryburg Formation. M13 and M24 potential mineralisation are possibly sourced from ultramafic debris transported from the Ghaap Group by the Orange River Catchment, however this potential target will require follow-up studies for verification. There is a very high Cu-Zn correlation coefficient calculated for samples near the Copperton deposit.

## 5.1 Recommendations

Indicator elements in stream sediments sample represents either mineralisation or post- mineralisation processes. The processes that affect the indicator elements distribution patterns, these process includes weathering, erosion of ore bodies and adjacent mineralised rock, contamination of pollutants, regolith, topographic gradient vegetation density and/ or climate. In this study integration of mineral exploration methods such as remote sensing, geophysics and petrography are recommended, this follow-up studies will assist in determining the extent of the anomaly.

The airborne geophysics studies must be conducted over the study area. Low level airborne electromagnetic (EM) surveys over the target area (M1-M29) especially the M2 and M3 which delineate the possibility of the base metal mineralisation is recommended. The high density stream sediments sampling on the grid and a depth of at least 50 meters to minimize the effect of Aeolian sand cover must be conducted. Petrography is another important tool, to understand the mineralogy of the study area underlying rocks. The detailed analysis of minerals by optical microscopy in thin section and micro-texture and structure is recommended in order to understand the origin and history of the rock.

Remote sensing will also be advantageous in conducting geological traverses of the study area in which anomalies of one or more of the above mentioned elements occur to establish the significance of the anomalies. Remote sensing imagery will also provide information on rock composition or rock alteration which is associated with the indicative of the presence of mineral deposits. Ore deposits are localized along regional and local fracture patterns, the Landsat and radar images are used to map these fracture pattern. Using multiple tools of exploration such as geology, structures, geochemistry, and drainage pattern are recommended for use in ArcGIS as thematic layers to generate the potential mineralisation targets.

**References**


Almond, J.E., 2018 Kuruman wind energy facility phase 3 near Kuruman, Kuruman district, Northern Cape. Natura Viva cc, Cape Town.

An, P., Moon, W.M., and Rencz, A.N., 1991. Application of fuzzy theory for integration of geological, geophysical and remotely sensed data. Canadian Jr. Explor. Geophy. 27: 1-11.

Anhaeusser C.R. (2019) Palaeo- Meso- and Neoarchaean Granite-Greenstone Basement Geology and Related Rocks of the Central and Western Kaapvaal Craton, South Africa. In: Kröner A., Hofmann A. (eds) The Archaean Geology of the Kaapvaal Craton, Southern Africa. Regional Geology Reviews

Armstrong, R. (1989). 1988 Annual Technical Report of the Geological Survey of South Africa.

Department of Mineral and Energy Affairs, pp. 22

Bailie, R. and Gutzmer, J., 2011. Age and primary architecture of the Copperton Zn-Cu VMS deposit, Northern Cape Province, South Africa. *Ore Geology Reviews* **39:** pp. 164–179.

Bailie, R., Gutzmer, J., Rajesh, H.M. and Armstrong, R., 2011. Age of ferroan A-type post-tectonic granitoids of the southern part of the Keimoes Suite, Northern Cape Province, South Africa. *Journal of African Earth Sciences*, **60**, pp. 153–174

Basson, I.J., Watkeys, M.K., and Phillips, D (2005) Structural evolution and tectonic context of the Mfongosi Group, Natal thrust front, Tugela terrane, South Africa. *African Earth Science* **43**. p.415-432

Basson, I.J., Watkeys, M.K., Perritt, S., and Menzies, H.A., (2004) Geochmistry Correlation Between Metasediments of the Mfongosi group of the Natal Sector of the Namaqua-Natal Metamorphis Province, South Affrica and the Ahlmannryggen group of the Grunehogna Province. *Gondwana Research* **7:1**, p.415-432

Black, D.E., 2015. Stratigraphic characterisation of the Collingham Formation in the context of shale gas from a borehole (SFT 2) near Jansenville, Eastern Cape, South Africa. Unpublished MSc. Thesis, Nelson Mandela Metropolitan University, South Africa

Boelema, R., 1994. The Metallogeny of the Upington and Kenhardt area, Northern Cape. MSc Thesis.

Rhodes University, Grahamstown.

Bokana, R.N., 2005. The Lithogeochemical characterization of the Hondekloof nickel mineralisation, Kliprand area, Garies terrane, Namaqualand, South Africa. University of the Western Cape.

Botha, B. J. Y., Grobler, N. J., Linstrom, W., and Smit, C. A. (1976). Stratigraphic correlation between the Kheis Matsap formations and their relation to the Namaqualand Metamorphic Complex. *Tram. Geol. Soc. S. Afr.,* **79**, p304-311.

Buhlmann, L, Philpott, D.E., Scott, M.J., and Sanders, R.N. 1975. The status of exploration geochemistry in southern Africa, in Geochemical Exploration 1974, Elsevier Pubi. Co~ Amsterdam, pp. 51-64.

Bumby, A.J., Eriksson, P.G., Catuneanu, O., Nelson, D.R., Rigby, M.J. 2012. Mesoarchaean and Palaeo-proterozoic sedimentary sequence stratigraphy of the Kaapvaal craton. J. Marine Petrol. Geol.

Boyle, R.W., 1982. Geochemical Prospecting for Thorium and Uranium Deposits. Developments in Economic Geology 16, 42 p.

Bradshaw, J. D., S. D. Weaver, and M. G. Laird, 1972 Suspect terranes and Cambrian tectonics in northern Victoria Land, Antarctica, in Tectonostratigraphic Terranes of the Circum-Pacific Region, Earth Sci. Ser., vol. 1, edited by D. G. Howell, pp. 467 – 479, Circum-Pac. Counc. for Energy and Miner. Resour., Houston, Tex.,

Carranza, E.J.M., 1994. A Catchment Basin Approach to the Analysis of Reconnaissance

Geochemica- Geological Data from Albay province, Phillipines. MSc thesis, Delft, ITC, pp. 206

Chork, C.Y. and Mazzuchelli, R.H., 1989. Spatial Filtering of Exploration Geochemical Data using EDA and Robust Statistics. *Journal of Geochemical Exploration*, **32 (3),** p. 221-243.

Cifti, E., Kolayli, H. and Tokel, S., 2005. Lead-Arsenic Soil Geochemical Study as an Exploration Guide over the Killik Volcanogenic Massive Sulfide Deposit, Northeastern Turkey. *Journal of Geochemical Exploration,* **86**, p. 49-59.

Cornell, D.H., 2019. Lithostratigraphy of the Copperton Formation, Areachap Group. *South African Journal of Geology (2019)* **122 (4),** p 561–570.

Cornell D. H., R.J. Thomas, H.F.G. Moen, D.L. Reid, J.M. Moore, R.L. Gibson, 2006: The Namaqua- Natal Province. *In*, Johnson M.R., C.R. Anhaeusser, R.J. Thomas (eds*), The Geology of South Africa*. Geological Society of South Africa, Johannesburg/ Council for geosciences, Pretoria, p. 325-379

Cornell D.H., Zack, T,. Andersen, T., Corfu, F., Frei, D. and van Schijndel, V,. 2016 The U-Pb zircon geochronology of the Palaeoproperozoic Hartley formation porphyry by six methods with age uncertainty approaching 1 Ma. *S. Afr. J. Geol.,* **119 (3)** p. 473-494

Cornell D.H., A Pettersson, 2007: Ion probe zircon dating of metasediments from the Areachap and Kakamas Terranes, Namaqua-Natal Province and the stratigraphic integrity of the Areachap Group. *South African Journal of Geology,* **v. 110**, p. 575-584.

Cornell, D.H., Hawkesworth, C.J., Van Calsteren, P. and Scott, W.D., 1986. Sm-Nd study of Precambrian crustal development in the Prieska-Copperton region, Cape Province. *Transactions of the Geological Society of South Africa*, **89**, p.17–28.

Council for Geoscience (CGS) ArcGIS database, accessed on 06 January 2020.

Dahlem, D.H., 1976. A national hydrogeochemical sampling program for uranium; *Soc. Min. Eng. /Am. Inst. Min. Met. Eng.,* Preprint 76-L-38, 22 p.

Deer, W.A., R.A. Howie, and J. Zussman (1963) Rock-forming minerals, v. 2, chain silicates, p.249-262.

Dewey, J.P., Robb, L. and Van Schalkwyk., 2006. Did Bushmanland extensionally unroof Namaqualand? Precambrian Research doi:10.1016/j.precamres.2006.07.007

De Villiers, J., Sohnge, P. G., 1959. The geology of the Richtersveld, memoir 48. Department of mines, Government Printer, 295

Duchesne, J.C., Auwera, J.V., Liegeois, J.P., Barton, E. S., Cliford, T. N., 2007. Geochemical constraints of the petrogenesis of the O'okiep Koperberg Duite and granitic plutons in Namaqualand, South Africa: A crustal source in Namaquan (Grenville) times. *Science Direct*, Volume 153, p116-142

Diener, J.F.A., White. R.W., Link. K., Dreyer. T.S and Moodley. A, 2012 Clockwise, low-P metamorphism of the Aus granulite terrain, southern Namibia, during the Mesoproterozoic Namaqua Orogeny. Precambrian Research, doi:10.1016/j.precamres.2012.11.009

Du Plessis, P.I. 1993. The Sedimentology of the Kalahari Group in Four study areas in Northern Botswana. MSc (thesis). University of Stellenbosch.

Elsenbroek, J.H. 1995. Instrumentation and Analytical technique for the analysis of regional geochemical samples used at the South African Council for Geoscience. An overview. DOI: 10.1039/an995200153

Eriksson, P, G,. Altermann, W., Catuneanu, O. Van der Merwe and Bumby A.J. (2001) Major influences on the evolution of the Kaapvaal craton. *Sedimentary Geology* **141-142**, p.205-231

Eriksson, P.G., (2012). Personal communication. University of Pretoria, Department of Geology.

Eriksson, P.G., Altermann, W., and Hattingth, P.J., (1993). Bushveld Complex, South Africa. *Minerial deposita* **30** 98p.

Eriksson, P.G., Altermann, W. and Hartzer, F.J. The Transvaal Super group and its Precursors. Johnson, M.R., Anhaeusser, C.R. and Thomas R.J. (2006). The Geology of South Africa*. Geology society of South Africa*, Johannesburg.

Fairey, B. Tsikos, H. Corfu, F and Polteau, S. 2013 U–Pb systematics in carbonates of the Postmasburg Group, Transvaal Supergroup, South Africa: primary versus metasomatic controls. *Precambrian Research,* **231** p. 194-205

Fifield, F.W. and Haines, P.J., 1995. Environment Analytical Chemistry, 3rd edition, Blackie Academic and Professional, London, pp. 424

Fletcher, W.K., Lahiri, R., Caughlin, B.L., and Blok, H., 1995, Use of a sensitive analytical method and the silt-clay fraction of stream sediments in exploration for gold in northern Thailand: J. *Geochem. Explor.,* **55,** pp. 301-307

Fransson, M., 2008: Pb-U zircon dating of metasedimentary rocks in the Areachap, Kakamas and Bushmanland Terranes in Namaqua Province, South Africa. Master thesis, Göteborgs.

Garret, R.G., 1989. The role of Computers in Exploration Geochemistry. In G.D. Garland (ed.) Proceedings of Exploration 87, *Ontario Geological Survey, Toronto*, **3**, p. 586-608.

Ghavami-Riabi, R. (2006). Geochemical exploration for base metal sulphide deposits in an arid environment (eastern Namaqua Metamorphic Province), South Africa. PhD thesis, University of Pretoria, Abstract

Ghavami-Riabi, R. Theart, H.F.J and De Jager, C. 2008. Detection of concealed Cu–Zn massive sulfide mineralisation below eolian sand and a calcrete cover in the eastern part of the Namaqua Metamorphic Province, *South Africa Journal of Geochemical Exploration,* **97 (2–3)** , p. 83- 101.

Ginsburg, I.I, 1960, Principles of geochemical prospecting New York, Pergamon Press 311.

Geerthsen, K. Maher, M.J. and Meyer R. 1991. The western edge of the Griqualand West Basin- A geophysical perspective. *S.Afr .I.Geol.* , **94(1)** p. 96-103

Greyling, L.N, Huizenga, J.M and Gutzmer, J. 2001. A Review Of Mississippi Valley-Type Deposits With Emphasis On the Palaeoproterozoic Pering Pb-Zn Deposit, South Africa. University of Witwatersrand, Johannesburg.

Geringer, G.J. Schoch, A.E. Sukanov, M. and Zhuravlev, D. 1998 Geochemical and isotopic characteristics of different types of anorthosite in the Namaqua mobile belt*, South Africa Chem. Geol.*, **145** p. 17-46

Grobbelaar, W.S. Burger, M.A. Pretorius, A.I. Marais, W. van Niekerk I.J.M. 1995 Stratigraphic and structural setting of the Griqualand West and Olifantshoek Sequences at Black Rock, Boshoek and Rooinekke Mines, Griqualand West, *South Africa Mineral. Deposita,* **30**, pp. 152-161

Gumsley, A. 2017. The Ongeluk LIP: a newly large defined large Igneous province on the critical Neoarchean-Paleoproterozoic boundary on the Kaapvaal Craton, South Africa. http://www.largeigneousprovinces.org/17mar Accessed (24/05/2018).

Gutzmer, J 2016. The Paleoproterozoic carbonate-hosted Pering Zn–Pb deposit, South Africa: I. Styles of brecciation and mineralisation. Available from: https://www.researchgate.net/publication/226551125_The_Paleoproterozoic_carbonate-hosted_Pering_Zn-

Pb_deposit_South_Africa_I_Styles_of_brecciation_and_mineralisation [accessed Jan 17 2019].

Hanekom, H.L. 1966. The crocidolite deposits of the Northern Cape Province. D.Sc. thesis (unpubl.), Univ. Pretoria, pp 213

Hart, H. P., 1988. Asbestos in South Africa. *J.* S. *Atr. Inst. Min. Metal/.* **88: 6**, p 185-198

Hilliard, P. 1999. Structural evolution and tectono stratigraphy of the Kheis Orogen and its relationship to the south western margin of the Kaapvaal Craton.

Howarth, R.J., 1984. Statistical Applications in Geochemical Prospecting: A Survey of recent Developments, *Journal, Geochemical Exploration*, **21**, p. 41-61.

Humphreys, H.C., Van Bever Donker, J.M., Scott, W.O., and Van Schalkwyk, L. 1988. The early deformational history of the eastern Namaqua Province: new evidence from Prieska Copper Mines. *S. Afr. J. Geol.* 91:174-183

Johnson, M.R., Anhaeusser, C.R. and Thomas, R.J. (Eds), 2006. The Geology of South Africa. Geological Society of South Africa, Johannesburg/Council for Geoscience, Pretoria, 507 p.

Johnston, S. T., McCourt, S., Mitchell, A., and Bisnath, A. (2003). The Tugela terrane, Natal belt, Kibaran magmatism and tectonism along the southeast margin of Kaapvaal craton. South Africa*. South African Journal of Geology* **106**.pp85-97

Kendall, B. van Acken, D. and Creaser, R.A., 2012. Depositional age of the early Paleoproterozoic Klipputs Member, Nelani Formation (Ghaap Group), Transvaal. *Precambrian Research* **237**:1-12

Land, J.S., Tsikos, H., Cousins, D., Luvizotto, G., Zack, T., 2017. Origin of red beds and paleosols in the Palaeoproterozoic Transvaal and Olifansthoek Supergroup of South Africa: provenance versus metasomatic controls*. Geol. J.*, (In Press). doi:10.1002/gj.2885

Ledwaba, P.F. 2014. Tiger's eye in the Northern Cape Province - potential for employment creation and poverty alleviation. *J. S. Afr. Inst. Min. Metall.* **114, 11p**.

Lepeltier, C., 1969. A Simplified Statistical Treatment of Geochemical Data by Graphical Representation: *Econ. Geol.,* **64.** Pp539-550

Manninen, T., Eerola, T., Makitie, H., Vuori, S., Luttinen, A., Senvano, A. and Manhica, V. 2008. The Karoo volcanic rocks and related intrusions in southern and central Mozambique. *Geological Survey of Finland, Special Paper* **48**, p211–250, 34

Mapukule, L.E., 2009. Interpretation of Regional Geochemical data as an aid to exploration Target Generation in the North West Province, South Africa. MSc (geology). University of Fort Hare. (Unpublished).

Maré L., de Kock M., Cairncross B. and Mouri H., 2014. Application of magnetic geothermometers in sedimentary basins: an example from the western Karoo Basin, South Africa. *South African Journal of Geology*, **117,** p 1–14.

Matmon A., Hidy A.J., Vainer S., Crouvi O., Fink D., Erel Y., ASTER Team, Horwitz L.K., & Chazan M. 2015. New chronology for the southern Kalahari Group sediments with implications for sediment-cycle dynamics and early hominin occupation. *Quaternary Research*.

**Appendices**

***Appendix 1: XRF and its principles.***

XRF has the advantage of being non-destructive, multi-elemental, fast and cost effective compared to other competitive techniques such as Atomic Absorption Spectrometry (ASS) or Inductively Coupled Plasma Spectrometry (ICP OES). A fairly uniform detection limits across a large portion of Periodic Table mean that the technique can be used for a wide range of concentrations from 100% to 0.01% (Van Grieken and Markowicz, 2002).

X-rays are produced by irradiating a sample with high energy photons produced by primary X-ray tube. When a high energy primary X-ray collides with an atom, an electron can be ejected from a low energy level creating an electron vacancy. When an electron from a higher energy level fills the vacancy, a secondary X-ray is created characteristic of that element. XRF analysis devices can be largely categorized into wavelength-dispersive X-ray spectrometry (WDX) and energy-dispersive X-ray spectrometry (EDX). WDX disperses the fluorescent X-ray generated in the sample using dispersion crystal and measures it using a goniometer, resulting in a large size. The detector in EDX on the other hand, has a superior energy resolution and requires no dispersion system, which enable downsizing of the device. Interaction of X-rays with sample creates secondary diffracted beams of X-rays related to inter-planner spacing in the crystalline powder according Bragg's Law:

$n = 2d\ sin\theta$ Equation 1.

Where: n is an integer, λ is the wavelength of X-rays; d is the inter-planar spacing generating the diffraction and is the $\theta$ diffraction angle.

***Appendix 2: The mean statistics of the each element relative or in association to the lithostratigraphic unit***

| LITHOSTRATIGRAPHY. | Ag | As_ | Ba | Ce | Co | Cr | Cu | Ga |
|---|---|---|---|---|---|---|---|---|
| | | | | | | | | |
| KALAHARI | 5.15 | 12.72 | 417.26 | 65.58 | 12.98 | 118.74 | 29.82 | 18.70 |
| DWYKA | 4.99 | 14.35 | 391.59 | 56.38 | 14.01 | 135.78 | 30.85 | 19.99 |
| WATERKOP | 5.29 | 14.66 | **474.63** | 56.96 | 15.80 | 143.51 | 33.95 | 21.24 |
| JACOMYNS PAN | **7.55** | 9.66 | 377.78 | 45.22 | 13.27 | 154.05 | 26.71 | 14.50 |
| SPIOENKOP | 4.02 | 6.77 | 468.12 | 64.24 | 15.00 | 118.87 | **42.20** | 24.02 |
| GROBLERSHOOP | 5.51 | 10.26 | 393.94 | 62.29 | 11.53 | 115.55 | 25.59 | 14.17 |
| UITDRAAI | 4.00 | 14.39 | 457.01 | 71.09 | 14.50 | 133.47 | 35.50 | 21.11 |
| BRULSAND | 5.02 | 44.58 | 400.53 | 71.57 | 18.88 | 185.49 | 38.97 | 18.15 |
| MATSAP | 4.00 | 6.96 | 429.50 | 66.83 | 15.26 | 130.54 | 36.91 | 21.92 |
| BOEGOEBERG DAM | 4.92 | 36.13 | 387.06 | 59.31 | 16.43 | 163.74 | 32.28 | 15.53 |
| OLIFANTSHOEK | 4.00 | 5.76 | 353.24 | 43.75 | 12.74 | 128.96 | 24.33 | 17.84 |
| GHAAP | 5.44 | 16.99 | 382.82 | 65.47 | 15.77 | 146.78 | 31.53 | 14.92 |
| ONGELUK | 4.00 | 5.59 | 382.09 | 54.99 | **22.68** | 180.52 | 41.84 | 19.02 |
| KOEGAS | 4.89 | 17.23 | 468.09 | 86.32 | 13.79 | 155.79 | 34.74 | 23.10 |
| ASBESTOS HILLS | 5.03 | 23.09 | 387.26 | **151.11** | 13.73 | 140.02 | 29.90 | 15.64 |
| CAMPBELLRAND | 5.58 | **31.17** | 388.51 | 57.56 | 15.52 | 147.32 | 33.21 | 15.50 |
| PRIESKASPOORT | 5.48 | 27.55 | 359.52 | 72.15 | 18.03 | **213.87** | 34.37 | 15.45 |
| DOORNFONTEIN | 4.00 | 16.81 | 356.31 | 46.00 | 13.89 | 127.61 | 31.68 | 15.09 |
| SKALKESPUT | 4.68 | 12.61 | 431.32 | 79.49 | 16.71 | 153.07 | 33.63 | 21.11 |
| DRAGHOENDER GRANITE | 4.00 | 4.00 | 293.09 | 36.16 | 10.32 | 94.26 | 26.93 | 13.32 |
| ZEEKOEBAART | 5.05 | 25.33 | 405.59 | 45.99 | 13.69 | 134.75 | 31.45 | **23.59** |

**Appendix 2: The mean statistics of the each element relative or in association to the lithostratigraphic unit**

| LITHOSTRATIGRAPHY. | Hf | Mo | Nb | Nd | Ni | Pb | Rb | S |
|---|---|---|---|---|---|---|---|---|
| | | | | | | | | |
| KALAHARI | 15.87 | 2.00 | 22.75 | 32.44 | 31.42 | 20.74 | 93.46 | 220.14 |
| DWYKA | 21.57 | 2.03 | 23.52 | 32.02 | 39.19 | 18.52 | 83.91 | 231.57 |
| WATERKOP | 18.08 | 2.11 | 27.10 | 34.87 | 44.26 | 19.66 | 88.67 | 330.74 |
| JACOMYNS PAN | 16.30 | 2.00 | 25.33 | 30.85 | 33.30 | 20.61 | 77.08 | 149.54 |
| SPIOENKOP | 14.89 | 2.00 | 21.29 | 34.03 | 39.55 | 18.48 | **105.22** | 128.54 |
| GROBLERSHOOP | 18.85 | 2.00 | 22.24 | 35.58 | 29.39 | 18.45 | 91.38 | 175.04 |
| UITDRAAI | 23.03 | 2.20 | 25.47 | 38.59 | 38.51 | 21.53 | 88.17 | 153.18 |
| BRULSAND | **41.97** | **2.85** | **33.22** | 33.88 | 43.48 | 18.65 | 83.74 | 109.66 |
| MATSAP | 18.54 | 2.00 | 25.59 | 28.71 | 42.81 | 19.14 | 94.04 | 174.34 |
| BOEGOEBERG DAM | 35.17 | 2.66 | 28.90 | 28.87 | 40.01 | 16.99 | 77.55 | 140.17 |
| OLIFANTSHOEK | 13.41 | 2.00 | 15.47 | 22.65 | 32.67 | 15.05 | 65.67 | 178.92 |
| GHAAP | 25.22 | 2.22 | 25.21 | 40.05 | 36.32 | 18.54 | 77.45 | 214.44 |
| ONGELUK | 11.29 | 2.28 | 15.98 | 28.20 | **58.53** | 16.30 | 70.76 | 168.61 |
| KOEGAS | 28.16 | 2.00 | 32.85 | 52.33 | 39.19 | **22.55** | 96.49 | 173.26 |
| ASBESTOS HILLS | 28.54 | 2.43 | 24.88 | **66.24** | 34.41 | 17.29 | 83.16 | 247.28 |
| CAMPBELLRAND | 31.67 | 2.41 | 29.15 | 25.09 | 38.24 | 16.19 | 79.14 | 164.96 |
| PRIESKASPOORT | 16.21 | 2.21 | 23.03 | 36.57 | 57.68 | 11.86 | 71.56 | **2628.70** |
| DOORNFONTEIN | 17.32 | 2.00 | 14.13 | 20.89 | 38.03 | 12.07 | 73.60 | 154.87 |
| SKALKESPUT | 19.58 | 2.00 | 20.17 | 39.33 | 40.00 | 16.83 | 86.63 | 176.37 |
| DRAGHOENDER GRANITE | 9.83 | 2.00 | 11.68 | 27.28 | 32.89 | 13.23 | 63.53 | 396.20 |
| ZEEKOEBAART | 24.84 | 2.00 | 32.14 | 29.28 | 37.57 | 17.85 | 89.17 | 227.44 |

| LITHOSTRATIGRAPHY. | Sc | Sn | Sr | Ta | Th | U | V |
|---|---|---|---|---|---|---|---|
| | | | | | | | |
| KALAHARI | 19.32 | **6.83** | 107.27 | 6.03 | 13.49 | 3.50 | 103.53 |
| DWYKA | 17.32 | 3.34 | 107.92 | 8.18 | 13.41 | 3.59 | 112.67 |
| WATERKOP | 17.02 | 3.00 | 118.88 | 6.73 | 13.36 | 3.29 | 135.72 |
| JACOMYNS PAN | 14.96 | 5.08 | 107.77 | 5.33 | 13.64 | 5.45 | 97.43 |
| SPIOENKOP | 17.16 | 3.00 | 110.07 | 4.64 | 12.38 | 3.00 | 129.83 |
| GROBLERSHOOP | 15.82 | 3.00 | 104.82 | 5.52 | 14.61 | 4.40 | 88.20 |
| UITDRAAI | 20.78 | 3.00 | 146.44 | 5.82 | 15.72 | 3.34 | 153.99 |
| BRULSAND | **25.73** | 3.00 | 97.54 | **14.00** | 15.29 | **6.59** | 132.14 |
| MATSAP | 18.92 | 3.00 | 110.11 | 4.44 | 14.08 | 3.00 | 131.39 |
| BOEGOEBERG DAM | 24.93 | 4.21 | 94.36 | 9.25 | 12.69 | 5.72 | 118.92 |
| OLIFANTSHOEK | 15.07 | 3.00 | 118.87 | 3.86 | 9.07 | 3.00 | 108.38 |
| GHAAP | 19.88 | 4.21 | 107.71 | 8.24 | 14.95 | 3.99 | 106.35 |
| ONGELUK | 19.29 | 3.00 | 116.08 | 3.00 | 10.74 | 6.17 | 134.83 |
| KOEGAS | 16.87 | 3.14 | 124.56 | 10.39 | **21.23** | 4.89 | **153.36** |
| ASBESTOS HILLS | 16.20 | 3.53 | 111.96 | 8.23 | 13.06 | 4.44 | 118.45 |
| CAMPBELLRAND | 20.66 | 3.30 | 88.95 | 7.87 | 12.76 | 5.76 | 112.80 |
| PRIESKASPOORT | 17.31 | 3.00 | **173.17** | 7.98 | 7.10 | 3.93 | 133.15 |
| DOORNFONTEIN | 14.74 | 3.00 | 90.36 | 5.72 | 7.95 | 3.00 | 102.87 |
| SKALKESPUT | 15.26 | 3.00 | 137.68 | 5.56 | 10.49 | 3.00 | 139.39 |
| DRAGHOENDER GRANITE | 3.00 | 3.00 | 112.77 | 3.00 | 7.56 | 3.00 | 97.31 |
| ZEEKOEBAART | 11.77 | 3.00 | 114.93 | 13.65 | 15.14 | 4.55 | 134.10 |

**Appendix 2: The mean statistics of the each element relative or in association to the lithostratigraphic unit**

| LITHOSTRATIGRAPHY. | W | Y | Zn | Zr |
|---|---|---|---|---|
| | | | | |
| KALAHARI | 5.48 | 23.92 | 60.16 | 707.42 |
| DWYKA | 7.64 | 24.53 | 57.03 | 910.74 |
| WATERKOP | 5.59 | 23.55 | 65.80 | 757.26 |
| JACOMYNS PAN | 6.06 | 19.97 | 47.99 | 789.83 |
| SPIOENKOP | 3.00 | 28.45 | **85.62** | 598.65 |
| GROBLERSHOOP | 5.14 | 21.81 | 47.48 | 936.93 |
| UITDRAAI | 4.72 | 27.06 | 75.77 | 939.96 |
| BRULSAND | 4.06 | **46.15** | 51.61 | **2119.99** |
| MATSAP | 3.53 | 28.31 | 69.25 | 774.83 |
| BOEGOEBERG DAM | 3.69 | 39.27 | 47.70 | 1795.59 |
| OLIFANTSHOEK | 4.17 | 20.70 | 49.41 | 566.31 |
| GHAAP | 6.42 | 24.03 | 51.86 | 1278.69 |
| ONGELUK | 3.81 | 20.97 | 80.35 | 439.88 |
| KOEGAS | 5.69 | 32.22 | 77.43 | 1221.34 |
| ASBESTOS HILLS | 7.38 | 29.99 | 53.83 | 1329.99 |
| CAMPBELLRAND | 3.61 | 36.20 | 47.25 | 1575.53 |
| PRIESKASPOORT | 7.78 | 17.83 | 58.55 | 679.37 |
| DOORNFONTEIN | 5.79 | 22.84 | 57.97 | 806.66 |
| SKALKESPUT | 4.03 | 25.17 | 70.20 | 826.65 |
| DRAGHOENDER GRANITE | 3.00 | 15.46 | 57.83 | 448.25 |
| ZEEKOEBAART | **12.13** | 23.90 | 60.11 | 1062.29 |

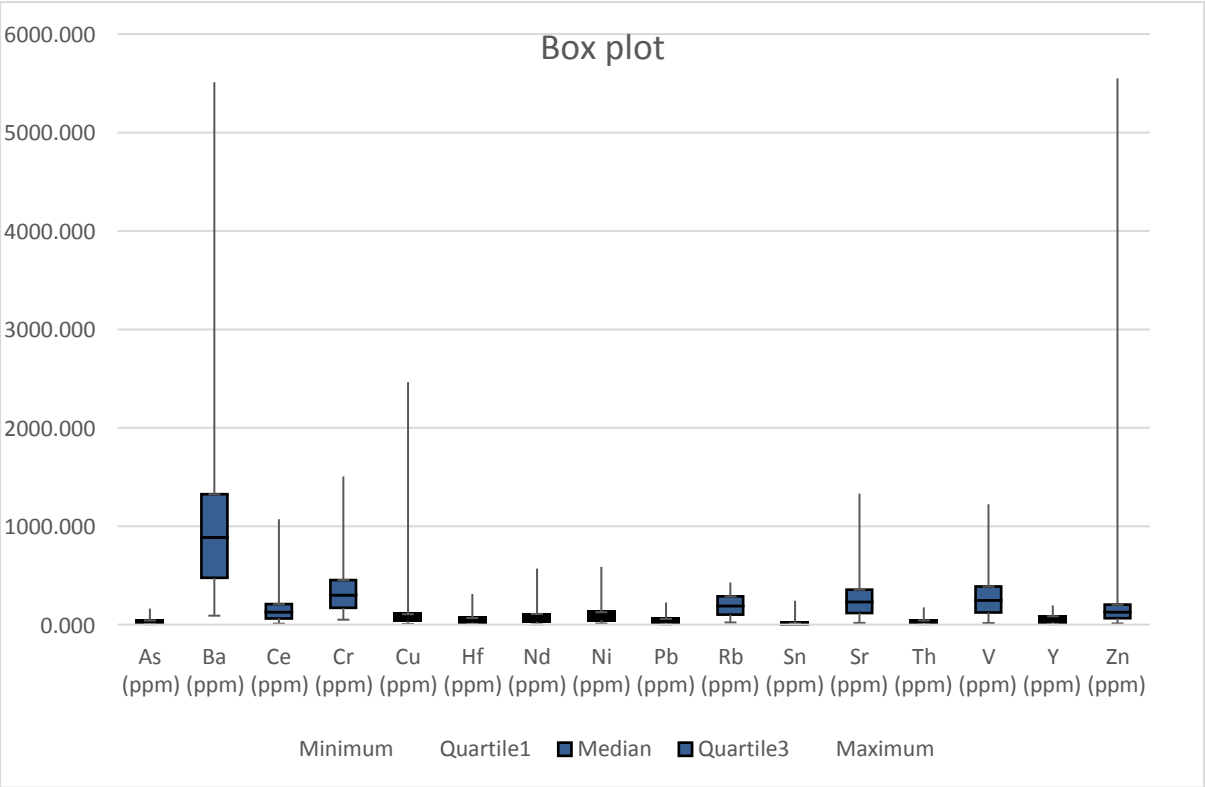
***Appendix 3: The descriptive statistics on geochemistry data of the Prieska area, and box plot.***

| Element | Minimum | Maximum | Mean | Standard Deviation | Skewness | Kurtosis | Quartile1 | Median | Quartile3 |
|---|---|---|---|---|---|---|---|---|---|
| **As (ppm)** | 4.000 | 120.910 | 15.802 | 13.874 | 2.235 | 9.991 | 6.145 | 11.450 | 20.240 |
| **Ag (ppm)** | 4.000 | 25.270 | 5.392 | 2.452 | 3.519 | 19.435 | 4.000 | 4.240 | 6.050 |
| **Ba (ppm)** | 91.180 | 4187.720 | 410.752 | 76.653 | 24.597 | 1080.028 | 382.565 | 409.805 | 439.865 |
| **Ce (ppm)** | 10.000 | 864.010 | 78.027 | 55.741 | 4.665 | 36.596 | 53.200 | 64.390 | 79.425 |
| **Co (ppm)** | 4.000 | 56.420 | 14.733 | 4.017 | 1.149 | 6.949 | 12.050 | 14.140 | 16.790 |
| **Cr (ppm)** | 49.790 | 1052.880 | 141.762 | 40.500 | 4.198 | 49.516 | 119.470 | 131.680 | 151.535 |
| **Cu (ppm)** | 7.370 | 2357.040 | 34.465 | 31.879 | 53.683 | 3534.044 | 28.510 | 32.780 | 37.740 |
| **Ga (ppm)** | 6.250 | 46.420 | 19.769 | 4.425 | 0.143 | 2.650 | 16.040 | 19.890 | 23.160 |
| **Hf (ppm)** | 5.000 | 245.440 | 23.292 | 14.397 | 3.954 | 30.123 | 15.850 | 19.820 | 25.720 |
| **Mo (ppm)** | 2.000 | 13.350 | 2.143 | 0.568 | 7.505 | 84.540 | 2.000 | 2.000 | 2.000 |
| **Nb (ppm)** | 3.000 | 112.200 | 25.264 | 8.482 | 2.075 | 13.720 | 20.650 | 24.060 | 28.115 |
| **Nd (ppm)** | 3.000 | 459.830 | 40.511 | 27.490 | 4.003 | 31.632 | 26.270 | 34.815 | 44.850 |
| **Ni (ppm)** | 11.360 | 460.500 | 39.559 | 12.345 | 7.908 | 192.598 | 33.180 | 37.620 | 43.905 |
| **Pb (ppm)** | 2.000 | 167.110 | 18.776 | 5.030 | 7.963 | 192.132 | 16.420 | 18.745 | 20.950 |
| **Rb (ppm)** | 21.170 | 142.690 | 86.942 | 13.467 | -0.688 | 4.017 | 80.355 | 88.400 | 95.525 |
| **Sb (ppm)** | 3.000 | 4.300 | 3.001 | 0.026 | 36.635 | 1554.275 | 3.000 | 3.000 | 3.000 |
| **S (ppm)** | 54.920 | 32965.370 | 233.027 | 471.570 | 49.696 | 3037.767 | 146.985 | 195.115 | 257.120 |
| **Sn (ppm)** | 3.000 | 230.040 | 3.611 | 3.976 | 31.589 | 1458.505 | 3.000 | 3.000 | 3.000 |
| **Sc (ppm)** | 3.000 | 50.180 | 18.183 | 5.077 | 0.135 | 3.687 | 14.930 | 17.930 | 21.355 |
| **Sr (ppm)** | 18.170 | 975.050 | 113.523 | 28.744 | 8.948 | 201.199 | 100.590 | 113.045 | 123.810 |
| **Ta (ppm)** | 3.000 | 61.570 | 7.556 | 6.478 | 2.620 | 12.424 | 3.000 | 5.285 | 9.130 |
| **Th (ppm)** | 3.000 | 132.240 | 13.868 | 6.750 | 4.161 | 40.510 | 10.270 | 12.970 | 15.890 |
| **U (ppm)** | 3.000 | 25.760 | 4.041 | 1.842 | 3.467 | 22.295 | 3.000 | 3.075 | 4.450 |
| **V (ppm)** | 16.180 | 836.190 | 126.384 | 33.836 | 3.657 | 41.490 | 108.250 | 123.520 | 137.885 |
| **W (ppm)** | 3.000 | 51.750 | 6.318 | 5.147 | 2.546 | 12.203 | 3.000 | 3.980 | 7.850 |
| **Y (ppm)** | 3.960 | 112.390 | 27.021 | 7.211 | 2.420 | 18.762 | 23.030 | 26.635 | 29.860 |
| **Zn (ppm)** | 11.990 | 5347.830 | 66.145 | 68.394 | 58.378 | 4155.871 | 53.120 | 62.850 | 74.285 |
| **Zr (ppm)** | 111.870 | 9242.850 | 1023.432 | 671.759 | 3.605 | 24.477 | 669.530 | 855.425 | 1144.235 |

## Appendix 3: The descriptive statistics on geochemistry data of the Prieska area, and box plot

| Element | Threshold values | Mean+3*SD | box 1 | box2 | box3 | whisker top | whisker bottom | CV |
|---|---|---|---|---|---|---|---|---|
| As (ppm) | 43.551 | 57.425 | 6.145 | 5.305 | 8.79 | 100.67 | 2.145 | 0.88 |
| Ag (ppm) | 10.296 | 12.748 | 4 | 0.24 | 1.81 | 19.22 | 0 | 0.45 |
| Ba (ppm) | 564.058 | 640.711 | 382.565 | 27.24 | 30.06 | 3747.855 | 291.385 | 0.19 |
| Ce (ppm) | 189.510 | 245.251 | 53.2 | 11.19 | 15.035 | 784.585 | 43.2 | 0.71 |
| Co (ppm) | 22.766 | 26.783 | 12.05 | 2.09 | 2.65 | 39.63 | 8.05 | 0.27 |
| Cr (ppm) | 222.762 | 263.262 | 119.47 | 12.21 | 19.855 | 901.345 | 69.68 | 0.29 |
| Cu (ppm) | 98.223 | 130.102 | 28.51 | 4.27 | 4.96 | 2319.3 | 21.14 | 0.92 |
| Ga (ppm) | 28.618 | 33.043 | 16.04 | 3.85 | 3.27 | 23.26 | 9.79 | 0.22 |
| Hf (ppm) | 52.085 | 66.482 | 15.85 | 3.97 | 5.9 | 219.72 | 10.85 | 0.62 |
| Mo (ppm) | 3.279 | 3.846 | 2 | 0 | 0 | 11.35 | 0 | 0.26 |
| Nb (ppm) | 42.229 | 50.711 | 20.65 | 3.41 | 4.055 | 84.085 | 17.65 | 0.34 |
| Nd (ppm) | 95.490 | 122.980 | 26.27 | 8.545 | 10.035 | 414.98 | 23.27 | 0.68 |
| Ni (ppm) | 64.250 | 76.595 | 33.18 | 4.44 | 6.285 | 416.595 | 21.82 | 0.31 |
| Pb (ppm) | 28.836 | 33.866 | 16.42 | 2.325 | 2.205 | 146.16 | 14.42 | 0.27 |
| Rb (ppm) | 113.876 | 127.343 | 80.355 | 8.045 | 7.125 | 47.165 | 59.185 | 0.15 |
| Sb (ppm) | 3.052 | 3.077 | 3 | 0 | 0 | 1.3 | 0 | 0.01 |
| S (ppm) | 1176.166 | 1647.735 | 146.985 | 48.13 | 62.005 | 32708.25 | 92.065 | 2.02 |
| Sn (ppm) | 11.562 | 15.538 | 3 | 0 | 0 | 227.04 | 0 | 1.10 |
| Sc (ppm) | 28.337 | 33.413 | 14.93 | 3 | 3.425 | 28.825 | 11.93 | 0.28 |
| Sr (ppm) | 171.010 | 199.754 | 100.59 | 12.455 | 10.765 | 851.24 | 82.42 | 0.25 |
| Ta (ppm) | 20.513 | 26.992 | 3 | 2.285 | 3.845 | 52.44 | 0 | 0.86 |
| Th (ppm) | 27.367 | 34.116 | 10.27 | 2.7 | 2.92 | 116.35 | 7.27 | 0.49 |
| U (ppm) | 7.726 | 9.568 | 3 | 0.075 | 1.375 | 21.31 | 0 | 0.46 |
| V (ppm) | 194.057 | 227.893 | 108.25 | 15.27 | 14.365 | 698.305 | 92.07 | 0.27 |
| W (ppm) | 16.612 | 21.759 | 3 | 0.98 | 3.87 | 43.9 | 0 | 0.81 |
| Y (ppm) | 41.443 | 48.654 | 23.03 | 3.605 | 3.225 | 82.53 | 19.07 | 0.27 |
| Zn (ppm) | 202.933 | 271.327 | 53.12 | 9.73 | 11.435 | 5273.545 | 41.13 | 1.03 |
| Zr (ppm) | 2366.950 | 3038.709 | 669.53 | 185.895 | 288.81 | 8098.615 | 557.66 | 0.66 |

***Appendix 4. The box plot of high coefficient of variation.***




Appendix 4 Box plot of high coefficient of variation continues….

